UiO : Department of Geosciences
University of Oslo

FEATURE DETECTION IN GLACIAL CHANNELS USING DRIFTERS

George Cowie

Master's Thesis,
Computational Geoscience, Spring 2022

Abstract

Drifting sensor platforms can be used to perform measurements in the harsh and inaccessible environments of glacial channels. These channels are predominantly responsible for the transfer of water from the surface to the glacier bed, where the water regulates many glacial processes (e.g. sliding, erosion). The water transit is thought to be partly controlled by morphological features in the channel. Using drifters to detect morphological features in glacial channels may therefore help to study this water transit. As drifters move through channels, they deliver a wealth of data, but computational methods to extract useful information out of these data are sparse. When they move over different morphological features in a channel, characteristic signals are recorded by the sensors onboard. This thesis uses a motif discovery algorithm, called a matrix profile query search on drifter pressure data, collected in supraglacial channels during field campaigns on Svalbard in 2020 and 2021, to detect the characteristic signal of a specific morphological feature, termed a step. Steps are areas of abrupt vertical slope change in channels. They modulate water flow through increased flow resistance and locally enhanced channel erosion. In the investigated data, up to 70% of the steps in two different supraglacial channels were correctly identified. These results indicate that steps can be detected using only pressure data from drifters. The method presented in this thesis is a starting point for automated feature detection in glacial channels using drifter data, but more work is needed to improve the accuracy of the method by collecting additional reference data and including more sensor modalities. As steps are responsible for most of the vertical elevation change in supra- and englacial channels, this method could, in combination with extended drifter studies, help to better understand the transit of water from the surface to the bed of glaciers. This might contribute to improved monitoring and prediction capabilities of glacier dynamics in a warming world.

Norsk sammendrag (Norwegian summary)

Flytende sensorplatformer "Driftere" kan brukes til å utføre målinger i de tøffe og utilgjengelige forholdene i smeltevannskanaler på bre. Drifterene kan levere et vell av data smeltevannskanaler, men metoder for å trekke ut nyttig informasjon fra dataene har enda ikke blitt utviklet. Når driftere beveger seg over ulike morfologiske former i en smeltevannskanal vil karakteristiske signaler bli målt av sensorene på drifteren. Denne oppgaven bruker en motivoppdagelsesalgoritme, kalt et matriseprofilsøk på trykkdata fra drifterene, samlet inn under feltkampanjer på Svalbard i 2020 og 2021, for å oppdage en spesiell morfologisk figur, kalt et trinn, i supraglasiale kanaler. Trinn er områder med brå vertikale skråningsendringer i supraglasiale kanaler og modulerer kanalstrømningen gjennom økt strømningsmotstand og øker kanalerosjon lokalt. Opptil 70% av trinnene i to undersøkte supraglasiale kanaler kunne identifiseres. Resultatene indikerer at trinn kan oppdages kun ved bruk av trykkdata fra driftere. Imidlertid begrenses nøyaktigheten av metoden av at kun en enkelt sensormodalitet brukes. Metoden presentert i denne oppgaven er et utgangspunkt for figurdeteksjon i glasiale kanaler ved bruk av drifterdata, men mer arbeid er nødvendig for å forbedre nøyaktigheten til metoden: ved å samle inn flere referansedata og å inkludere flere sensormodaliteter. Å bruke driftere for å oppdage morfologiske trekk i brekanaler kan bidra til å forbedre forståelsen av hele det hydrologiske systemet av isbreer og isdekker, fra overflaten til bunnen. Ettersom trinnene er ansvarlige for mesteparten av den vertikale høydeendringen av supra- og englasiale kanaler, kan denne metoden i kombinasjon med utvidede drifterstudier bidra til bedre forståelsen av vanntransport fra overflaten til bunnen av breer. Dette er av relevans da vann ved brebunnen regulerer mange prosesser ved breen (f.eks. ved bunnglidning, erosjon) og en bedre forståelse av sammenhengen mellom økt overflatesmelting og transporten av dette vannet til underflaten vil derfor bidra til å bedre forstå og forutsi den fremtidige utviklingen av til isbreer i en varmende verden.

Acknowledgements

First i would like to thank Andreas Alexander for his solid guidance and supervision through the whole process of creating this thesis, from proposal writing, to fieldwork, to the finished thesis. I thank him for spreading his enthusiasm about glaciers and fieldwork and for making it possible for me to travel up to Svalbard again.
Thank you to my supervisor Thomas Schuler for valuable discussions and feedback on my thesis.
I am deeply grateful to Nele Schimpf for all the support, opinions, comments, and for putting up with me ranting about steps throughout the last year.
Thank you to everyone who was involved in the fieldwork 2021, Léo Decaux, Livia Piermattei, Laura Piho, Maarja Kruusma, Jaan Rebane, the Sverdrup station personnel, Kingsbay staff, the SIOS Knowledge centre, particularly Inger Jennings, UNIS for safety training and logistical support and all the other great people in Ny-Ålesund.
I gratefully acknowledge everyone who was involved in the 2020 field campaign on Austre Brøggerbreen who provided me with invaluable data for this thesis. Fieldwork in 2020 was funded by the Research Council of Norway via an Arctic Field Grant (2020/310689) and POLARPROG (2020/317905)
Thank you to the Research Council of Norway for providing me with a grant that made my fieldwork possible (Arctic Field Grant 2021, grant number 322678) and to all the other grants that contributed:
Grants to Andreas Alexander:
- Research Council of Norway, project number 291644, Svalbard Integrated Arctic Earth Observing System -Knowledge Centre, operational phase: Access Grant 2020_0007
- Robert og Ella Wenzins legat ved Universitetet i Oslo
- Familien Stillesen og Professor S. A. Sexes legat
- Hans og Helga Reuschs legat til fremme av studiet av geografi og geologi
Grants to Livia Piermattei
- University of Oslo, Department of Geosciences, Industrial Liason
Grants to Maarja Kruusma:
- EU INTERACT Transnational Access: Deep Sense 2021
Other grants:
- Research Council of Norway, grant number 301837 MAMMAMIA: Multi-scale multi-method analysis of mechanisms causing ice acceleration
- University of Oslo, Department of Geosciences
A big thanks goes out to everyone at Lesesal 2418B for two great years working on our masters, wouldn't have been nearly as fun without you.
And finally, thank you to the cold waters of Voldsfjorden for giving me a massively time saving epiphany.

George Cowie
May 2022
Oslo

Contents

List of Figures

List of Tables

CHAPTER 1

Introduction

Water plays a dominant role in many glacial processes and in the impact of glaciers on the larger environment (Eyles, 2006). A major component of the available water on glaciers is meltwater. The main source of glacial meltwater are the ablation of snow and ice at the glacier surface. During winter, seasonal snowpacks on glacier surfaces renew. With the onset of the melt season this snow begins to melt, generating the bulk of the early season glacial meltwater. Later in the melt season, as the snowpack begins to exhaust, exposed ice begins to melt and takes over as the main source of meltwater (Armstrong et al., 2019). Water flow through the glacial system influences aspects of glacier dynamics by for example reducing basal friction or modulating ice viscosity (Phillips et al., 2010). Melt controls the quantity and quality of water delivered to downstream environments (Brown, 2002) and thereby shape landscapes through material erosion and sediment deposition (Eyles, 2006). Besides the importance for the glacial environment, meltwater is also of great significance to humans. Many countries are critically reliant on glacial meltwater as a source of drinking water, irrigation and hydropower production (Li et al., 2015). One of the most profound societal effects of glacial melt is that it contributes directly to sea level rise. Millions of humans who inhabit coastal lowlands are threatened by rising sea levels and the economic costs for damage and mitigation for this rise have been estimated from hundreds to thousands of billion dollars (Anthoff et al., 2010).

With an ever warming climate, glacial melt is occurring at higher altitudes and melt seasons are extending, leading to increased global meltwater production (IPCC, 2019). The Arctic in particular, is experiencing increased air temperatures and thus glacier melt. For example, the arctic archipelago of Svalbard is one of the most rapidly warming regions on Earth (Schuler et al., 2020). It has already experienced an increase in average annual air temperature of 3-5°C from 1971 to 2017 (Adakudlu et al., 2019). The rapid warming on Svalbard has led to a great mass loss of glaciers on the archipelago in recent decades. The mass balance estimates for the last two decades are -7 $\pm$ 4 Gt a^{-1} (2000-2019) for the climatic mass balance, and -8 $\pm$ 6 Gt a^{-1} for the total mass balance (Schuler et al., 2020). In a report from Adakudlu et al., 2019, the air temperature on Svalbard is predicted to increase by 7° to 10° C by 2100. This is predicted to lead to more intense and frequent rainfall, decrease in snow cover and a severe reduction in glacier area and increasingly negative glacier mass balance. The rapid warming on Svalbard makes the archipelago an indicator of what is to come for other glaciated areas on the planet. Research in this geographic area is therefore needed to develop methods and better scientific understanding of processes, to better understand the ongoing and upcoming changes to the worlds glaciers.

Due to various ecological, climatic and societal impacts of glacial hydrology and accelerating mass loss trends of glaciers (Hugonnet et al., 2021), there is an ever growing realisation of the importance of this system. However, in situ data on the topic remains sparse because of difficult measuring conditions. (Pitcher and Smith, 2019). New technologies are needed to access previously inaccessible study areas. With the advent of remote sensing methods, large inaccessible areas can be mapped using satellites, aircraft or by the use of unmanned aerial vehicles (UAVs) (Bhardwaj

et al., 2016; Nuth et al., 2013; McKean et al., 2009). These methods have also made repeat mapping easy, reducing the complicated logistics of fieldwork. However, results obtained from remote sensing still need validation from in situ measurements (Gleason et al., 2016). Glaciers are often in remote areas where logistics are difficult and expensive to organise. Glaciers also present a number of hazards, such as crevasses, moulins, cold meltwater channels, harsh and freezing weather conditions and, in the Arctic polar bears, to name a few.

Direct measurements are important for a number of reasons: as model input, to validate results obtained by remote sensing, modelling studies, and to provide data from sub- and englacial channels, which are inaccessible to remote sensing techniques. Current methods of in situ measurements within glacier hydrology include among others: dye tracing, doppler current profiling, salt injection, ground penetrating radar (GPR) and gas tracing. These methods are often limited in either temporal or spatially distributed information in glacial channels. A suite of floating sensors, commonly named drifters, have been developed to resolve some of the issues of fieldwork in glacial hydrology. These drifters can be deployed into channels where they log data autonomously, floating passively with the water flow. This allows profiling of long channel segments and the possibility to profile the sub- and englacial system without having to physically enter them. The data can then be recovered by instrument recovery or by wireless data transfer. Previous tests of drifter platforms have shown great promise for measurements in glacial channels (Alexander, Kruusmaa et al., 2020; E. Bagshaw et al., 2014; E. A. Bagshaw et al., 2012; Tuhtan et al., 2020; Piho, Alexander et al., 2022).

1.1 Aims

Drifter technology has created the potential to study underexplored areas in glacial hydrology, by collecting data from previously inaccessible places like the sub- and englacial system. Collected data can be complex and hard to interpret, especially where visual inspection is not possible and other reference data is not available (as in sub- and englacial channels). Therefore robust methods that can transfer collected data into scientific information are needed. Numerous computational methods exist to analyse data within earth sciences, but few have been applied to this platform. Therefore, the aim of this thesis is to find a computational method that is able detect morphological features in glacial channels based on the data collected by two different drifter platforms.

1.2 Research objective

To improve the capability of drifter measurements, this thesis aims to develop a set of algorithms for data analysis. For this, two different drifter platforms were used in the field and the data from two field seasons analysed. Different features present in supraglacial channels, like meander bends and step-risers, yield characteristic signals (Tuhtan et al., 2020). There is a wide variety of signal processing tools available for classifying signals. In this thesis, matrix profile query searches were found to be suitable for this kind of investigation. This is a simple and fast method that can be used to find repeating patterns in time series data. Comparing drifter-detected signals to in situ reference data and classifying these into different glacier features, will allow for the development of a baseline method that can be used to analyse drifter data without the need for reference data.

The work has focused on classifying one specific morphological feature called a step. Steps are one of the most prominent features in supraglacial channels and are easily detected in video footage that serves as reference.

CHAPTER 2

Theoretical background

2.1 Supraglacial channels

Supraglacial channels are channels transporting water across the surface of an ice body. They are found in all glaciated regions and are most active during the summer melt. The term "supraglacial channel" is used generically for both streams and rivers (Pitcher and Smith, 2019). Rivers and streams are classified as follows,

- "Supraglacial rivers are primarily main-stem channels with high stream orders that are perennially occupied. They are regularly spaced, form parallel to ice flow directions, have elongated patterns, and often terminate in moulins." (Pitcher and Smith, 2019)
- "Supraglacial streams are low order with shallow depths, are annual or transient on multiyear timescales, and are often tributary to larger rivers." (Pitcher and Smith, 2019)

Supraglacial channels form and develop via erosion into the ice. The primary drivers of erosion in supraglacial streams are frictional dissipation of heat from flowing water (Karlstrom et al., 2013), mechanical erosion (Ferguson, 1973) and thermal erosion from solar radiation. Solar energy input in shallow channels is higher than in the surroundings because glacial channels have an albedo of around half that of bare ice, due to the lower albedo of water present in the channel (Ryan et al., 2018). The enhanced thermal energy absorbed by the water is available for ablation of the channel bed and to increase the temperature of the water. These processes, along with other properties like variable melt rates from topographic shading, extensional and compressional ice flow, nonuniform surface slope, variations in ice structure and variations in water input, govern channel morphology (Karlstrom et al., 2013).

Supraglacial channels terminate by draining directly into the sea, into the terrestrial hydrological system or by entering the subglacial or englacial system through moulins, crevasses or cut and closure systems. Supraglacial channels vary in width from just a few centimetres to tens of meters (Pitcher and Smith, 2019). Englacial and subglacial channels are distinct from supraglacial channels in that they exist below the surface of the ice. Englacial channels flow within the ice, below the surface and above the bed, while subglacial channels flow at the bed of the glacier. Meltwater entering the subglacial drainage system can modulate the subglacial thermal properties (Alexander, Obu et al., 2020) and increase the water pressure, promoting dynamic properties like sliding (Iken et al., 1983). Meltwater can also remain stored in channels, moulins or lakes throughout the winter both in the supra-, en-, and subglacial system (Arnold et al., 2014). See figure 2.1 for examples of drainage systems.

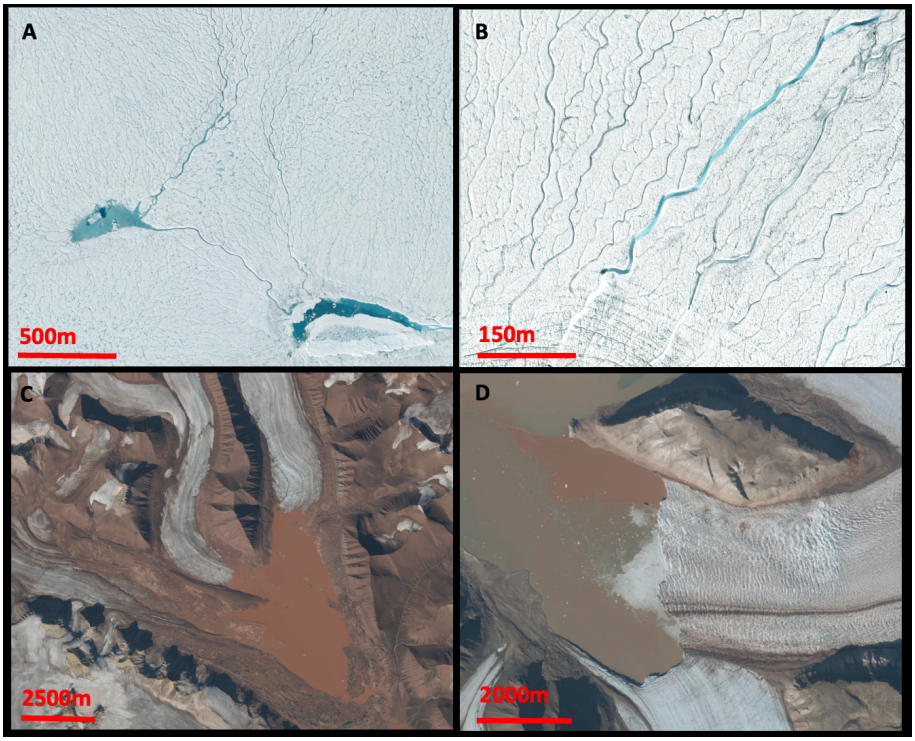

Figure 2.1: A) Supraglacial channels running into supraglacial lakes, Bråsvellbreen Svalbard. B) Multiple supraglacial channels terminating into moulins along a crevasse. Old snow filled channels downstream of the moulins still visible. Bråsvellbreen Svalbard. C) Proglacial lake, Trebrevatnet, Svalbard. D) Sediment plume in Kongsfjorden in front of Kronebreen and Kongsvegen, Svalbard.

Steps

In fluvial rivers, singular features of abrupt slope changes are commonly termed knickpoints (Davis, 1932). A series of knickpoints along a channel are termed knickzones and often appear in rapid succession with a regular frequency (Vatne and Irvine-Fynn, 2016). Knickpoints migrate upstream as the erosion rates around these points is faster than in other areas of the channel (Vatne and Irvine-Fynn, 2016). The enhanced erosion is driven by frictional thermal erosion and mechanical weathering (Kamintzis et al., 2019). Enhanced erosion around knickpoints is thought to be the main mode of channel adjustment to perturbations (Vatne and Irvine-Fynn, 2016). This has also been reported as a mechanism by which supraglacial channels can incise into ice and become englacial channels (Gulley et al., 2009; Vatne and Irvine-Fynn, 2016). If channel incision rates exceed the surface ablation a canyon is formed that can be covered by winter snow, refreezing meltwater or plugged by detached blocks of ice, roof collapse or by deformation of ice. These processes can isolate the channel from the surface creating an englacial channel (Gulley et al., 2009).

Step-pools are staircase-like longitudinal profiles that occur in knickzones and consist of two components: a knickpoint followed by a plunge pool (see figure 2.2). The channel segment with a steep inclination following a knickpoint is referred to as a step-riser (Chartrand and Whiting, 2000). Step-risers are commonly preceded by a pool segment (Vatne and Irvine-Fynn, 2016). An example of a sequence of steps can be seen in figure 2.3. As the water passes down a step-riser the flow velocity increases, enhancing erosional scour in the plunge pool and creating recirculating currents in the pool (Vatne and Irvine-Fynn, 2016). A set of distinct hydraulic conditions occur within a step-pool: subcritical flow upstream of the step, critical flow across the knickpoint lip, supercritical flow down the step-riser and finally a hydraulic jump in the plunge pool. A hydraulic jump is the rapid and sudden transition from a supercritical flow to a subcritical flow (Murzyn and Chanson, 2009). Step-pools are important in channels because they reinforce channel bed stability, provide much of the change in elevation and cause much of the hydraulic roughness in channels (Vatne and Irvine-Fynn, 2016). In englacial channels, step-pools may account for more than 80% of the descent in flow path elevation (Vatne, 2001). In artificial spillways, stepped chutes are used as a method to dissipate energy in flood water Chanson, 1994. In fluvial rivers the energy dissipation caused by transitions from supercritical to subcritical flow found in steps-pools can account for up to 90 % of the flow resistance in the entire river (Curran and Wohl, 2003).

Knickpoints, knickzones, step-pools and step-risers come in a range of forms within channels. As these forms are not discriminated between in this thesis, all areas of abrupt longitudinal slope change will from here on out be referred to as steps.

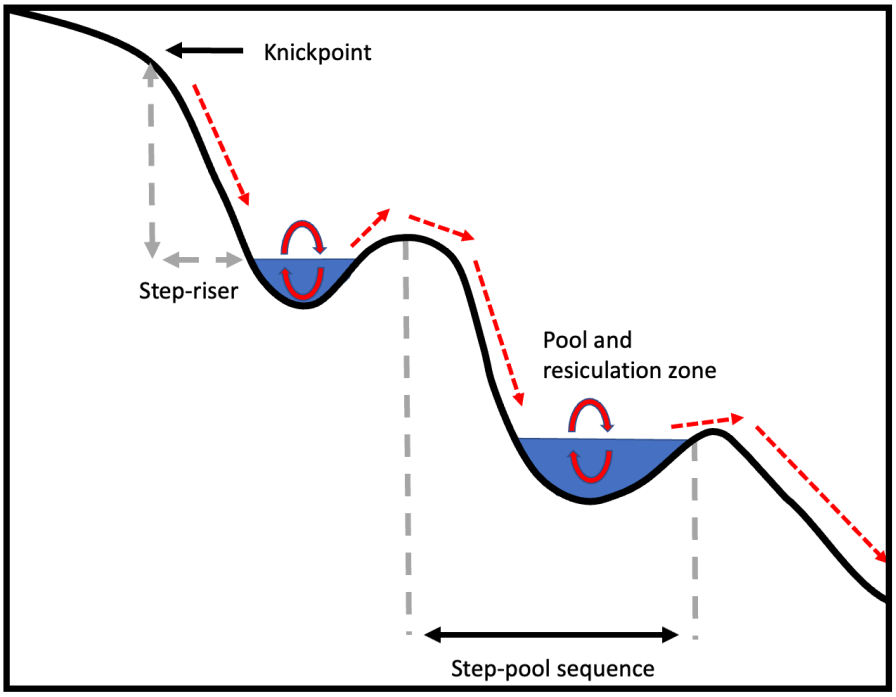

Figure 2.2: Schematic of a step-pool sequence. Dashed red lines indicate the flow direction. Recirculation zones are shown by curved red arrows. Modified from Vatne and Irvine-Fynn, 2016
.

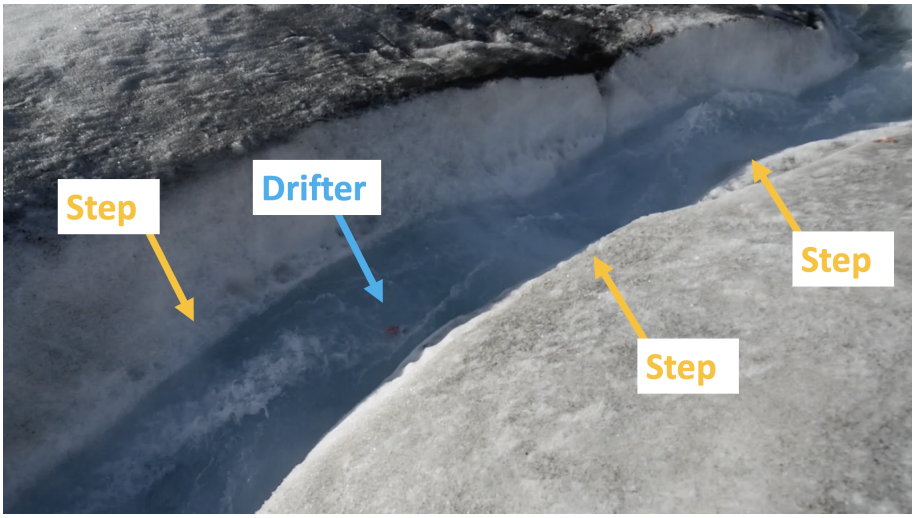

Figure 2.3: Sequence of steps from a channel on Austre Brøggerbreen. The image was taken on the 18.08.2020. In the image the drifter is located in the plunge pool of a small step.

Hydraulic equations

Hydraulic geometry measurements of channel width, depth and water velocity can be used to describe flow conditions in a supraglacial channel (Pitcher and Smith, 2019). Flow conditions can be categorised as subcritical, critical or supercritical or turbulent versus laminar, among others. In subcritical flow, gravity and friction are in balance and the flow velocity divided by the water depth in the channel is constant over short time intervals (Pitcher and Smith, 2019). In critical and supercritical flow, velocity and water depth change abruptly over short time intervals. These different flow conditions can be described using the dimensionless Froude number (F_r), which describes the ratio between water velocity, gravity and depth (Pitcher and Smith, 2019).

$$F_r = \frac{v}{\sqrt{g \cdot d}} \tag{2.1}$$

Where v is the average water velocity in the centre of the channel, d is the water depth at the cross section and g is the gravitational acceleration, set to 9.81 ms^{-2}. Froude numbers equal to 1 indicate critical flow, numbers larger than 1 indicate supercritcal flow, and numbers smaller than 1 subcritical flow.

In order to characterise channel flow as laminar or turbulent the dimensionless Reynolds number R_e can be used (Ponce, 1979).

$$R_e = \frac{v \cdot d}{k_v}, \tag{2.2}$$

where v is the average water velocity in the centre of the channel, d is the flow depth and k_v is the kinematic viscosity of water at 0° C with a value of $1.787 \cdot 10^{-6}$ $\mathrm{m}^2\mathrm{s}^{-1}$. High Reynolds numbers, $R_e > 3000$, indicate turbulent flow and low number, $R_e < 1000$, laminar flow. Reynolds numbers with values between $1000 < R_e < 3000$ are in the transitional range between laminar flow and turbulent flow, although the transitional range is not clearly defined (Ponce, 1979).

2.2 Drifters

The data used in this thesis were collected using two drifting sensor platforms. The platforms each consist of a buoyant tube equipped with pressure and inertial measurement unit (IMU) sensors. Each drifter is deployed directly into meltwater channels where it floats passively with the flow of the water while collecting data. These sensor platforms are a promising method for the study of the glacial hydrologic system (Alexander, Kruusmaa et al., 2020; Piho, Alexander et al., 2022; Tuhtan et al., 2020). The drifters can be equipped with a range of sensors that collect data along the flow paths of glacial channels (Alexander, Kruusmaa et al., 2020). As they are able to collect data along the flow path, they provide the possibility of a larger spatial range of observational data than conventional static measurement stations (Alexander, Kruusmaa et al., 2020). They also hold the potential to be deployed into areas that are inaccessible for manual measurements, for instance englacial or subglacial systems (Piho and Kruusmaa, 2021). However, in order to interpret time series data collected by drifters, substantial reference data are required and computational methods to extract useful information need to be developed.

2.3 Data mining

Mining time series data for information is an ever expanding field. The number of instruments providing such data is proliferating, along with methods to analyse them (Bagnall et al., 2016). A time series is a series of values separated by a time step. The definition of a time series $T \in \mathbb{R}^n$ is a sequence of real valued numbers $t_i \in \mathbb{R} : T = [t_1, t_2, ..., t_n]$ where n is the length of T (Dau and Keogh, 2017). Data of this kind could be anything from air temperature records to power consumption records of a kitchen fridge (Yeh et al., 2017). When analysing time series data,

common objectives include: looking for trends, anomalies or recurring patterns. Using a time series of air temperature records over Svalbard as an example, a trend could be increasing air temperatures during the industrial era, anomalies could be extreme heat waves and repeating patterns could be seasonal temperature swings. Another domain of time series data analysis, that is currently growing rapidly, is that of extracting information from small devices logging different variables. For instance, many mobile phones are equipped with triaxial accelerometers that can be used to classify human motion behaviour (Thang et al., 2012). Such small accelerometers have also been mounted on chickens to monitor feeding behaviours (Yang et al., 2021).

The drifters are equipped with similar sensors and are measuring the same variables, but in a different system. Analysing the data collected by the drifters is at its core very similar to analysis of human motion or animal behaviour. We are trying to gain some physical insight about a real system based on the motion of the drifter through that system. To this end, I have utilised a motif discovery algorithm called a Matrix profile. In the context of time series, motifs are recurring patterns in the time series (Van Benschoten et al., 2020). This algorithm has been applied to solving problems in a range of fields like bioinformatics, speech processing, robotics, neurology and etymology (Zhu et al., 2016).

Matrix profile

The matrix profile is a conceptually easy and computationally cheap method to detect motifs and anomalies in time series data. A matrix profile is a vector that stores the normalised Euclidean distance between a subsequence of a time series and its nearest neighbour (Akbarinia and Cloez, 2019). It can be used to find global similarities in a time series or to detect similar features by a query search using sliding windows (Van Benschoten et al., 2020).

The basic idea is to take a subsequence of length m from a time series and compute the normalised Euclidean distance to all other possible subsequences and store index and distance to the closest match to this subsequence. This process is repeated with a sliding window for all possible subsequences until you have a list of nearest neighbours for every subsequence in the time series (Akbarinia and Cloez, 2019).

The normalised Euclidean distance, DZ, between to subsequences of equal length m, $T_{i,m}$ and $T_{j,m}$, is defined by Akbarinia and Cloez, 2019 as follows:

$$DZ_{i,j} = \sqrt{\sum_{l=0}^{m-1} \left(\frac{t_{i+l} - \mu_i}{\sigma_i} - \frac{t_{j+l} - \mu_j}{\sigma_j} \right)^2}, \tag{2.3}$$

where μ_i and μ_j are the mean of the values in two subsequences $T_{i,m}$ and $T_{j,m}$ respectively. m is the length of the subsequence. σ_i and σ_j are the standard deviation of the values in $T_{i,m}$ and $T_{j,m}$ respectively.

Figure 2.4 shows a simple matrix profile where one window is held fixed and one window is slid along the data. This results in a vector of normalised Euclidean distances. The smallest of these distances is selected as the nearest neighbour of the subsequence (Van Benschoten et al., 2020). Since only the best match for each subsequence needs to be stored this gives a spatial complexity of $O(n)$. This example compares subsequences of the same time series, but it is also possible to compare different time series to each other. One of the advantages of the matrix profile is that it can compare time series of different lengths, because it only relies on subsequences.

When all possible subsequences of one time series are compared to themselves or to another time series, the resulting matrix profile will reveal motifs and anomalies. Motifs are shown by low distances and anomalies by high distances (Van Benschoten et al., 2020).

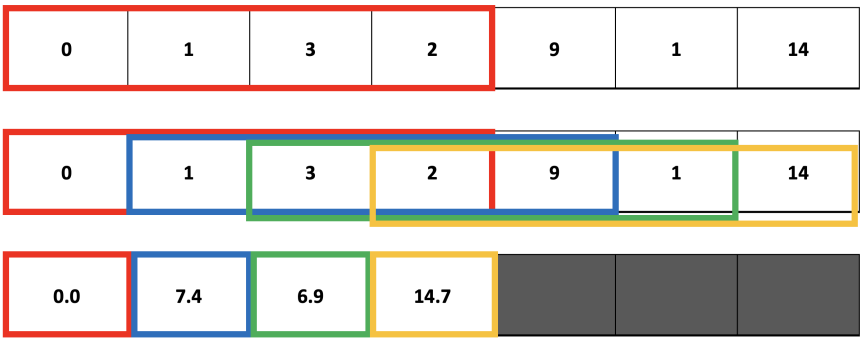

Figure 2.4: Results of a matrix profile from one subsequence. The top row shows a simple time series with a subsequence length of 4 boxes in red. The second row is the same time series with all possible subsequences with a length of 4 (different colours). The last row shows the euclidian distance between the subsequence in the first row with all the possible subsequences in the second row. The red window shows the trivial match where the subsequences are the same. Adapted from *The matrix profile* 2022.

The goal of this thesis is to detect specific features in the drifter data. Computing global matrix profiles may reveal repeated patterns in the data, but these patterns may not provide the wanted information, as they would only indicate patterns are repeating in the data, but not what these patterns are. Another possibility using matrix profile framework is to search by query. When searching by query, only a selected subsequence of the data is compared to the time series. The resulting matrix profile will show the distances of all subsequences in a time series to the query. If the location of a channel feature is known within a time series, a subsequence around this location can be chosen as a query.

CHAPTER 3

Methods

3.1 Study area

The measurements used in this thesis were collected from two different supraglacial channels, on the Kongsvegen (2021) and Austre Brøggerbreen (2020) glaciers on Svalbard (Norwegian arctic). The data from the channel on Austre Brøggerbreen was used as a reference case, whereas the data from the channel on Kongsvegen was used as a test case to see if the method is transferable between different channels and drifter platforms.

Austre Brøggerbreen

Fieldwork on Austre Broggerbreen was conducted in August 2020 between the 15.08 and 18.08. The data from this field campaign was provided to me for the purpose of this study.
Austre Brøggerbreen is an approximately 5 km long land terminating valley glacier located at 78°50N, 11°50 E on the Svalbard archipelago (Piho, Alexander et al., 2022). The elevation range of the glacier is between 80 to 600 m a.s.l., with a surface area of 9.35 km^2 (Vatne and Irvine-Fynn, 2016). The glacier was selected as a study site due to it being easily accessible by foot from the research settlement of Ny-Ålesund. The glacier has been rapidly downwasting, with an average negative net balance of -0.4 m w.e.a^{-1} since 1967, and current rates of -0.62 m w.e.a^{-1} (2000-2019) (Schuler et al., 2020). There are very few open crevasses on the glacier, but the ice is characterised by water-healed crevasses and crevasse traces (Jennings et al., 2016). The glacier is primarily cold based with most of the ice temperature below the pressure melting point (Vatne, 2001). The glacier has been retreating since 1918 causing it to have slow surface flow velocities, around 2 m a^{-1} during the 1980's (Vatne, 2001).

On the upper part of Austre Brøggerbreen a 1080 m long supraglacial channel transect was used for drifter deployments. The channel contained a number of different channel features like meanders, step-pools and knickzones. The channel was subdivided into multiple cross sections. A schematic overview of these cross sections can be viewed in figure 3.2. Cross sections were named with a prefix A and increasing numbers from the recovery point A1, up to cross section A25, with the distance from A25-A1 covering the entire 1080 m channel. In the field, the cross sections were attempted to be placed at roughly regular intervals. However, the planned spacing was too dense to be able to cover the entire channel transect of 1080m within the time constraints of the fieldwork. Therefore, the cross sections from A15 to A25 had a larger space between them than A1 to A15. Due to the malfunction of the used differential GPS the positions of the cross sections were not recorded. Cross sections were used as deployment points for drifters and as locations to measure hydraulic geometry. Multiple sets of drifters were deployed from each cross section down to the recovery point A1.

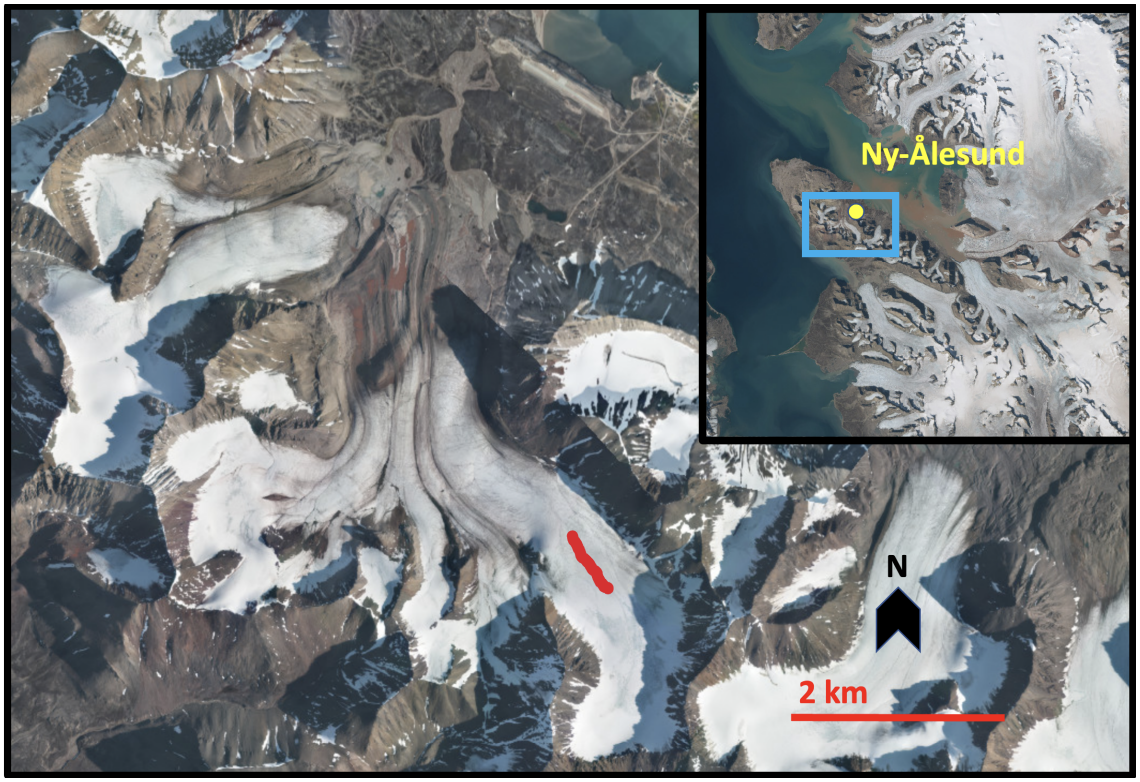

Figure 3.1: 2020 fieldwork site on Austre Brøggerbreen. The supraglacial channel that drifters were deployed into can be seen as a red line on the glacier.

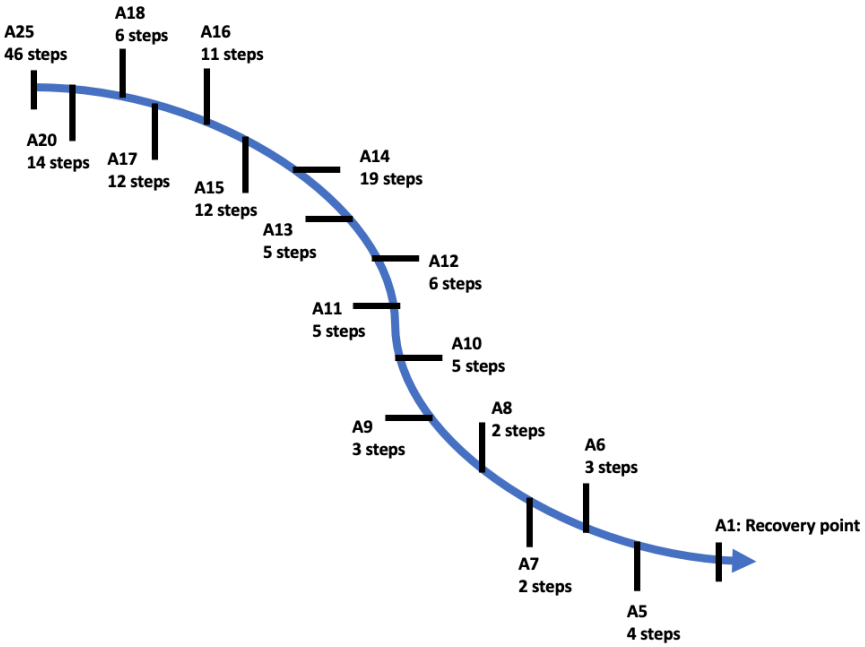

Figure 3.2: Conceptual map of the cross sections on the Austre Brøggerbreen supraglacial channel. The spacing of the cross section does not reflect the real spacing. The number of steps shown at each cross section refers to the number of steps between the current cross section and the next one downstream. The direction of flow is from left to right. I did not include deployments from cross sections A2-A4 in my analysis because they were judged too short to add much information. Cross sections A19, A21, A22, A23 and A24 were not recorded in the field due to time constraints. These cross sections are therefore not included in the figure.

Figure 3.3: A deployment from cross section A2-A1 of the supraglacial channel on Austre Brøggerbreen. The recovery point A1 can be seen where a person is standing across the channel, ready to recover drifters. In the foreground drifters are lined up on the ice, ready for deployment. In the lower left corner of the image there is a hydraulic jump in the plunge pool of a step. The hydraulic jump is followed by two steps down to the recovery point

Kongsvegen

Kongsvegen is a large polythermal glacier and is located on the west coast of the Norwegian Arctic archipelago of Svalbard, near the research settlement Ny-Ålesund [3.4]. Kongsvegen is 26 km long, with a total surface area of ∼100 km (Karner et al., 2013). The glacier terminates into Kongsfjorden with an approximately 2 km wide tidewater front. On the glacier, there are surface slopes ranging from 0.5 - 2.5° (König et al., 2002). The net mass balance of Kongsvegen is currently -0.15 m w.e.a^{-1} (Schuler et al., 2020).

Drifter deployments on Kongsvegen took place between the 13.07.2021 and the 18.07.2021. The drifters were deployed and retrieved by hand in a 652 m transect of a supraglacial channel on Kongsvegen. The channel length was estimated from measurements made from a Trimble net R9 dGPS. The dGPS was placed on a pole in the middle of the channel and carried from the deployment site to the recovery site, along the centreline of the channel, with the bottom of the pole on the channel bottom. The measurements were post-processed using RTKlib and local correction data from the Ny-Ålesund geodetic observatory. In addition to the drifter deployments, measurements of hydraulic geometry were made.

The selected channel was located approximately 0.5 km from the glacier terminus. The channel ran parallel to a medial moraine and terminated in a larger lateral channel on the western side of Kongsvegen. Along the channel there were several closed crevasses crossing the channel. Small tributary channels often flowed along closed crevasses into the main channel and the closed crevasses often coincided with channel features like hydraulic jumps. There was a significant amount of debris, medium to small sized rocks and sediments covering the ice around the channel. An aerial overview of the fieldwork site can be seen in figure 3.5.

Kongsvegen was deemed a good site to test the drifter platforms for multiple reasons. The glacier exhibits a wealth of different channel systems during the melt season. Aerial imagery confirmed the seasonal presence of channels spanning multiple kilometres, creating the possibility to deploy the drifters in long transects of the channel. Kongsvegen is a surge-type glacier and is thought to be currently building up to a new surge phase (Kohler et al., 2018). Surge-type glaciers oscillate between a quiescent phase, where ice velocities are low and the glacier geometry steepens, and a period of rapid ice movement that flattens out the glacier geometry. Surge events thought to be closely related to the subglacial hydrologic system. They are rare, short lived and poorly understood (Burgess et al., 2012). Therefore, it was an interesting site in which to conduct fieldwork, given that there was the possibility to observe surge related processes as they were happening. Finally, there was a parallel project monitoring the glacier lake outburst flood of Setevatnet, a glacier lake on Kongsvegen. This project created interesting synergies with my project, allowing us to share data and logistics.

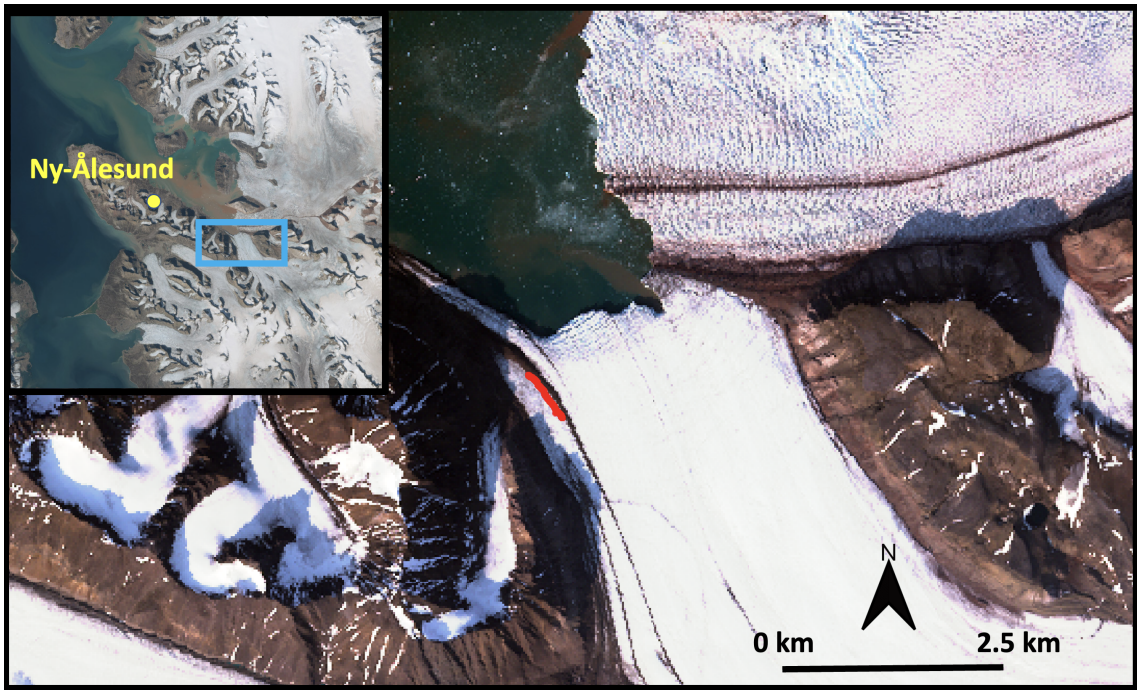

Figure 3.4: Study area on Kongsvegen. The red line on the left hand side of the glacier shows a GPS track taken along the supraglacial channel on Kongsvegen.

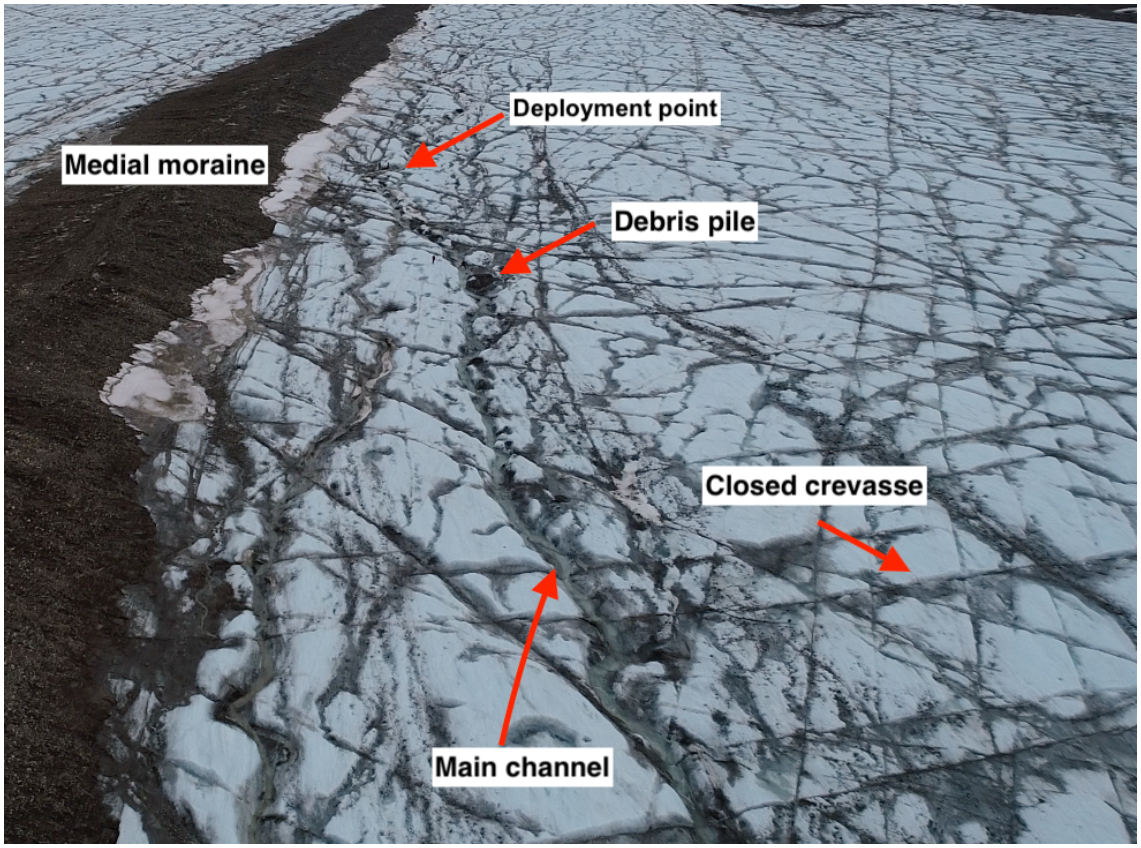

Figure 3.5: The fieldwork site on Kongsvegen captured with a drone. The channel is located roughly in the middle of the image. To the left is a medial moraine. There are numerous debris piles located along the channel, one large one is marked close to the deployment point. Closed crevasses cross the channel at several locations. The deployment point is marked towards the top of the image, while the recovery point is not in the image. For a sense of scale, a fieldworker is barely visible on the ice just beside the debris pile.

3.2 Drifters

In the field, two types of drifters were utilised, named Mammamia-series (M-series) and Barotrauma-series (B-series). The majority of deployments analysed in this thesis are from the B-series drifters. The following section contains a description of the two platforms and their sensor payloads.

B-series

The B-series drifters are tube shaped and are 12 cm long with a 4 cm outer diameter (figure 3.6). The tube has a plastic cap at each end, one hemispherical and one flat. Three pressure transducers are mounted in the hemispherical end cap. The two outer pressure sensors record at 2 bar, while the central one records at 30 bar. The 30 bar sensor was not used in this thesis because it did not have the necessary sensitivity. The two other pressure sensors are designed for a maximum pressure of 2 bar (MS5837-2BA, TE Connectivity, Switzerland) and a sensitivity of 0.02 mbar (2 mm water column). The resolution of the pressure sensor was recorded at 0.01 mbar. The accuracy of the sensors was 1 mbar (*TE connectivity sensors* 2017). The sampling frequency of the pressure sensor was 100 Hz. The devices are turned on by a magnetic switch. When activated, they log pressure for 15 s to calibrate to atmospheric pressure. After the 15 s, the local atmospheric pressure is set to 100 kPa. This removes the need for manual post processing. The pressure recorded by the pressure sensors in the channel is the sum of atmospheric, hydrostatic and hydrodynamic pressure. The devices are also mounted with an IMU (BNO055, Bosch Sensortec, Germany) including accelerometers, gyroscopes and magnetometer. The data from the accelerometers were not used in this study as it proved difficult to resolve vertical motion from the acceleration data. The accelerometers all measure the acceleration of gravity at all times. Lining up multiple drifter units with no movement showed that they were measuring the value of the gravitational acceleration differently. Manually correcting the value of the gravitational acceleration introduces a large error in the vertical acceleration (Piho, Alexander et al., 2022). The magnetometer and gyroscope are primarily sensors used to orient the accelerometer data into a fixed reference frame. As the accelerometer data was not used, the magnetometer and gyroscope were not used either. Each drifter unit had a unique identifier with a prefix B, followed by the serial number identifying the unit. See Alexander, Kruusmaa et al., 2020 for more details on the B-series drifters.

M-series

The M-series drifters are similar to the B-series devices but are larger and have some differing characteristics. They have a plastic casing which is 22 cm long and 8 cm in diameter. Some drifters had a hemispherical silicone nose to soften hard impacts. With the silicone nose, the drifters were designed for a shock impact of 100 m free fall onto rock. The sampling frequency of the pressure sensors was 50 Hz. The different sensors on the drifters are listed below (Manufacturer, product, board info):

- 2x 30 bar Pressure sensors: TE Connectivity, MS583730BA01-50, custom printed circuit board
- 3-axis IMU (accelerometer, gyroscope, magnetometer): Bosch Sensortec, BMX160, breakout board SEN0373 by DFRobot
- High-g accelerometer: ST Microelectronics, H3LIS331DL, breakout board SEN-14480 by Sparkfun Electronics
- GNSS module: U-blox, ZOE-M8Q, breakout board GPS-15193 by Sparkfun Electronics
- Radio: Radiocrafts RC1701HP-MBUS4
- Logging microcontroller: Adafruit Feather M0 Adalogger, Adafruit product 2796

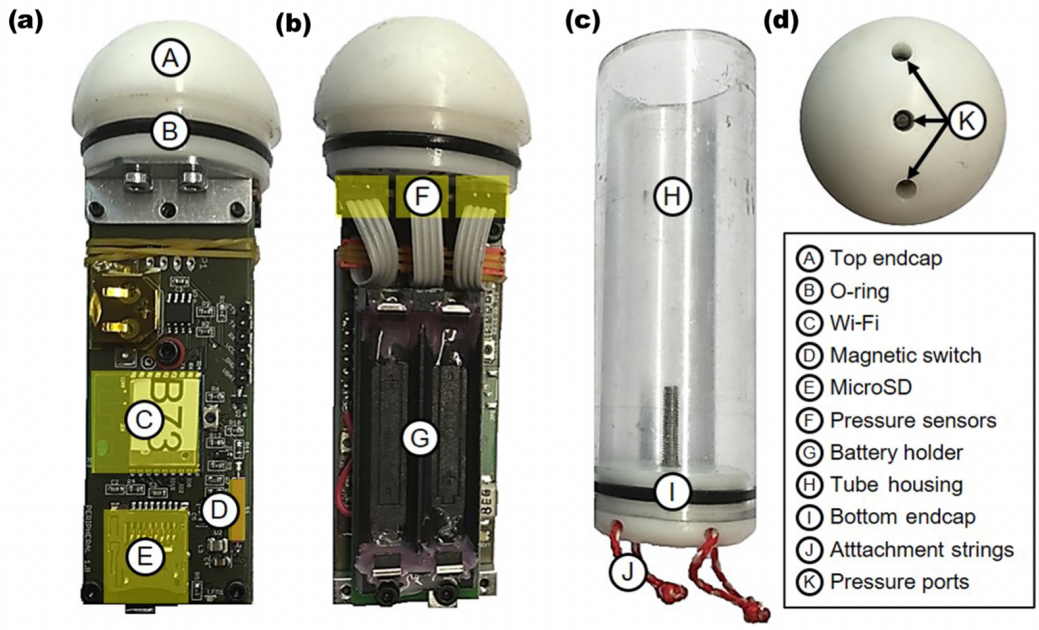

Figure 3.6: Components of the B-series drifters. Figure from Alexander, Kruusmaa et al., 2020.

- 2x batteries: Keeppower ICR18650-320PCM (3.7 V, 3200 mAh)

The pressure sensor can measure pressures up to 30 bar and has a sensitivity of 50 mbar. The M-series drifters were designed to be deployed down moulins where the expected pressure was between 5-20 bar, the 2 bar sensors used on the B-series would break at such pressures and were therefore replaced with 30 bar sensors.

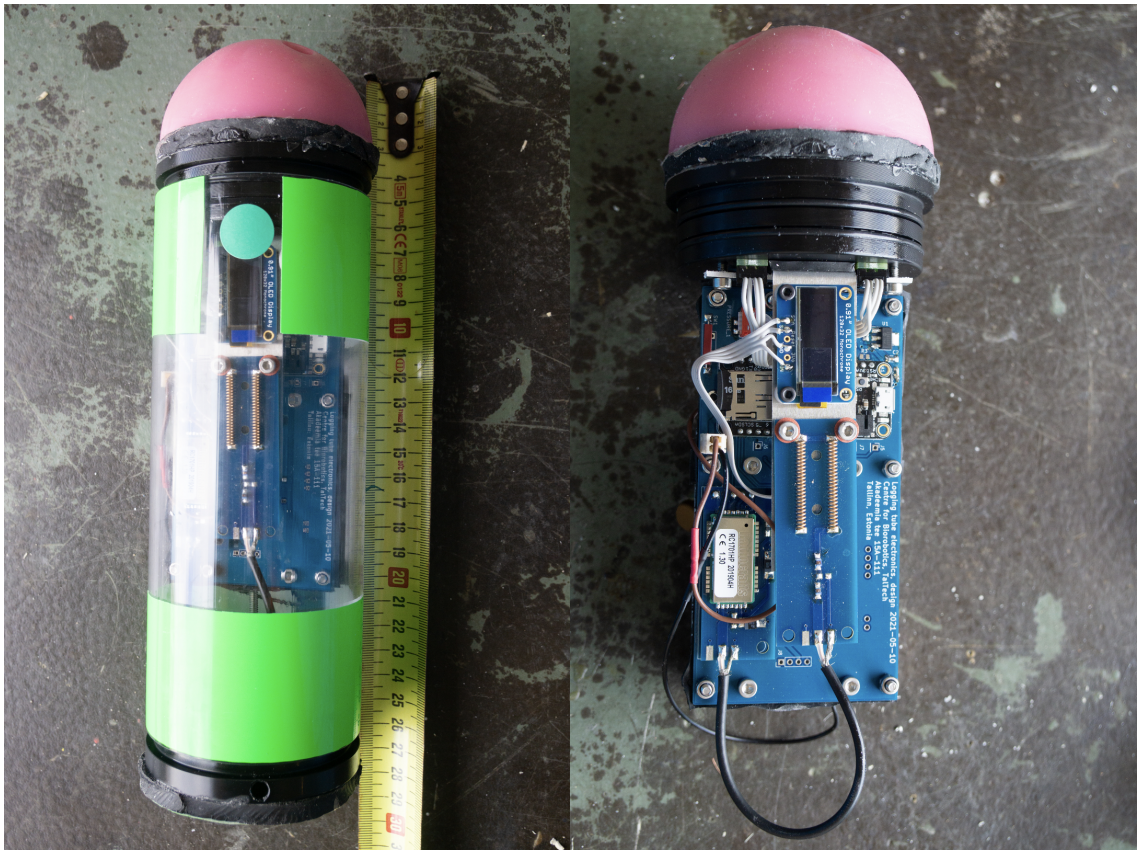

Figure 3.7: M-series drifter with a silicone nose. The left image shows the drifter with its plastic casing on. The right image shows the drifter without its casing.

3.3 Measurements

This section describes how the drifters were deployed in the field and how reference measurements were collected. The field methods were similar for the fieldwork in 2020 and 2021. See Tesaker, 2021 for a more in depth description of the field methods used in 2020.

Drifter deployments

The drifters were deployed and retrieved by hand in each channel. At the deployment point the drifters were turned on using a magnetic switch. When turned on they automatically began logging data. One team deployed up to 10 drifters at a defined start location, with a short time interval (1 min - 30 sec) between each drifter deployment. The time of each deployment was noted down in a fieldbook. The drifters flowed through the channel to the defined recovery point where they were retrieved and turned off (figure 3.8). In cases where drifters got stuck on rocks, in eddies or were washed to the channel bank, they were pushed back into the channel again. Some deployments were filmed with a handheld camera or a drone, allowing comparison of the data to the observed flow within the channel.

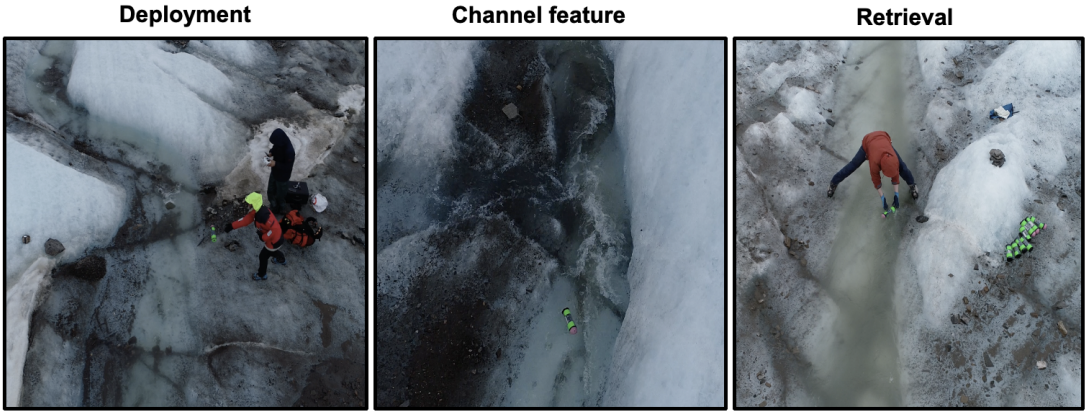

Figure 3.8: Drifter deployment (left), flow (middle) and retrieval (right) in the supraglacial channel on Kongsvegen, filmed by drone.

Video data

Certain drifter deployments were filmed by handheld camera. One deployment in the supraglacial channel on Kongsvegen in 2021 was filmed by a DJI Phantom Pro RTK UAV. Different features in the channel, like meanders, steps and hydraulic jumps, were noted down with the time of the feature in the deployment. The drifter unit used for the deployment was noted down so the data from the drifter could later be paired with the video. Each feature was given one time stamp corresponding to the judged middle of the feature. For a step this was in the slope after a knickpoint and before it plunged into a pool. For a meander this was when the drifter was in the extreme of the outer bank. However, what constitutes the middle of a given feature is a rather subjective measure and had to be judged from case to case. The time was noted in a resolution of 10 ms. Unfortunately, many of the units filmed during the 2020 fieldwork failed during their deployments. Failures included faulty sensors and loss of battery contact. In total, I used 3 videos of deployments in 2020 as references, one each, between transects A7-A1, A8-A1 and from A14-A1. Three videos were taken of drifters that failed during deployment and were therefore not used. These included transect A15-A1 (no data), A13-A1 (pressure sensor malfunction) and A8-A1 (lost battery contact mid deployment). The features detected in the videos were paired with the data by aligning the time of the deployment and recovery with the pressure data of the drifter.

Hydraulic geometries

Measurements of hydraulic geometries were made at each of the 25 cross sections in the supraglacial channel on Austre Brøggerbreen by Tesaker, 2021 on the 18.08.2020. Channel width, water depth, wetted perimeter and water velocity were measured (figure 3.2). The measurements were made twice during the day, starting at cross section A1 and ending at A25. The time of the measurements was between 12:00-13:00 and 15:45-17:20. Tables of these measurements can be found in the appendix (table A.1 and A.2).

On Kongsvegen, hydraulic geometries were measured on three separate days: 13.07, 15.07 and 18.07.2021. Water width, water depth, wetted perimeter and water velocity were measured at 9 cross sections that were roughly evenly spaced along the 652 m channel transect from the deployment point to the recovery point. Cross sections were named C1,C2,...C9, with C1 being the recovery point and C9 being the deployment point. Measurements were repeated from the same cross sections on each day. The exact time of measurement was not recorded. Water velocity was measured from the centre of the channel with a stream flowmeter. Water depth was measured with an aluminium pole from the centre of the channel. Water width was measured with a tape measure perpendicular to the flow direction. The wetted perimeter was measured with a heavy steel chain, laid across the bottom of the channel.

Reynolds (equation 2.2) and Froude (equation 2.1) numbers were calculated using the water depth and velocity at each cross section. Drifters deployed from cross sections experience the channel conditions from where the drifter was deployed, down to the recovery point. Therefore, the mean Froude and Reynolds numbers from each cross section, down to the recovery point were calculated. For example, the mean Reynolds number from the Austre Brøggerbreen cross section A4 was calculated as follows.

$$\bar{Re}_{A4} = \frac{Re_{A1} + Re_{A2} + Re_{A3} + Re_{A4}}{4} \tag{3.1}$$

3.4 Data processing

The processing of all the resulting data files collected from deployments from cross sections over multiple days is described below (flowchart of data processing, figure 3.9).

Data preparation

As the B-series drifter logs data in a binary format, it was converted to ASCII.txt files using a Matlab script. Drifter data was then loaded into a python script and data from each file was plotted to check that the data was usable. Sometimes drifters were turned on and off without being deployed resulting in a flat pressure signal. Successful deployments were easy to identify as they first showed constant reading, corresponding to drifters laying on the ice, followed by a section of pressure spikes when the drifter was in the water, followed by another section of constant readings where the drifter was lying motionless on the ice after retrieval. The drifters were purposefully left lying still for this reason.

The next step was to remove the data where the drifter was lying still on the ice before and after deployment, by visually inspecting the pressure readings. When the drifter is submerged in water the pressure readings increase, marking the beginning of the deployment. At the end of the deployment the pressure readings drop back to atmospheric pressure marking the end of the deployment. For most deployments this was a straightforward process, but sometimes the pressure sensors needed some time to equalise to the water pressure in the channel, making the transition from air to water pressure less clear. At the retrieval site the drifter was often pushed down slightly before being pulled out of the water. This created an artificial spike in the pressure readings that

could be misinterpreted as a channel feature. However, the retrieval point was the same for all deployments, and, just before the retrieval point there were three step-pools. These were often clearly visible in the data as three distinct pressure spikes, and since there were no features after these step-pools subsequent pressure peaks were considered artefacts and therefore removed.

Data was then processed through a low pass filter to remove high frequency noise. The cutoff frequency was set to 3 Hz. This limit was chosen because it preserves changes that occur over half a second, which is roughly the minimum time it takes for a drifter to pass over a step. After this, the mean of the left and right pressure sensor was taken in order to smooth out irregular readings from one of the sensors.

The M-series data were logged at 50 Hz, in order to make this work with the query search using the B-series data which was logged in 100 Hz artificial datapoint were added. This was done by doubling the number of datapoints. The artificial datapoints added were the mean of the two surrounding points.

Matrix profiles

Two methods were used to detect step-pools using matrix profile query searches. Both methods were implemented using the MatrixProfile Python 3 library (Van Benschoten et al., 2020).

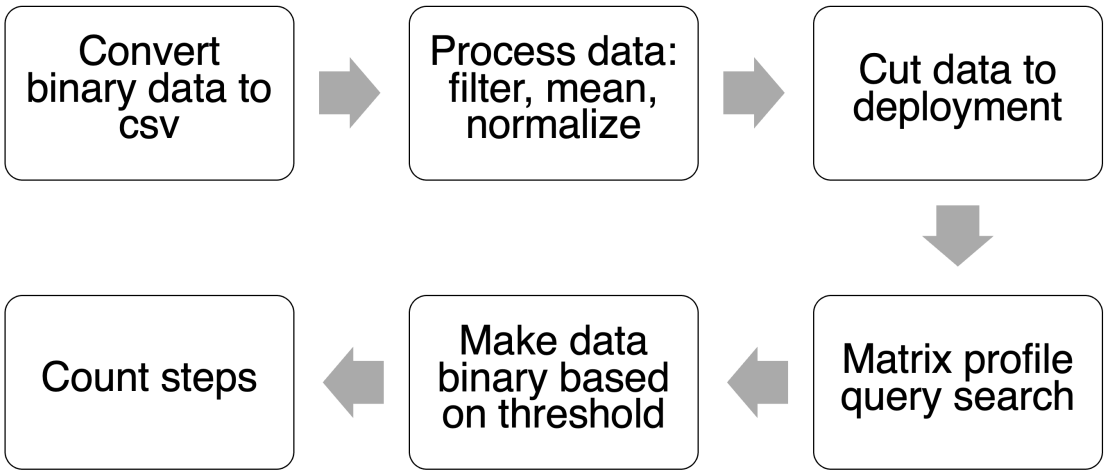

Figure 3.9: Flowchart of data processing and analysis using the matrix profile query search to detect steps in channels using drifter pressure data.

Single query search

In the single query search, an entire pressure time series is compared to one subsequence of pressure data, that is known to contain a step. This method therefore rests on the assumption that steps create a characteristic pattern in the pressure data. The normalised euclidean distance between the chosen subsequence and all possible subsequences in the queried data, of the same length as the query, are stored in a distance profile. The distance profile is then made binary by applying a threshold. All values below the threshold are considered steps and are set to 0, while all other values are set to 100. These values were chosen for visualisation purposes, but as long as they can be separated by value, the choice of what value to give them, is arbitrary. This produces a countable list of the number of steps detected in a given time series. The indexes of detected steps were also stored so that they could be referenced back to the data.

Figure 3.10 shows a simplified example of a query search using a dummy time series with three signals, two triangular and one square. The query in this case is the triangle in the top plot marked by dashed yellow lines. The dummy time series is then searched for similarities with this query. This creates a trivial match where the query is equal to itself. The next triangular signal in the dummy time series has the exact same shape as the query triangle, but double the magnitude. In the distance profile this produces the exact same distance, because the normalised euclidean distance is used. Essentially, only the shape of the data is compared, not the magnitude. The square signal shows some similarity to the query, but not as much as the perfect match with the triangles. A threshold line is added to the distance profile, and only values below this line are considered matches; in this case there are two matches. Using real data matches will likely never be perfect. For the real data the value of the threshold was determined by trial and error. Steps detected using different thresholds were compared to known steps and the threshold was iteratively tuned to include as many correctly detected steps as possible. Starting off with a low threshold and one high threshold, both were run and the number of correctly identified steps were compared. The difference between the high and low threshold was then narrowed and compared them again. This process was repeated until the optimum value was found.

Queries were tested by creating subsequences around known steps from reference videos and using these subsequences as queries. The suitability of the queries was judged by comparing the detected steps to the steps found in the video. Steps in the channel had different durations, typically taking around 0.5 - 1 s to pass through the step. If the step had a large plunge pool after it, this time could be longer. Therefore, it was not possible to determine if a detected step was a correct match to an actual step automatically. Detected steps were scrutinised visually to see if they matched the step signature as the real step. The fraction of correct matches compared to the total number of matches was used as the indicator for the suitability of the query. For each query, both the window size of the subsequence and the threshold value had to be tweaked to get optimum results. Setting the threshold too high included more detected steps, but suffered from wrong matches. Setting the threshold too low may give a higher fraction of correctly identified steps, but too few matches in total. The same is true for the window size. Increasing the window size gives fewer matches while decreasing it gives more. The window size has an upper constraint which is the length of a step, typically in the range of one to two seconds.

After the optimal query was identified, the query was applied to other datasets. Few of the datasets have a reference video to asses the accuracy of the identified steps. For these deployments the performance of the detection was evaluated using the total number of detected steps against the known total number of steps in the channel.

The query that was used in this investigation was a step between 118.6 s and 119.34 s into the deployment of drifter unit B56 from cross section A14 to A1 on the 18.08.2020. The drifters were sampling at 100 Hz so this gave a window length of 74 datapoints. The threshold that was used for this query was 5. The threshold has no unit because of the normalisation. This particular step was selected because it gave the best ratio of correctly identified steps to total steps of all the queries that were tested. The same query was tested on the 2021 datasets, both on the B- and M-series drifters.

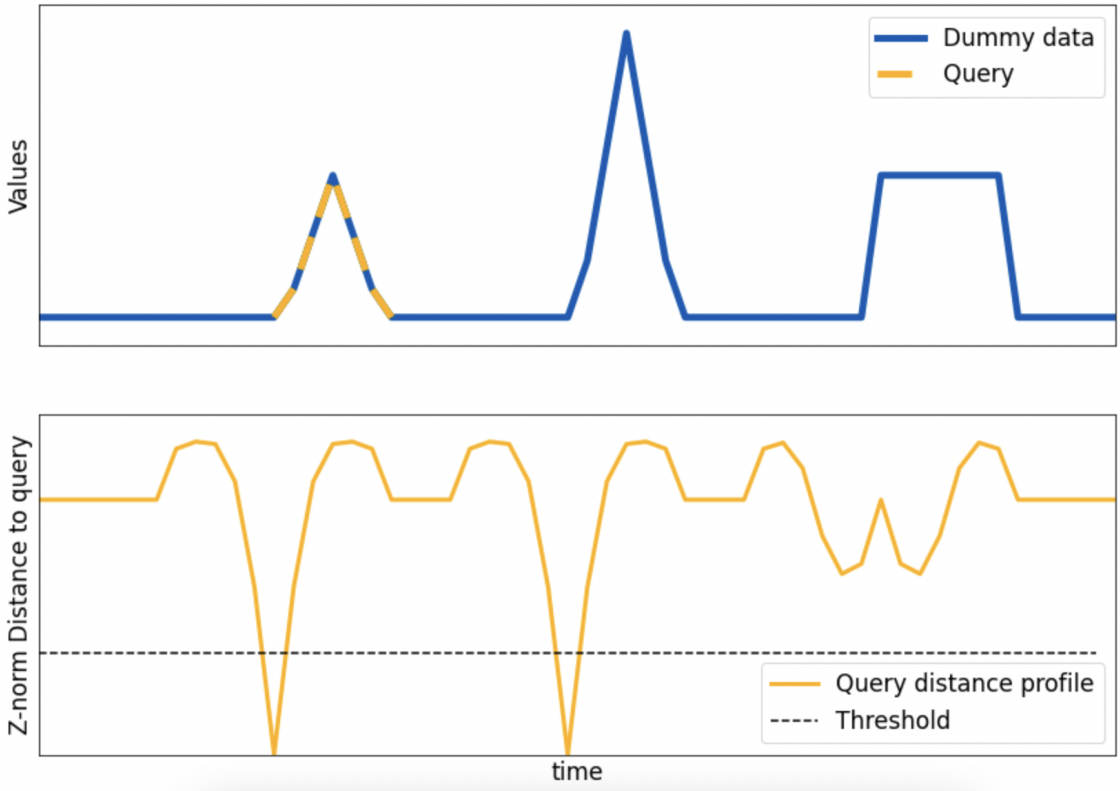

Figure 3.10: A simplified example of a single query search. The top plot shows a time series with three distinct signals, two triangular and one square. The triangular shapes have a different magnitude but have identical proportions. A query is made from the first triangle (dashed yellow lines). The bottom plot shows the distance profile of the query to all possible subsequences of the time series. There are two identical structures beneath the two triangular signals, that both have the same minimum value because the two shapes are identical to the query when normalised. The square signal shows some degree of similarity to the query. On all the signals, the distance first increases as the query subsequence begins sliding over a signal in the data. This is because the query and the signal are out of phase. In real drifter data, values below the dashed black threshold line were counted as steps.

Iterative query search

The iterative query search is similar to the single query search except that multiple queries are considered. In this method, one subsequence of the pressure data was created for each step from all the steps identified by video. A query of a time series was then run on each of the subsequences iteratively. The resulting distance profile from each iteration was aggregated to one distance profile, which was then divided by the number of iterations to scale the distance profile to the number of queries. The result of this was that subsequences of the data that had an overall good agreement with many of the queries had a low value in the distance profile and vice versa. This made this method a majority consensus approach. The approach to optimise the parameters of this method differed from the single query search. Instead of finding the optimal fraction of correctly identified steps to total detected steps, the method was run on multiple cross sections of different lengths with the goal of most accurately detecting the total number of steps from each cross section.

For the iterative query search method, a dummy time series was created with two distinct signals, one triangular and one square signal, (figure 3.11) as a simple example of this approach. Two subsequences were extracted to be used as queries, one of the triangular signal and one of the square. The queries were then run on the dummy time series, producing two different distance profiles. One showed a perfect match to the triangular signal and one to the square signal. These two distance profiles were then aggregated to produce the mean distance profile, seen in the bottom of figure 3.11. Note that in the two single distance profiles only one signal match produces a distance that goes below the set threshold, but in the aggregated distance profile both signals drop below the threshold. This is useful if there are signals in the data that are caused by the same phenomenon, but produce differently shaped signals. In the drifter pressure data, the shape of the pressure signal will never be identical when moving over a step, because there are many factors that govern what the pressure signal may look like. For instance, the orientation of the drifter in the flow, the pressure sensor's depth in the water column, turbulence or differing shapes of steps. By using the iterative query, a variety of signal patterns, that correspond to a known step in the channel, can be classified as a step by the algorithm. The subset of queries was created from 54 identified steps in the deployment of drifter unit B56 between A14 and A1 on the 18.08.2020. Using the known timestamp of the steps in the time series, a subsequence was extracted by creating a time window of 0.9 s, ± 0.45 s around the step location in the time series. A threshold of 12.28 and a query window length of 0.9 s was used on the drifter pressure data.

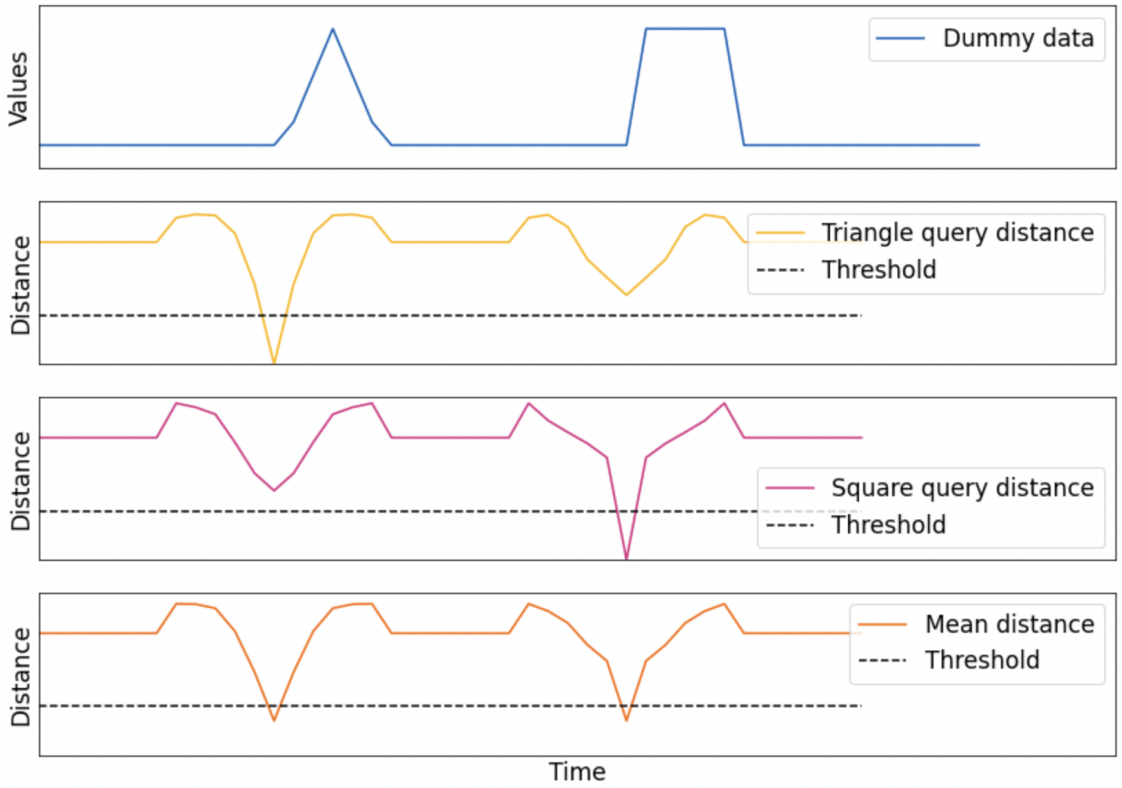

Figure 3.11: A simplified example of the iterative query search method. The top plot shows dummy data with a triangular and a square signal. The second plot shows a distance profile from a triangular query. The third plot shows a distance profile for a square query and the last plot shows the mean of the two distance profiles. Values under the dashed threshold line would be classified as a step using this method.

Velocity correction

Daily variations in water velocity within the supraglacial channels led to large differences in the deployment time of drifter deployed between different days. Longer drifter datasets consistently produced more detected steps than shorter datasets in the same channel transect. This necessitated a correction factor for the velocity of the drifter. Equation 3.2 was used to correct data for velocity. This equation is purely empirical and was created based on the data. n_{corr} is the corrected step count, $n_{detected}$ is the original step count, v_d is the velocity difference between the deployed drifter and a reference measurement and C is the correction constant. The factor v_d is quadratic so the correction term grows larger for velocities far away from the reference velocity.

$$n_{corr} = n_{detected} + v_d * |v_d| \cdot C. \tag{3.2}$$

The value of the reference velocity v_0 was 2.6 m/s and was derived from the mean deployment time of drifters traversing the full channel length from A25-A1 and the estimated channel length between the two cross sections. The path length of the channel from A25 to A1 was estimated by Piho and Kruusmaa, 2021 to be 1080 m.

Minimum sample size

To evaluate the feasibility of the step detection method with drifter data, an assessment of the minimum sample size needed to achieve a given precision was made. This assessment was made using the following equation from Hou et al., 2018

$$n = \frac{Z^2_{1-\frac{\alpha}{2}}}{\varepsilon^2} \cdot \left(\frac{\sigma}{\mu}\right)^2, \tag{3.3}$$

where $Z^2_{1-\frac{\alpha}{2}}$ is the standard normal deviate (e.g., $Z_{0.975} = 1.96$ for the 95 % confidence interval), μ is the population mean. ε is the defined precision, set to $\varepsilon = 0.1$. σ is the standard deviation of the population.

Random index test

A test was performed to see if the single query search method performed better than randomly generated indexes along the time series. The test was performed by creating a list of randomly generated numbers with values between 0 and the length of a pressure time series of drifter unit B56, deployed from cross section A14 on the 18.08.2020. The number of randomly generated indexes was the same as the number of steps detected by the single query search on the same time series. Each index then corresponded to a specific time in the time series. Each index represented a "detected" step in the time series and was then evaluated using the same criteria as with the single query search. If a point was judged to be within the pressure signature of a real step feature it was counted as a hit. Since the number of features in the channel was quite dense, it was expected that even randomly distributed false hits would match step features in some cases. The test was repeated 10 times with different sets of indexes generated from pythons random module (*Generate pseudo-random numbers* 2022). Each set of indexes was generated using a unique seed to initialise the random number generator, to ensure that the tests are repeatable. The output of each seed was not known beforehand.

CHAPTER 4

Results

In this chapter, I will present the results of my step detection algorithms. The results from the fieldwork done in 2020 on Austre Brøggerbreen will be presented first, followed by the results from the 2021 fieldwork on Kongsvegen.

4.1 Supraglacial channel, Austre Brøggerbreen 2020

In this section, step detection results of deployments from the different cross sections to the recovery point on the 18.08.2020 will be presented first, followed by step detection applied to the entire channel (A25-A1) on the 15.08, 16.08, 17.08 and 18.08.

Single query search

Figure 4.1 and table 4.1 show the detected steps of drifter unit B56 from A14-A1 on the 18.08.2020. This deployment was filmed, so it was possible to reference the detected steps to the actual steps in the channel. There were 54 steps observed in the video. 45 steps were detected using the single query search in this deployment, of which 33 steps were counted as hits (61% of the true number) and 12 were counted as false positive matches. One of the matches was a trivial match where the query was identical to itself. The detected steps were counted as a hit if they were within a step-like signal that also had a step found in the video - a step signal being a rise and peak-trough-peak sequence (see figure 4.2 for an example of such a sequence). These signals did not always have a very similar shape in the pressure data so a degree of subjectivity was inherent in the count.

The query used to detect steps in figure 4.1 can be seen in figure 4.2. The query spans the time period from the drifter moving over the entire step-pool. A image of the actual step feature that corresponds to the query can be seen in figure 4.3.

Table 4.1: The number of steps identified from cross section A14, A8 and A7 down to A1, compared to the number of steps identified by video. The column **Deployment cross section** refers to the cross section that the drifter was deployed from. All deployments flowed from the the deployment cross section, down to the same recovery point A1. The column **Total matches** shows the total number of steps detected in each deployment. The detected steps were classified as a positive match where the detected step matches a real step and as false positive where a detected step does not match a real step. The column **True number of steps** shows the real number of steps in the channel between each cross section down to A1.

Deployment cross section	True number of steps	Total matches	Positive	False positive
A14	55	45	33	12
A8	11	12	10	2
A7	9	11	7	4

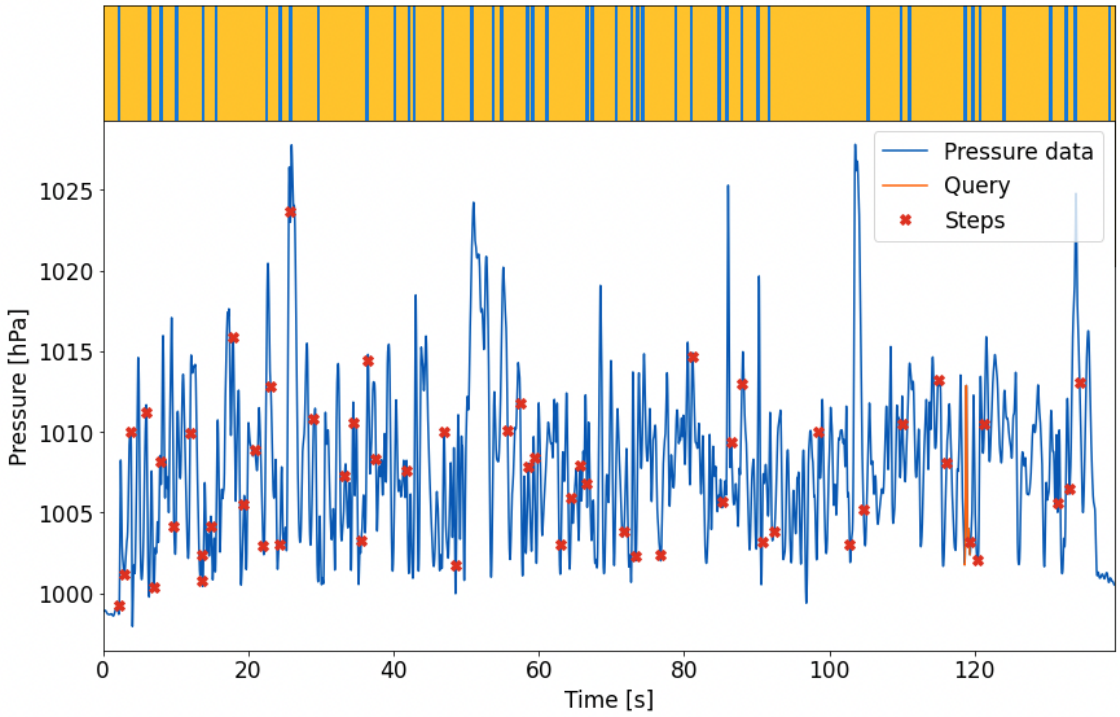

Figure 4.1: Deployment of drifter unit B56 from cross section A14-A1 on Austre Brøggerbreen 18.08.2020. The upper plot shows the binary distance profile (yellow bar with dashed blue lines), using the single query search. Of this deployment, blue lines are detected steps. The blue line in the lower plot shows mean pressure of the left and right pressure sensor. Steps identified in a video are marked by red crosses. A subsequence of the pressure data is highlighted in orange, this is the subsequence that was used as a query. A bigger version of this subsequence can be seen in figure 4.2.

Figure 4.4 shows the number of steps detected in each deployment from the different cross sections down to the recovery point. For shorter channel segments deployed from A5-A12, the number of detected steps was closely grouped around the real number of steps in the channel. For longer channel segments deployed from A13-A25, the spread of the detected steps increases and the number of detected steps begin falling below the real number.

The results in table 4.2 were produced using a total 117 deployments of drifters from the different channel cross sections. The difference between the number of steps detected and the true number of steps from the deployment cross section was calculated for each individual deployment. Adding up the difference for each deployment gave a total of 787 steps. Dividing this by the number of deployments gave an error per deployment of 6.7 steps. Doing the same calculation, but using the mean number of detected steps for sets of deployments from each cross section gave an average error of 6.4. The difference between the true number of steps and the mean detected steps varied between a minimum of 0.3 (deployments from cross section A11) and a maximum of 15.2 (deployments from cross section A18).

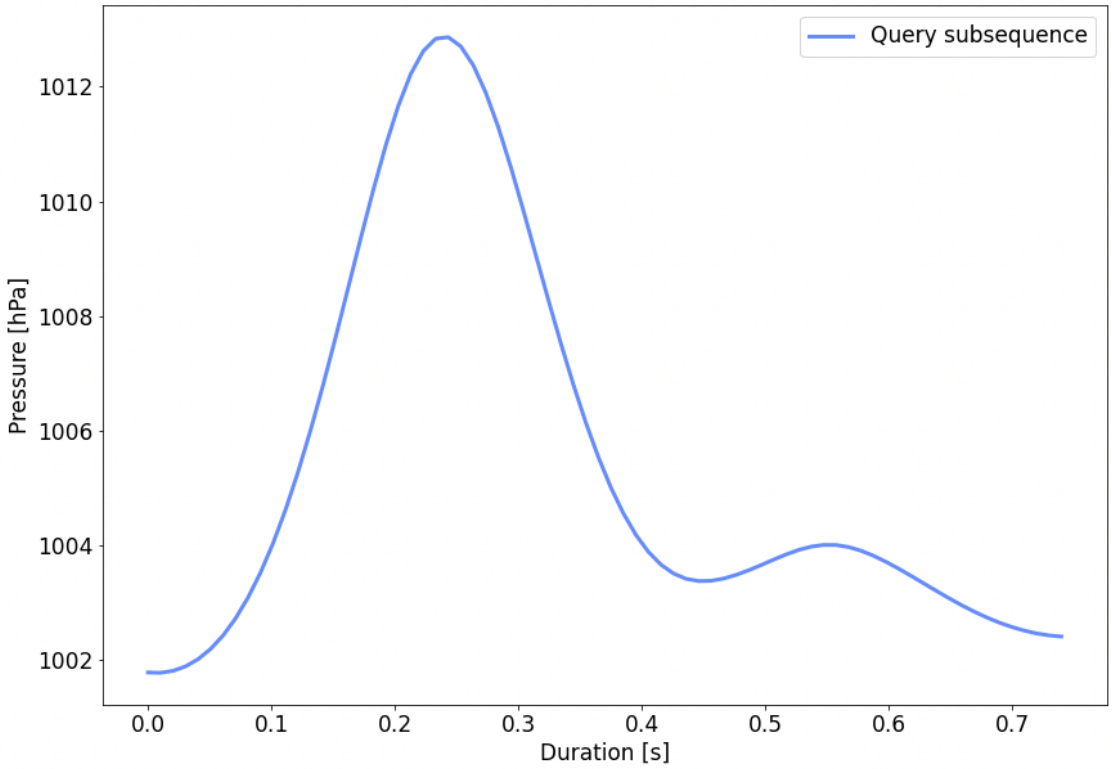

Figure 4.2: A subsequence of pressure data taken as drifter B56 passed over a step between cross section A6-A5, on the 18.08.2020. This subsequence was used as a query to find the detected steps in figure 4.1. The sequence was taken from 120.65 s to 121.39 s into the deployment.

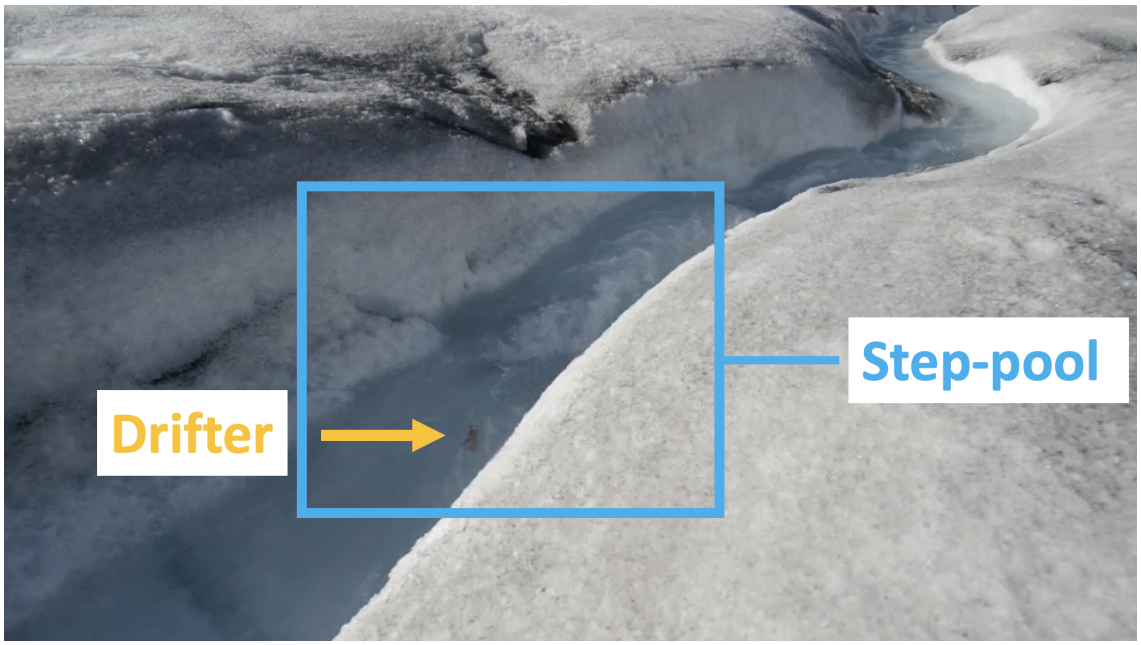

Figure 4.3: The step feature that produced the signal that was used as the query (figure 4.2). The drifter can be seen in the image as a dark dot in the channel. The step feature is inside the blue box.

Table 4.2: Mean and median detected steps from different channel cross sections to the recovery point A1 using the single query search. The mean and median are calculated from all the deployments made from a given cross section on the 18.08.2020. The number of deployments from each cross section is shown in the column **Number of deployments** and the true number of steps between each cross section and A1 is shown in the column **True number of steps**. The absolute difference between the true number of steps and the mean detected steps is shown in the column **Difference**. The query shown in figure 4.2 is used for all deployments. Deployments are made from the deployment point **Deployment cross section** to the same recovery point A1. The column σ shows the standard deviation of the number of detected steps of all deployments made from a cross section.

Deployment cross section	**Mean steps detected**	**Median steps detected**	**True number of steps**	**Difference |true-mean|**	**Number of deployments**	σ
A5	3.0	3	4	1	9	0.83
A6	5.1	5.5	7	1.9	8	2.32
A7	8.6	8	9	0.4	9	1.89
A8	10.6	10.5	11	0.4	10	2.87
A9	14.6	13.5	14	0.6	10	4.0
A10	22.6	23	19	3.6	9	3.69
A11	23.7	24.5	24	0.3	6	3.35
A12	26.1	25	30	3.9	9	2.13
A13	35.6	33	35	0.6	7	5.72
A14	43.5	43	54	10.5	7	1.5
A15	52.5	51.5	66	13.5	6	3.2
A16	65.3	62.5	77	11.7	6	9.76
A17	71	70	89	18	3	2.16
A18	79.8	75	95	15.2	8	15.8
A20	101.8	101.5	109	7.2	6	9.58
A25	141.0	141	155	14	4	5.7

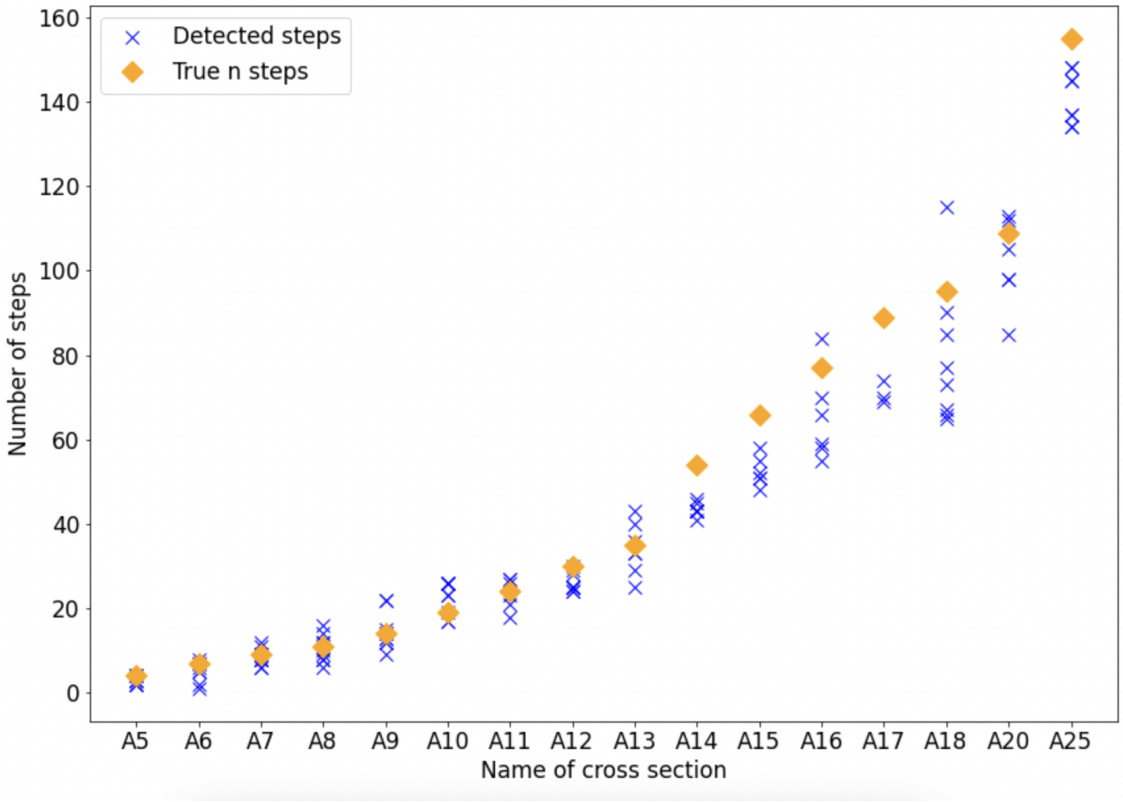

Figure 4.4: Number of detected steps in deployments from each channel cross section on the 18.08.2020 using the single query search. Blue crosses show the number of detected steps for each deployment. Orange diamonds show the true number of steps counted from videos in the channel. Note that a detected step is not necessarily a real step in the channel but could also include a number of false positive detections. These false positives cannot be distinguished since there is no video reference data for these deployments.

Random index test

Ten sets of 45 random indexes were generated as pseudo detected steps on the pressure data of deployment A14-A1 B56 on the 18.08.2020 (see figure 4.5) for an example. Every set was analysed to assess how many of the randomly placed indexes corresponded to a real step in the channel, which can be seen in table 4.3. Each index that corresponded to a real step was classified as a **Positive match**. The real number of steps in this channel segment was 54. The average number of positive matches for all 10 tests was 20.5 (38% of the real steps). The best number of positive matches was 24 (44% of the real steps). The number of correct matches using the single query search was 33 (61% of the real steps).

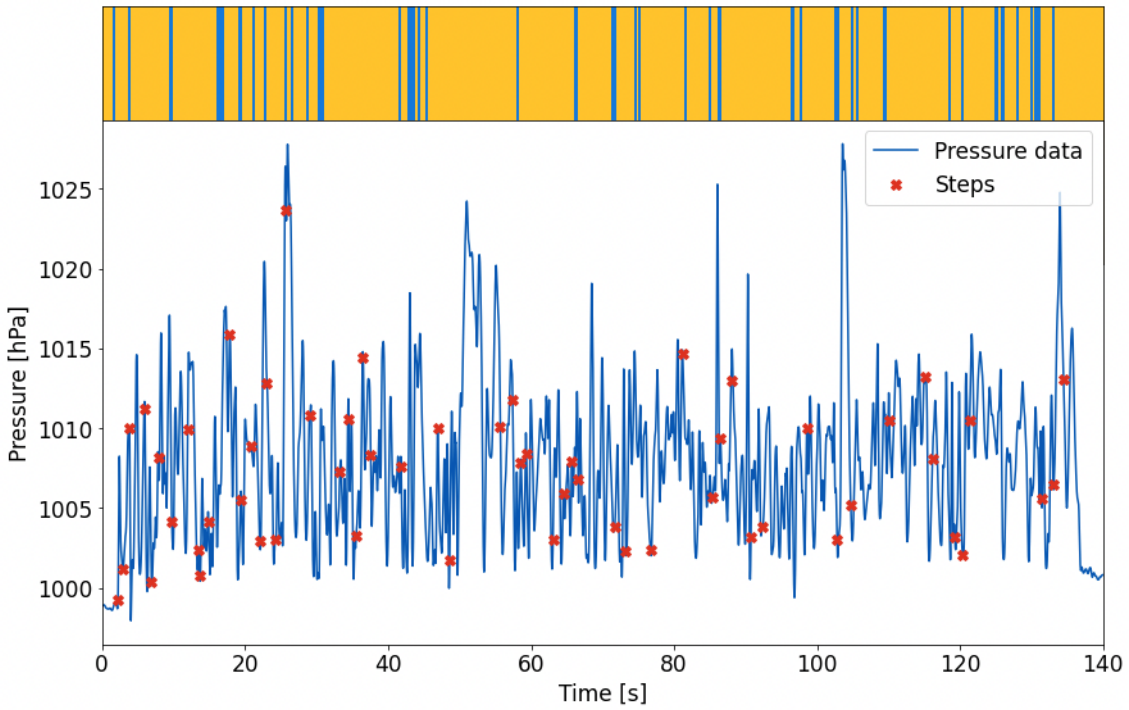

Figure 4.5: Random index test on deployment A14-A1 B56 on the 18.08.2020 with randomly placed steps. The blue stripes on the yellow bar in the top plot represent the position of the randomly placed steps. The steps identified by video are represented by red crosses.

Table 4.3: The number of positive matches found using 10 different sets of random indexes on a dataset from the channel segment A14-A1 with drifter unit B56 on the 18.08.2020. A positive match is defined by a random index being within a real step feature found by video. The seed is the seed used to initialise the random indexes using python random.

Drifter ID	**Positive match**	**% of real steps**	**Seed**
B56	23	41	10
B56	21	39	35
B56	23	41	63
B56	19	35	1034
B56	18	33	10084
B56	17	32	20459
B56	20	37	55459
B56	17	31	25759
B56	23	41	207759
B56	24	44	2090459
Mean	20.5		

Iterative query search

Figure 4.6 shows the detected steps in a deployment from A14 to A1 that was filmed. It is the same deployment that was shown for the single query (figure 4.1). Using this method, 55 steps were detected, of which 38 were positive matches (70% of the true number) and 17 were false positive matches, compared to 33 positive matches (61% of the true number) and 12 false positive matches using the single query. The true number of steps in this channel segment was 54. The method was

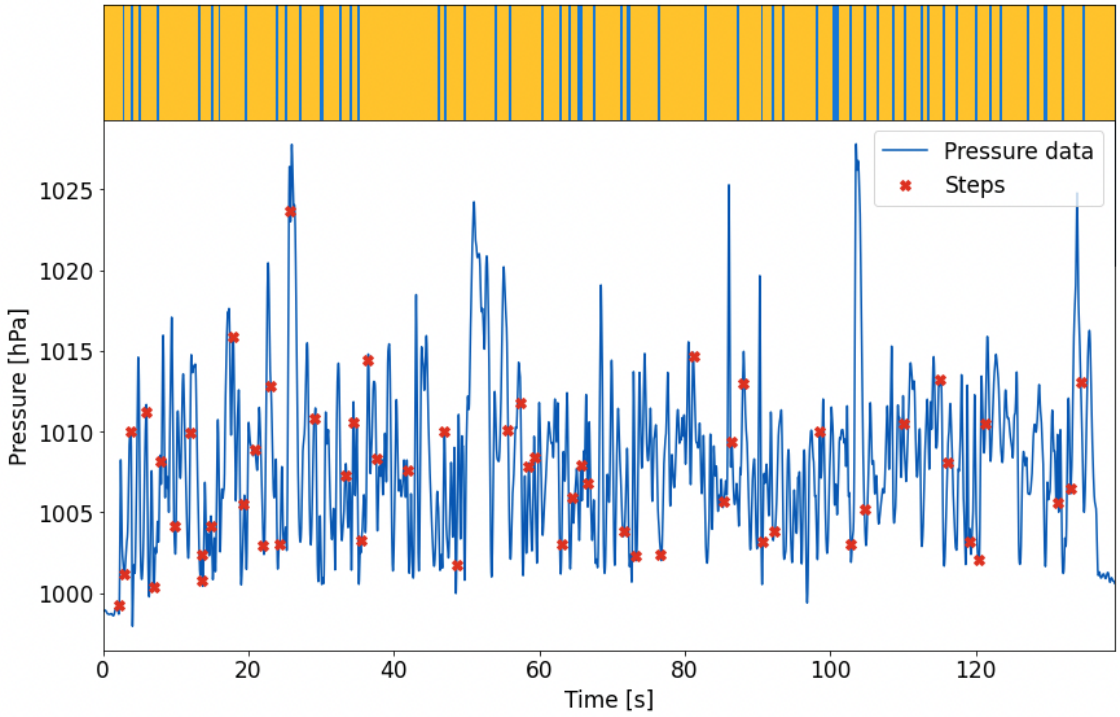

Figure 4.6: Deployment of drifter unit B56 from cross section A14-A1 on Austre Brøggerbreen 18.08.2020. The upper plot shows the binary distance profile of this deployment using the iterative query search (yellow bar with dashed blue lines), blue lines are detected steps. The blue line in the lower plot shows mean pressure of the left and right pressure sensor. Steps identified in a video are marked by red crosses.

also tested on a filmed deployment starting from A8. Figure 4.7 shows the detected steps in the deployment from A8 to A1. 13 steps were detected, of which 9 were positive matches (81% of the true number of steps) and 4 were false positive matches. The true number of steps in this section was 11.

Figure 4.8 shows that for shorter channel sections starting between A5-A11, the number of detected steps is closely grouped around the real number of steps in the channel, but the number of steps is slightly over estimated in most deployments. At longer channel transects, starting between A14-A20, the number of detected steps begin falling below the real number. However, at the longest channel section A25 the number of counted steps is very close to the real value.

The results in table 4.5 were produced using a total of 117 deployments of drifters from the different channel cross sections. The difference between the number of detected steps and the true number of steps from the deployment cross section was calculated for each individual deployment. Adding up the difference for each of the 117 deployments gave a total of 669 steps. Dividing this by the number of deployments gave an error per deployment of 5.7 steps, using the single query search this number was 6.7. Doing the same calculation, but using the mean number

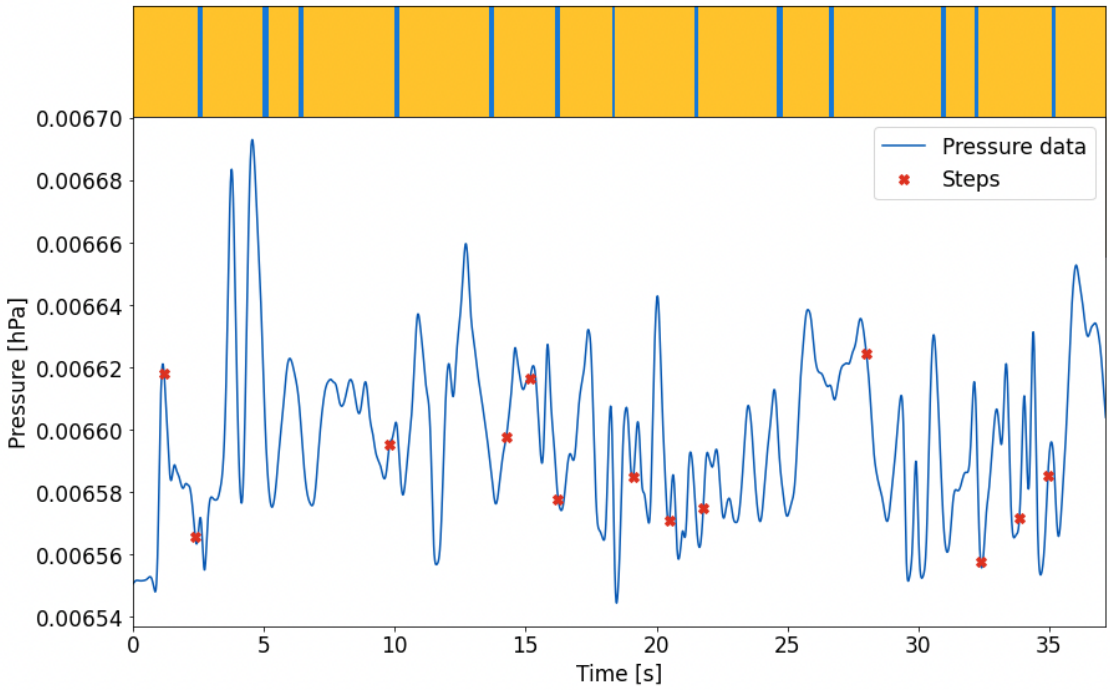

Figure 4.7: Single deployment of drifter unit B13 from cross section A8-A1 on Austre Brøggerbreen 18.08.2020. The blue line in the lower plot shows pressure readings from the drifter in the channel. Steps identified by video are marked by red crosses. The yellow bar at the top shows the binary distance profile made using the iterative query method. Blue lines are detected steps.

Table 4.4: Steps identified using the iterative query search from cross section A14, A8 and A7 compared steps identified by video. The column **Total matches** shows the total number of steps detected in each deployment. The detected steps were classified as a positive match where the detected step matches a real step. False positive where a detected step does not match a real step. The column **True number of steps** shows the real number of steps from each cross section down to A1.

Deployment cross section	True number of steps	Total matches	Positive	False positive
A14	55	55	38	17
A8	11	13	9	4
A7	9	9	4	5

of detected steps for sets of deployments from each cross section, gave an average error of 4.4; using the single query this was 6.4. The difference between the true number of steps and the mean detected steps varied between a minimum of 0.2 (deployments from cross section A18) and a maximum of 15.7 (deployments from cross section A16).

Table 4.5: Mean and median detected steps in deployments from different channel cross sections using the iterative query search. The mean and median are calculated from all the deployments made from a given cross section on the 18.08.2020. The number of deployments from each cross section is shown in the **Number of deployments** and the true number of steps between each cross section and A1 is shown in the column **True number of steps**. The absolute difference between the true number of steps and the mean detected steps is shown in the column **Difference**. Deployments were made from the deployment point **Deployment cross section** to the same recovery point A1. The standard deviation of the number of steps detected from each cross section are shown in the column σ

Deployment cross section	**Mean steps detected**	**Median steps detected**	**True number of steps**	**Difference |true-mean|**	**Number of deployments**	σ
A5	5.3	6	4	1.3	9	1.63
A6	8.4	8	7	1.4	8	1.11
A7	10.0	10	9	1	9	1.83
A8	16.0	16.5	11	4	10	3.71
A9	19.8	19	14	5.8	10	1.66
A10	26.6	26	19	7.6	9	3.77
A11	26.7	27	24	2.7	6	2.13
A12	32.9	35	30	2.9	9	5.0
A13	38.7	40	35	3.7	7	3.15
A14	50.3	54	54	3.7	7	6.47
A15	58.8	59	66	7.2	6	6.2
A16	61.3	62	77	15.7	6	3.99
A17	78.7	80	89	10.3	3	6.6
A18	94.8	95.5	95	0.2	8	11.31
A20	109.7	108.5	109	0.7	6	10.73
A25	156.75	153	155	1.75	4	7.73

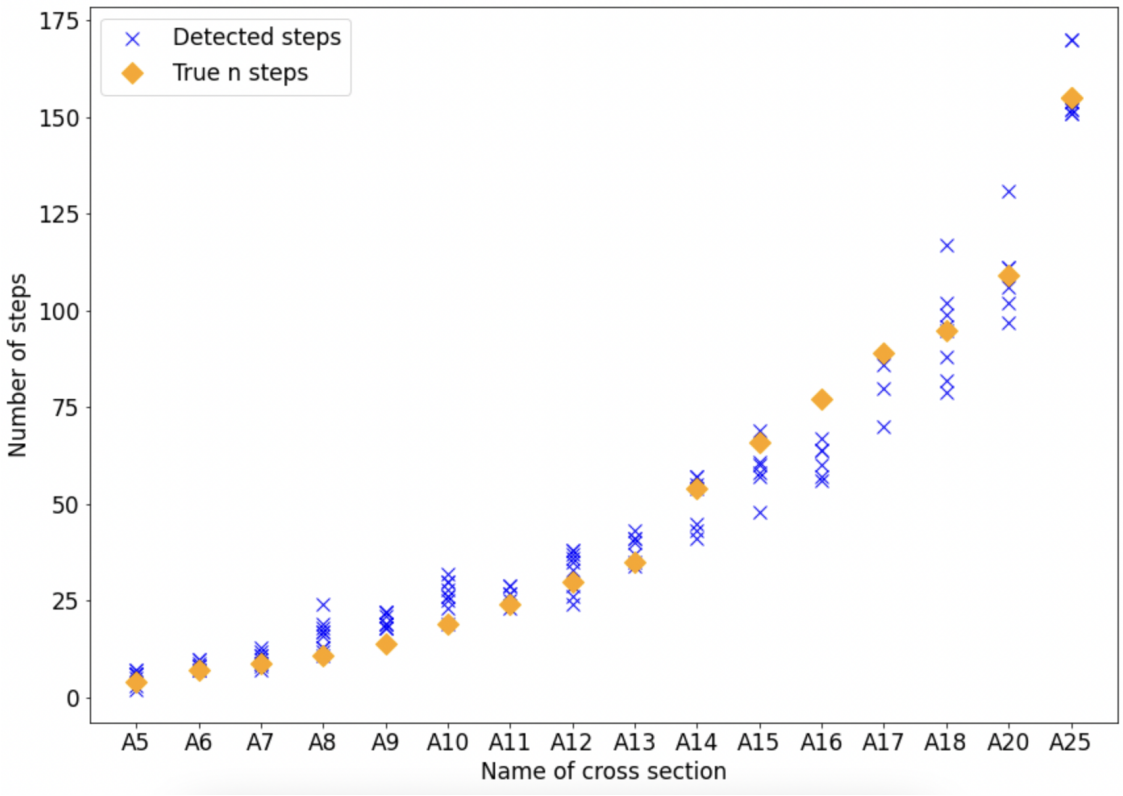

Figure 4.8: Number of detected steps in deployments from each channel cross section on the 18.08.2020 using the iterative query search. Each blue cross shows the number of steps detected in a single deployment from a given cross section down to A1. Yellow diamonds show the number of steps counted in a video from each cross section down to A1. The mean values of deployments from each cross section can be seen in table 4.5.

Deployments on other days, Austre Brøggerbreen

So far, the results have focused on the deployments from a single day on the 18.08.2020. During the same fieldwork season, drifters were also deployed on the 15.08, 16.08 and 17.08.2020. During these days the drifters were only deployed from A25 to A1.

Drifters deployed between A25 and A1 on the 15.08 and 16.08 and 17.08.2020 showed higher step counts than drifters deployed on the 18.08.2020 (figure 4.9). The number of detected steps in the channel generally increased with deployment time.

In order to remove the trend of increasing step counts with increasing time a velocity

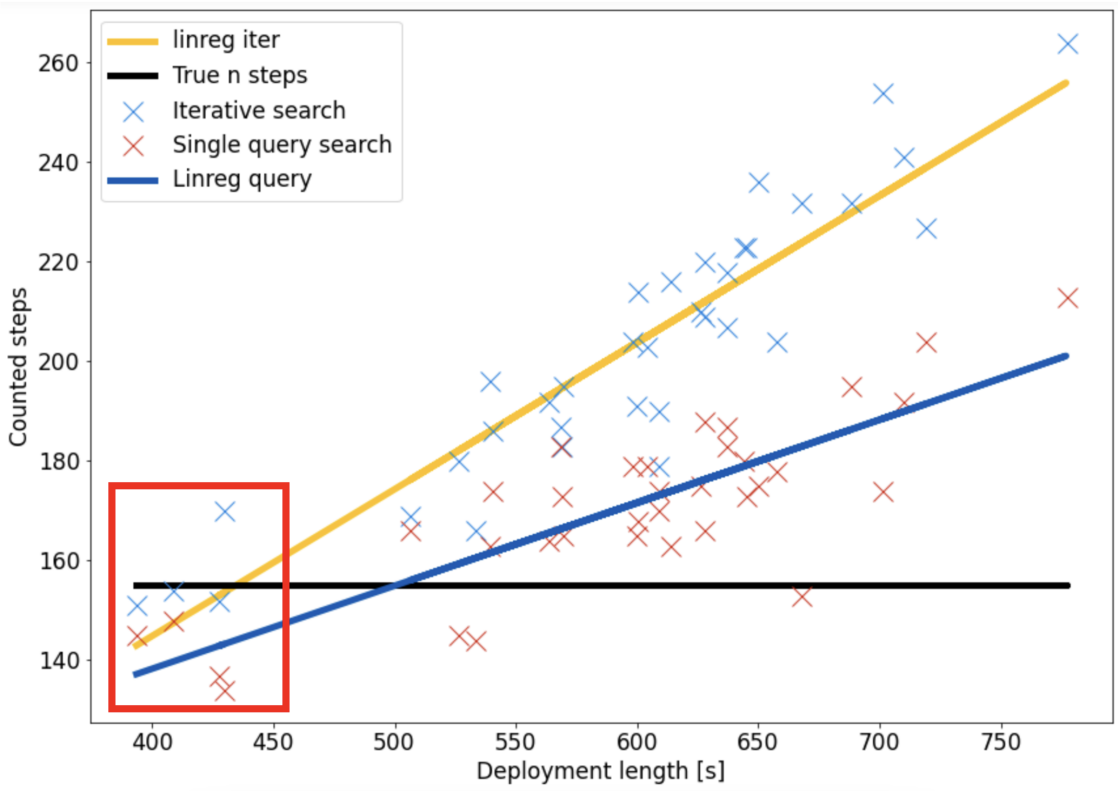

Figure 4.9: Step count of deployments from A25. Results include deployments from 4 separate days (15.08.2020,16.08.2020,17.08.2020, 18.08.2020). Two methods were used to estimate the number of hits. Single query search (red crosses) and iterative query search (blue crosses). The points inside the red square are from the 18.08.2020, the day the data was tuned for. Linear regressions (linreg) calculated from the results of the two methods (yellow line: iterative query, blue line: single query).

correction was applied to all deployments made on the 15.08, 16.08, and 17.08.2020. The correction was made using equation 3.2. The original step count and the corrected step count for the single query method can be seen in figure 4.10. The original step count and the corrected step count for the iterative query method can be seen in figure 4.11. The mean values found for each day can be seen in table 4.6. The largest error using the corrected step count was on the 15.08 for both methods, the iterative query method produced a difference of 5.5 steps to the true number of steps (155, an error of 4%), while the single query method had an difference of 8.8 steps (an error of 6%). The best result of the iterative query method was on the 17.08 where it produced the exact same number of steps as the true steps (155). The result closest to the real number of steps, using the single query method, was on the 16.08 with a difference of 4.7 steps (3%). The average percentage

error from deployments from A25 for all the field days was 2% for the iterative query and 6% for the single query.

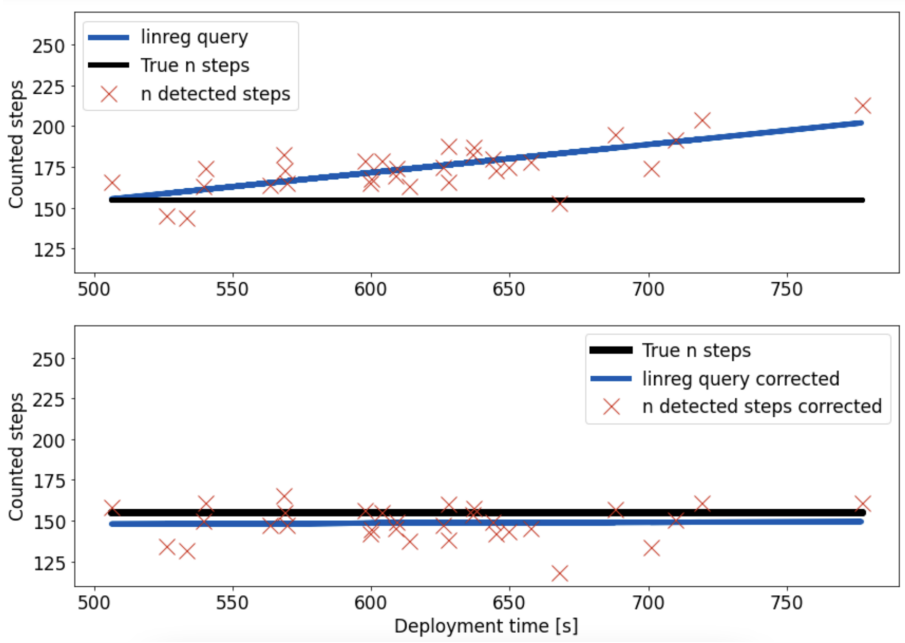

Figure 4.10: Number of detected steps using the single query method in deployments from A25 on the 15.08, 16.08 and 17.08. The top plot shows uncorrected results. The bottom plot shows results corrected using equation 3.2. Linear regression lines (blue) are fitted to the data, named **linreg query** in the legend. The black horizontal line shows the real number of steps in the channel segment (155)

Table 4.6: Mean step count of all drifter deployments during three days. The column **Step count i** shows the results from the iterative method. The column **Step count q** shows results from the single query search. The results have been corrected for velocity using equation 3.2. Deployments from the 18.08.2021 are not included since they have the baseline velocity from which the velocity correction was made.

Date	Step count i	Step count q
15.08.2020	149.5	146.2
16.08.2020	157.1	150.3
17.08.2020	155	148.9

A stationary pressure logger was installed in the bottom of the channel at cross section A25, measuring the absolute water pressure in the channel from about 18:00 16.08 to 18:00 18.08 (figure 4.12). The measured pressure increased over time from a minimum of around 967 hPa to a maximum of 985 hPa. There is one full day of pressure measurements on the 17.08, during which there is a diurnal variation in the pressure with a peak at 16:00. The drifters were deployed between 18:08 and 21:05 on the 15.08, 20:40 to 21:34 on the 16.08, 17:55 and 19:57 on the 17.08 and 12:53 and 13:08 on the 18.08. All deployments were made from A25-A1. For each successive day, the water pressure was greater than the previous at the deployment time. The number and spread of steps detected on each day decreased with increasing pressure. The pressure readings may be a proxy for increased discharge, since it indicates that the water column above the pressure sensor is deepening. The average velocity of deployments from A25-A1 was 1.6m/s, 1.8m/s and 2.6m/s on the 16.08, 17.08 and 18.08 respectively, so the water velocity increased with increasing

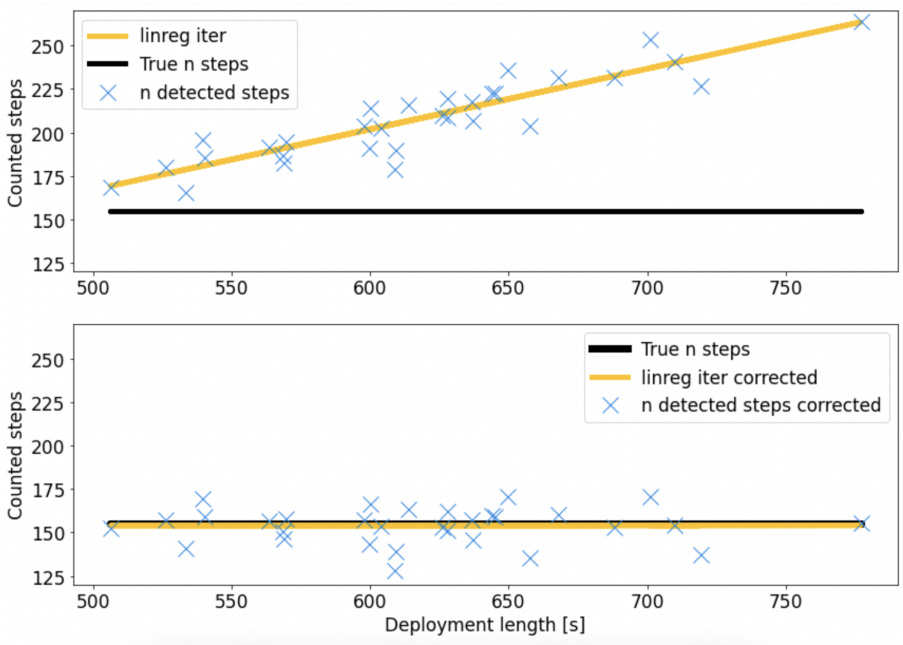

Figure 4.11: Number of detected steps from iterative query search in deployments from A25 on the 15.08, 16.08 and 17.08. The top plot shows uncorrected results. The bottom plot show results corrected by velocity estimate. Linear regression lines are fitted to the data, named **linreg iter** in the legend.

pressure. The velocity was calculated from the channel section length (1080 m) divided by the average transit time of the deployments on this day.

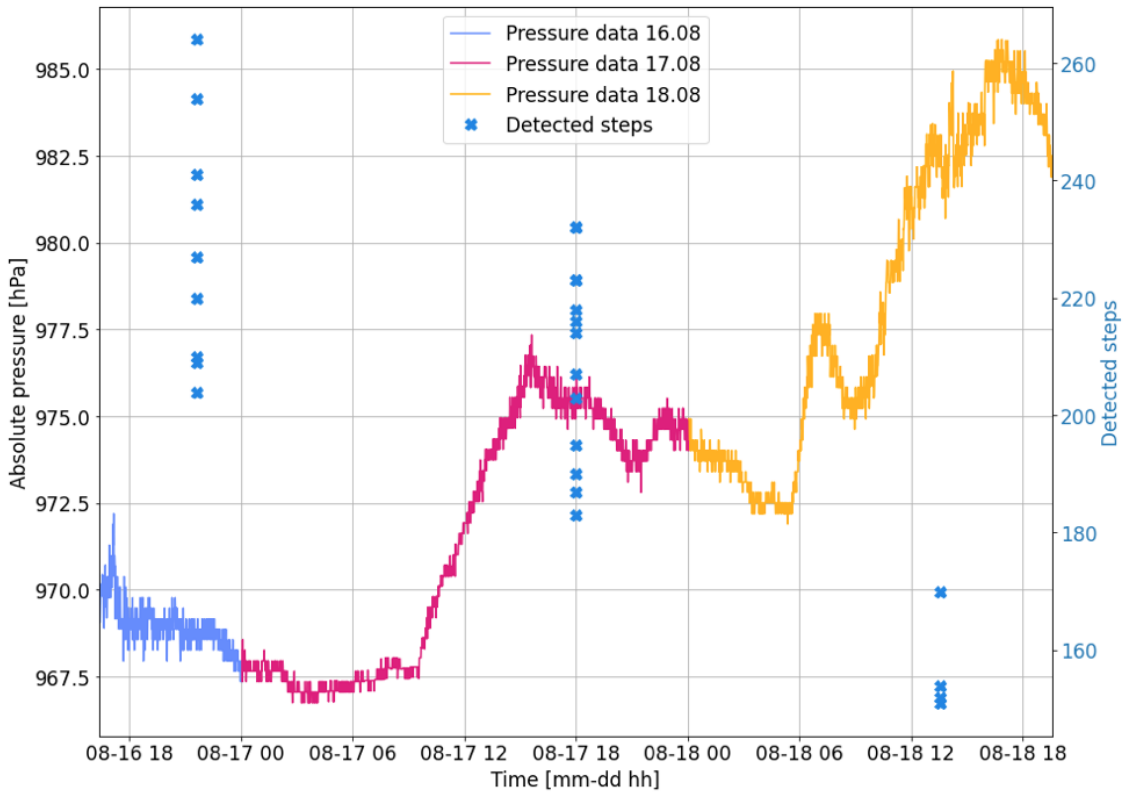

Figure 4.12: Pressure data from a static HOBO pressure logger placed in the channel together with the number of detected steps on the different days. The left y-axis shows the absolute pressure measured by the logger, the right y-axis shows the number of detected steps. The different colours show the pressure on different days. Blue crosses show detected steps per deployment. The crosses are placed at the approximate time of deployment.

4.2 Supraglacial channel, Konsvegen 2021

The following results were produced from a supraglacial channel on Kongsvegen during fieldwork conducted in the summer of 2021. The methods and queries used on this data are identical to the ones used for the 2020 deployments.

One set of B-series drifters were deployed on Kongsvegen on the 13.07.2021. During that day, no video was taken to count the number of steps in the channel. However, the channel was filmed by drone on the 15.07.2021, two days later. In this video, 95 step-pools were identified. Running the single query search with the 2020 query yielded a mean step count of 122.5 (129 % of the true number of steps) for eight deployments. With a velocity correction the number of detected steps was 99.8 (105 % of the true number of steps). Running the iterative query search yielded a mean step count of 133.5 (140 % of the true number of steps) over eight deployments. Applying the velocity correction to the deployments gave a value of 87.2 (92 % of the true number of steps). The velocity was derived from the deployment time of each drifter unit and the channel length that was measured by a DGPS. The channel length was estimated to be 652 m.

The M-series drifters were deployed on four different days on Kongsvegen (13.08, 15.08, 17.08, 18.08). The total number of counted steps per deployment can be seen in figure 4.13. This figure shows the step count found by directly applying the same method as the B-series drifters with no modifications, meaning the same queries were used as in 2020. Figure 4.14 shows the step count found by tuning the threshold of the iterative query search and applying the velocity correction. The single query method was also used, but yielded poor results that are not included here. Using this method, more than 200 % of the real steps were detected. Applying the method used for the B-series directly gave a mean step count of 89.0, 100.8, 79.3 and 129.3 on the 13.08, 15.08, 17.08 and 18.08 respectively. Using the adjusted threshold and velocity correction the mean step count was 95.1, 108, 94.2 and 95.5. The adjusted threshold was set to 12.337.

In the channel on Kongsvegen most step-pools were located around closed crevasses (figure 4.16). The closed crevasses created a very erratic channel flow. Abrupt changes in channel direction often occurred around closed crevasses. They also occasionally made step pools in diagonal angles, compared to the flow direction in the channel. This differs from the channel on Austre Brøggerbreen, where step-pool sequences only occur along the flow direction of the water.

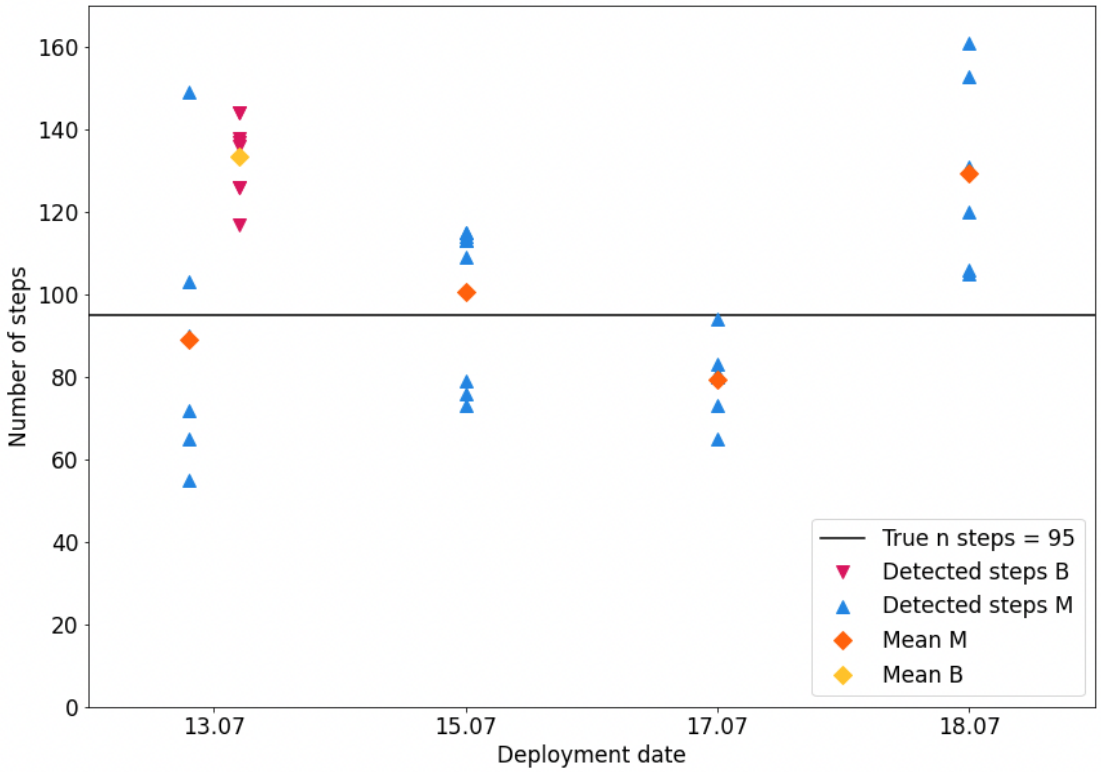

Figure 4.13: Step counts in the supraglacial channel on Kongsvegen. The number of steps detected using the iterative query search with the same parameters as the B-series drifters. Each triangular marker represents a single deployment. Diamond shaped markers show the mean of the deployments on each day. On the 13.07 both B-series and M-series drifters were deployed. The M-series are shown in blue and the B-series in red.

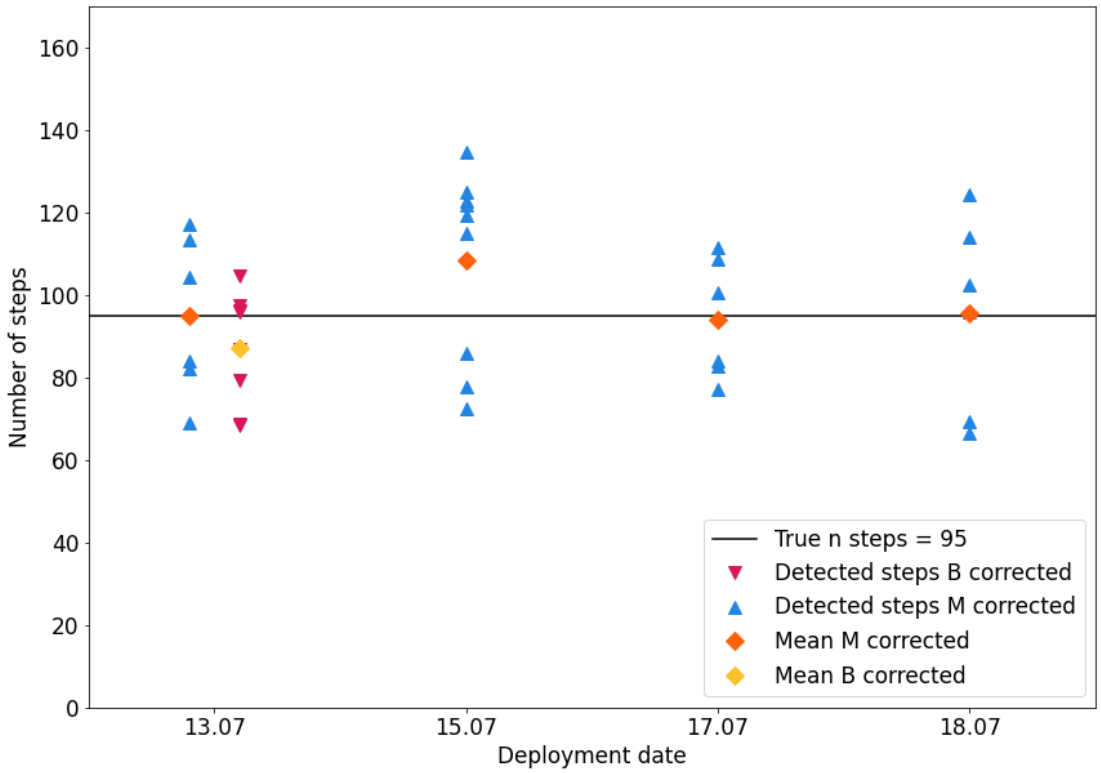

Figure 4.14: Step counts in the supraglacial channel on Kongsvegen using M-series drifters. The number of steps detected using the iterative query search with the same parameters as the B-series drifters. Each triangular marker is a single deployment. Diamond shaped markers show the mean of the deployments on each day. On the 13.07 both B-series and M-series drifters were deployed. The M-series are shown in blue and the B-series in red.

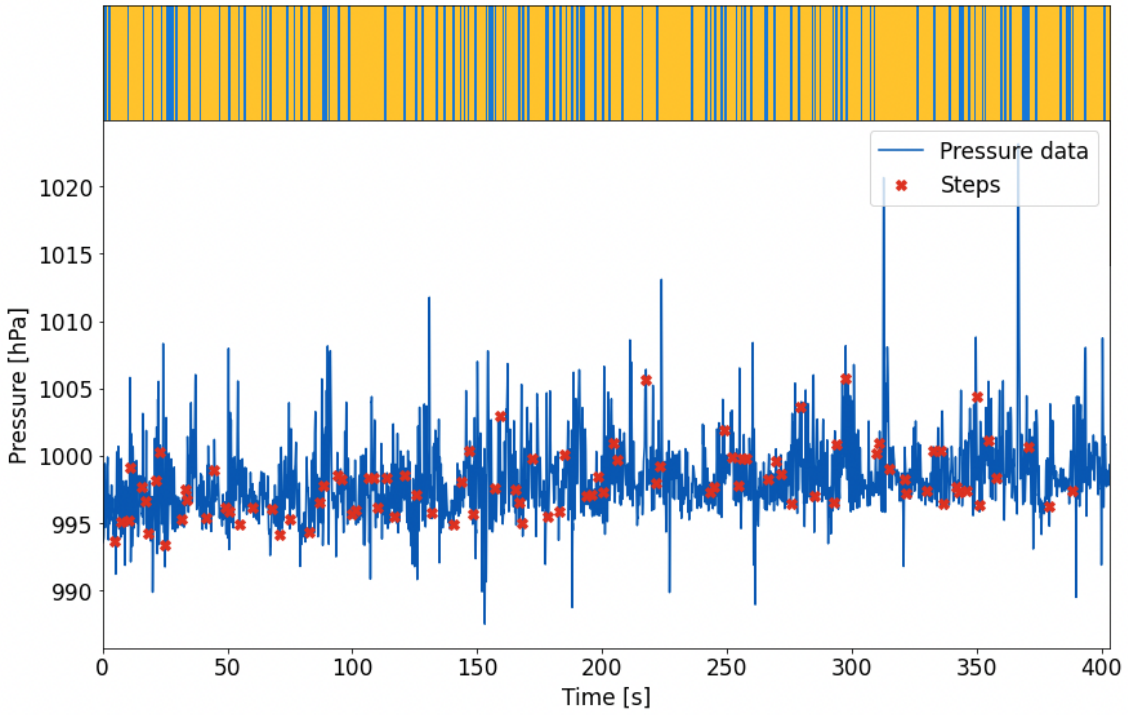

Figure 4.15: Single deployment of M-series drifter unit M09 in the supraglacial channel on Kongsvegen on the 15.07.2020. The blue line shows pressure readings from the drifter in the channel. Steps identified in a drone video are marked by red crosses. The yellow bar at the top of the plot shows the binary distance profile, made using the iterative query method, blue lines are detected steps. In this deployment 113 steps were detected. 66 of these corresponded to real steps (70% of the true number of steps).

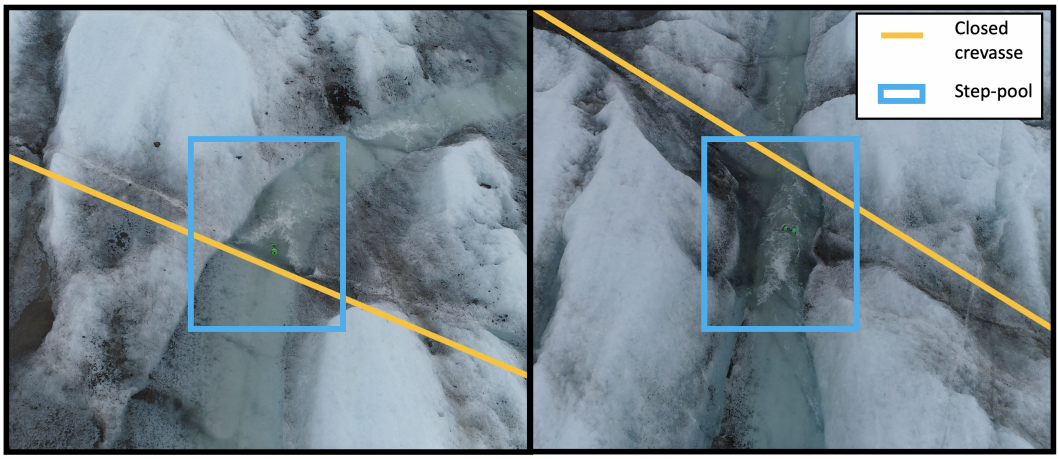

Figure 4.16: Step-pools located along closed crevasses in the supraglacial channel on Kongsvegen, 15.03.2021. In the left image the step forms after the closed crevasse. The closed crevasse can be seen as a white line through the ice, just above the yellow line. In the right image the step forms before the closed crevasse. The closed crevasse can be seen as a dark line just below the yellow line.

4.3 Hydraulic geometry

Austre Brøggerbreen

The Reynolds numbers calculated for the 18.08.2020 indicated that the flow was turbulent, $Re < 3000$, at all cross sections at both 12:00-13:00 and 15:45-17:20 (figure 4.17). The mean Reynolds number was higher at 15:45-17:20 for all cross sections than for 12:00-13:00. There was a notable difference between the mean Reynolds number at the two measurement times, the mean Reynolds number increased upstream from A5 to A25 at 12:00-13:00, while at 15:45-17:20 the mean Reynolds number decreased upstream from A5 (figure 4.18).

The Froude numbers calculated for the 18.08.2020 showed that the flow was supercrit-

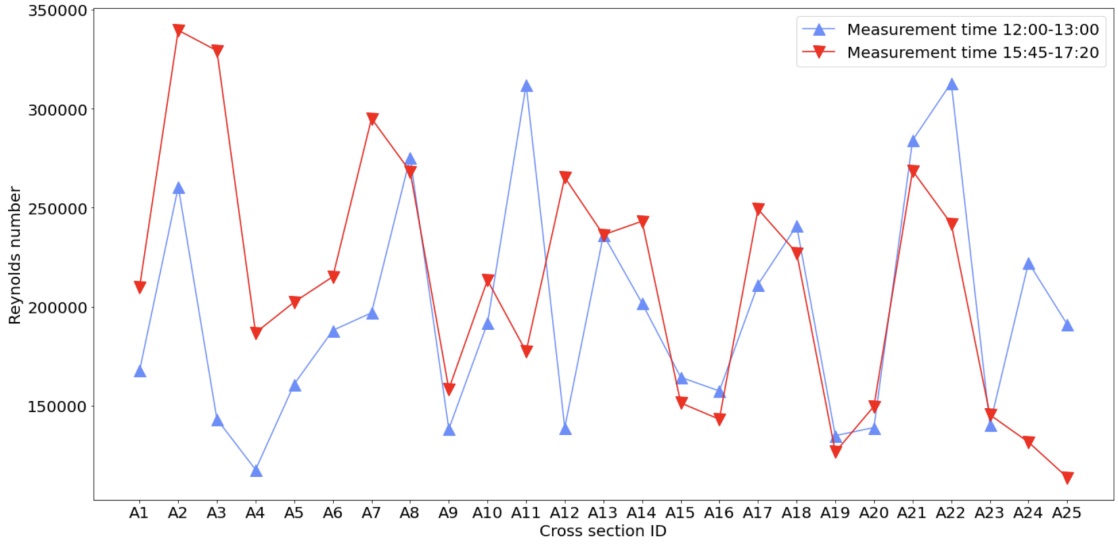

Figure 4.17: Reynolds numbers at all cross sections in the supraglacial channel on Austre Brøggerbreen on the 18.08.2020. Hydraulic geometry measurements were carried out at two separate times during the day. Blue triangles show the measurements taken between 12:00 and 13:00, while red triangles show measurements taken between 15:45-17:20. Lines are included between the measurement points as a visual aid.

ical, $Fr > 1$, at most cross sections, both at 12:00-13:00 and 15:45-17:20. Between 12:00-13:00 there was near critical flow at cross section A5 $Fr = 1.03$ and at A19 $Fr = 1.10$. Between 15:45-17:20 there was subcritical flow at A11 $Fr = 0.76$ and critical flow at A25, $Fr = 1.02$. The mean Froude number was larger from A1 to A16 between 15:45-17:20 than for measurements at 12:00-13:00, excluding A11 which was lower. From A16 to A25 the mean Froude number was lower between 15:45-17:20.

Kongsvegen

The Reynolds numbers calculated for Kongsvegen indicated that the flow was turbulent, $Re < 3000$, at all cross sections on all days (figure 4.21). The mean Reynolds numbers showed that the overall turbulence was largest on the 15.07.2021, and lowest on the 18.07.2021. The mean Reynolds number increased with upstream distance on the 18.07 and 15.07. On the 13.07 the mean Reynolds number increased with upstream distance until C6 after which it began decreasing again.

The Froude numbers showed that the flow was subcritical at 6 out of 9 cross sections on the 18.07. On the 13.07, the flow was subritical at 2 out of 9 cross sections and on the 15.07

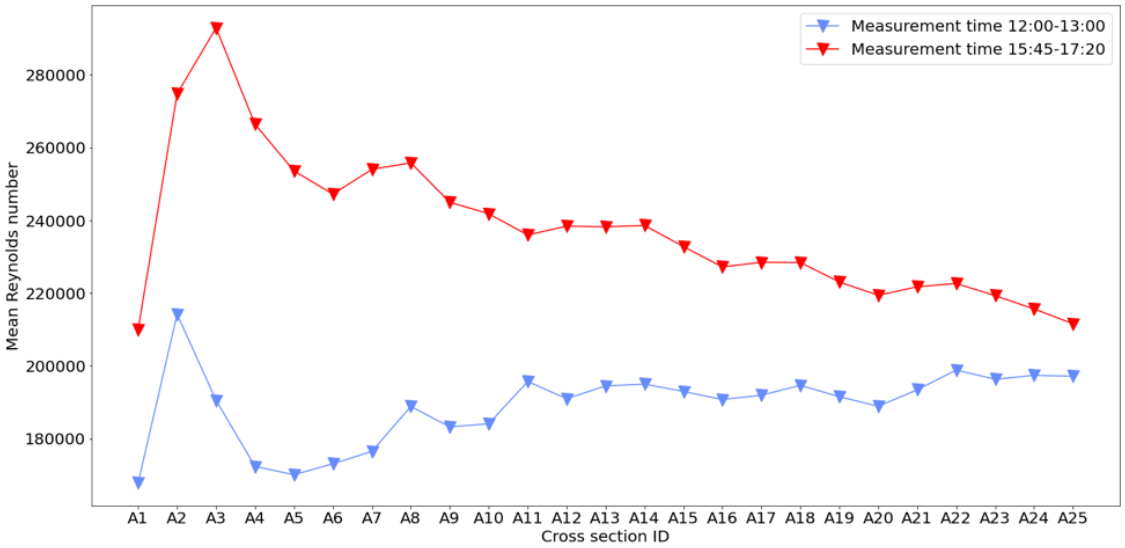

Figure 4.18: Mean Reynolds numbers from different cross sections down to cross section A1 in the supraglacial channel on Austre Brøggerbreen 18.08.2020 at two different times 12:00-13:00 in blue and 15:45-17:20 in red. The mean was calculated from all cross sections between the cross section in question and A1.

only one cross section was subcritical. Other than this, all cross sections were supercritical. On the 13.07 and 15.07, the Froude numbers were largely the same, while the mean Froude number were lower on the 18.07.

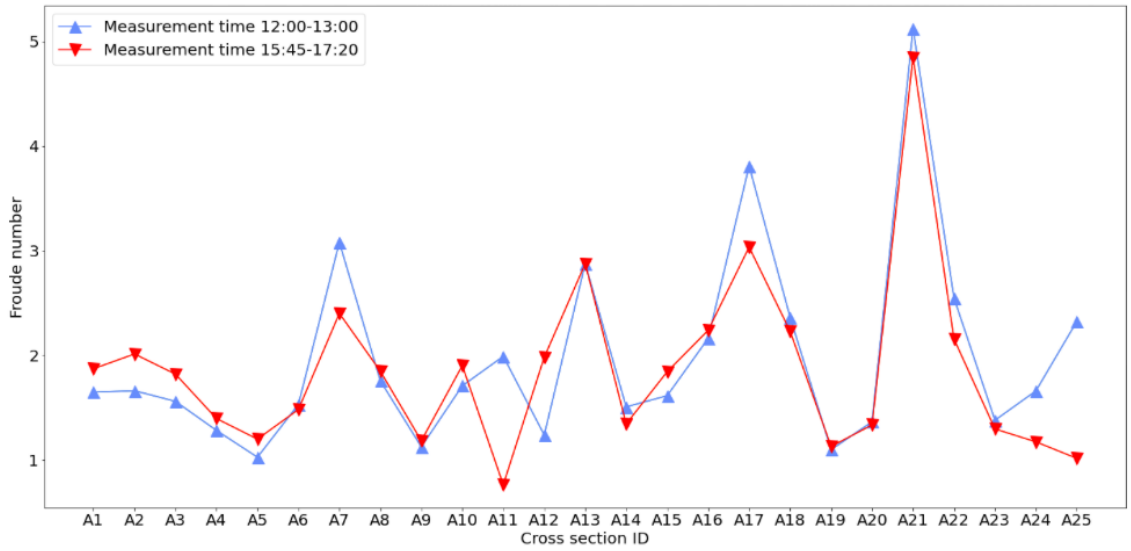

Figure 4.19: Froude numbers at all cross sections in the supraglacial channel on Austre Brøggerbreen on the 18.08.2020. Hydraulic geometry measurements were carried out at two separate times during the day. Blue triangles show the measurements taken between 12:00 and 13:00, while red triangles show measurements taken between 15:45-17:20. Lines are included between the measurement points as a visual aid.

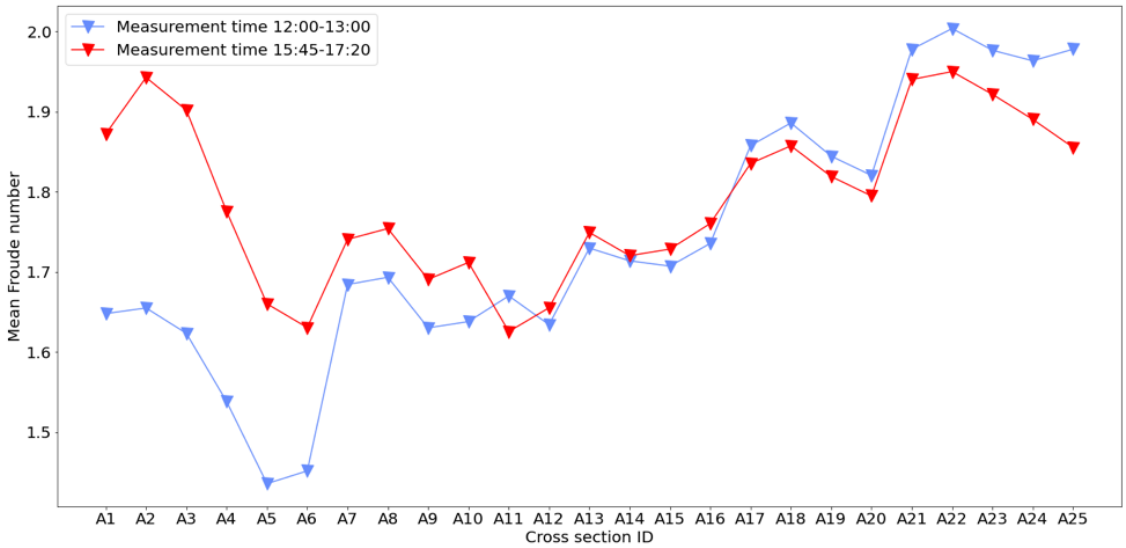

Figure 4.20: Mean Froude numbers from different cross sections down to cross section A1 in the supraglacial channel on Austre Brøggerbreen 18.08.2020. The mean was calculated from all cross sections between the cross section in question and A1. Blue and red lines represent Reynolds numbers at all cross sections measured at two different times on the 18.08.2020, 12:00-13:00 in blue and 15:45-17:20 in red.

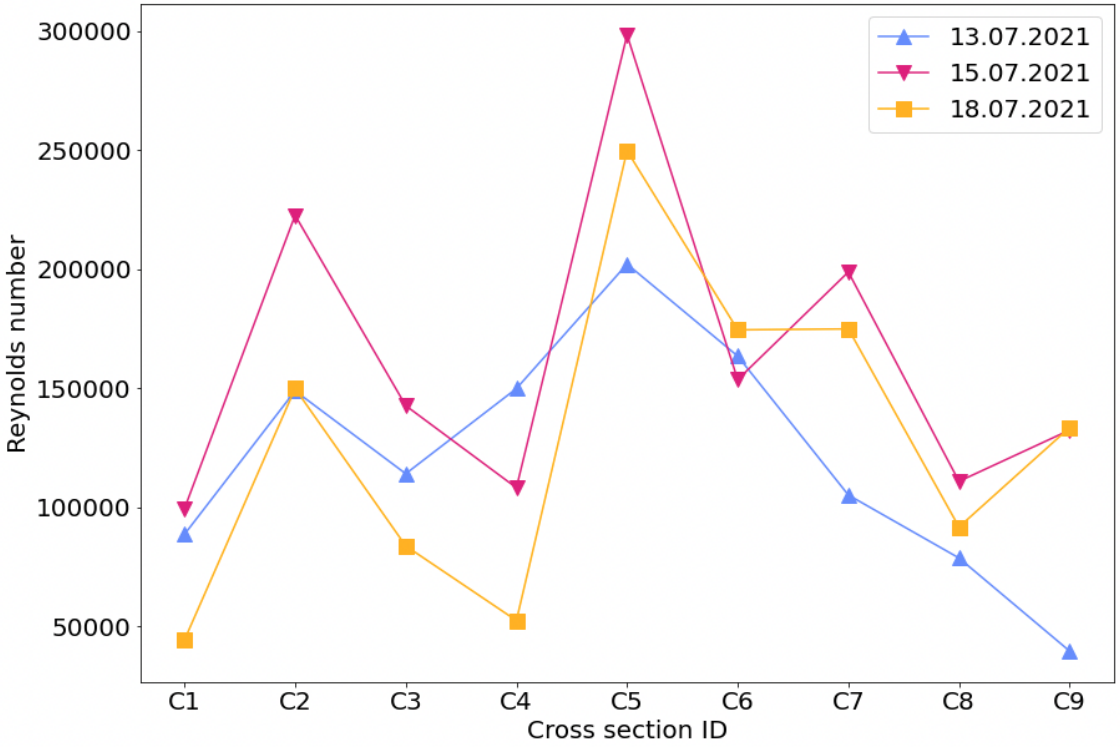

Figure 4.21: Reynolds numbers at all cross sections in the supraglacial channel on Kongsvegen on the 13.07 (blue), 15.07 (pink) and 18.07.2021 (yellow). Cross section C1 is the recovery point and C9 the deployment point.

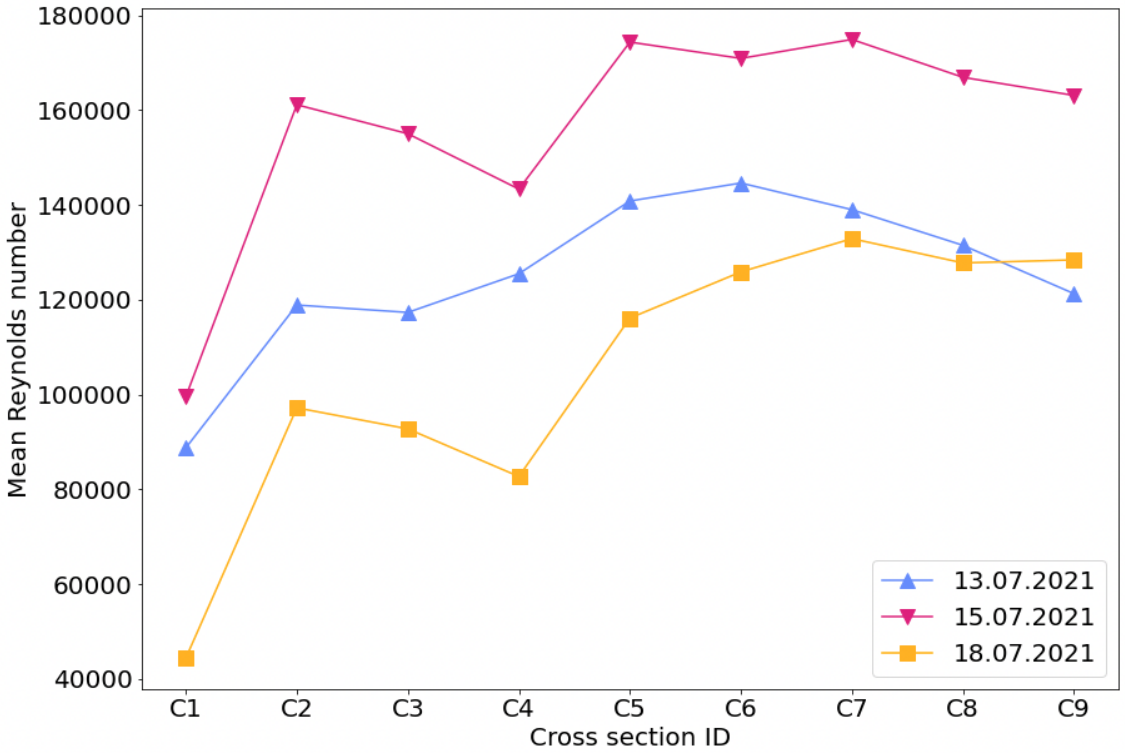

Figure 4.22: Mean Reynolds numbers at all cross sections in the supraglacial channel on Kongsvegen on the 13.07 (blue), 15.07 (pink) and 18.07.2021 (yellow). Cross section C1 was the recovery point and C9 the deployment point. The mean was calculated from all values from a given cross section down to the recovery point.

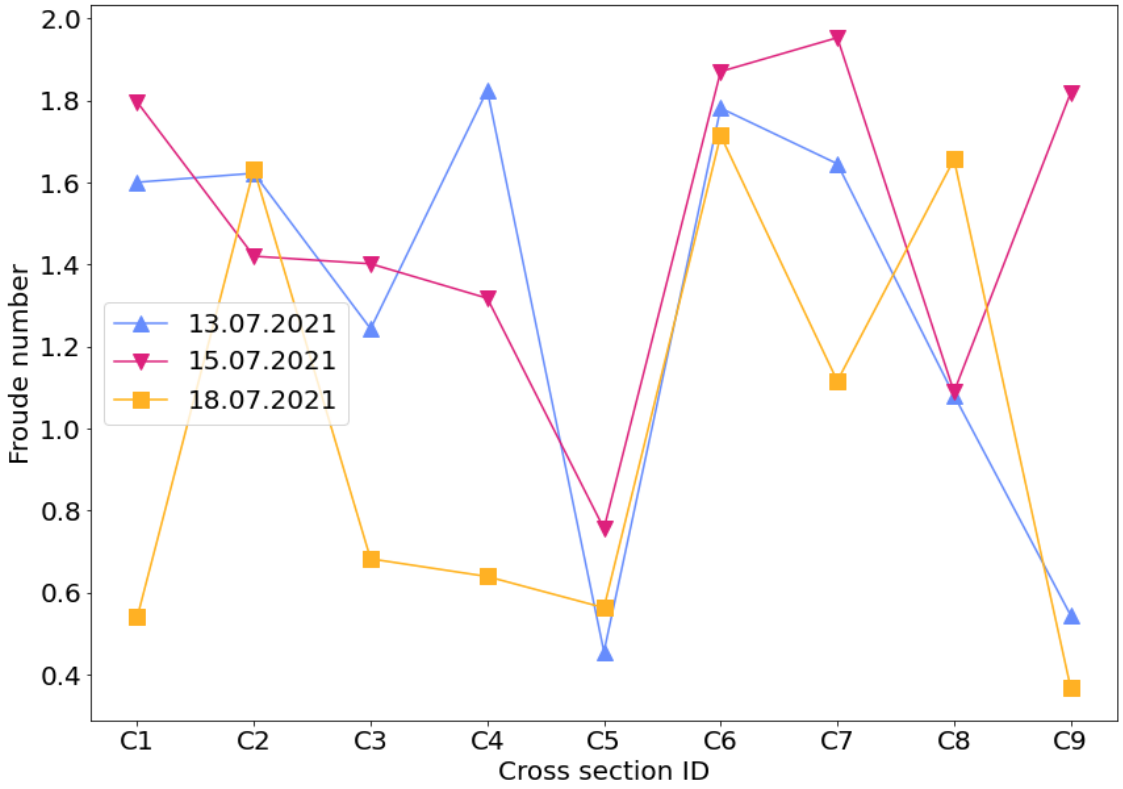

Figure 4.23: Froude numbers at all cross sections in the supraglacial channel on Kongsvegen on the 13.07 (blue), 15.07 (pink) and 18.07.2021 (yellow). Cross section C1 represents the recovery point and C9 the deployment point.

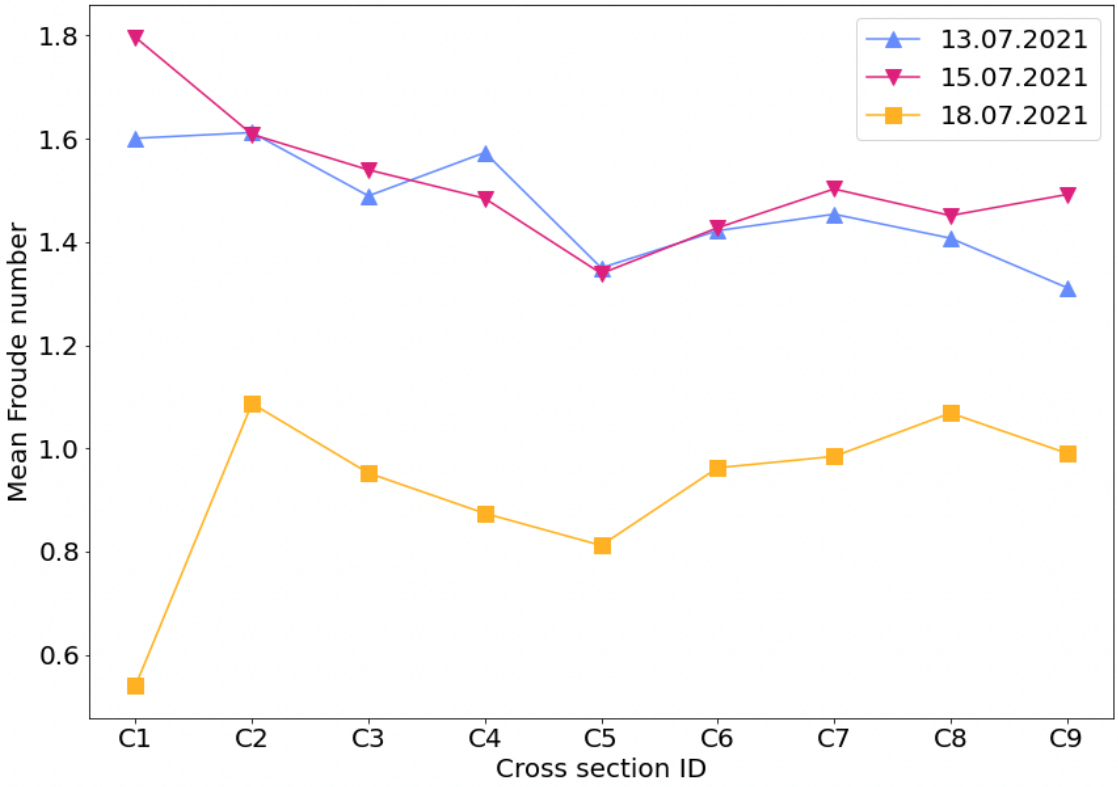

Figure 4.24: Mean Froude numbers at all cross sections in the supraglacial channel on Kongsvegen on the 13.07 (blue), 15.07 (pink) and 18.07.2021 (yellow). Cross section C1 was the recovery point and C9 the deployment point. The mean was calculated from all values from a given cross section down to the recovery point.

CHAPTER 5

Discussion

In this chapter I will first discuss and evaluate the main results obtained from the step detection methods; how the method performed on the reference channel on Austre Brøggerbreen and how it transferred to the test case on Kongsvegen. Next, I will postulate some potential uses for step detection in glacial channels and lastly, I will discuss some of the limitations and future improvements that could be made in this kind of investigation.

5.1 Step detection

Using the single query method on the Austre Brøggerbreen channel, 73.3% of the steps detected in figure 4.1 were correctly detected, meaning that they corresponded to real steps in the channel. Overall, method proved to be a undersensitive, counting too few steps in some channel segments (see figure 4.1). This under sensitivity may be mitigated by increasing the threshold in the distance profile. Currently, the threshold was chosen based on the best ratio of correct step detections to false positives, but it could instead be chosen based on correct detection of the total number of steps. Increasing the threshold allows more subsequences of the time series to be classified as steps, but reduces the accuracy of the steps detected, i.e. more false positives. The selection of what threshold to use then becomes a question of what information is required from the data. Detecting the correct number of steps could be useful for estimating the hydraulic roughness of the channel or for following the development of steps in the channel. Detecting the correct location of steps within a time series is useful for mapping channels and improving geometric and morphological reconstructions of channels. Using a low threshold could give more certainty to the location of pronounced steps, and provide more accurate reconstructions.

The query used to search for steps (figure 4.2) was chosen based on a process of trial and error. Numerous subsequences of the pressure data around known steps were tested, and this one yielded the best results. Observing the data around steps revealed that this was a common signal for a step: a sharp rise in pressure as the drifter moves towards the edge of a step, a drop in pressure as the drifter moves over the edge, and a slight increase in pressure as the drifter plunges into the pool. The physical origin of this signal was interpreted from the movement of the drifter over the step feature used to create the query in figure 4.2. The video showed that at the beginning of the step, before the knickpoint, the drifter was floating with the pressure sensor at the water surface, oriented upstream. As it passed over the knickpoint, the sensor was submerged in water, possibly explaining the first sharp rise in pressure. After passing the knickpoint, the sensor was ejected further out of the water column as it moved over the step riser, which could explain the drop in pressure. At the end of the step riser, the drifter plunged into a turbulent pool, possibly explaining the second pressure peak. A similar step signal was observed by Alexander, Kruusmaa et al., 2020 using the same drifters, but their interpretation of the signal differed from the one mentioned previously. They interpreted the signal as a sharp increase in pressure as the drifter dropped over the edge of the step and into the pool. The pressure increase was a response to increased depth as the drifter dove into the pool and the neutral buoyancy of the drifter then

brought it back to the water surface decreasing the pressure. Due to currents in the pool, the drifter made a second dive, creating the smaller secondary pressure peak. This interpretation leads to the conclusion that the video reference data used in this thesis could be slightly misaligned to the pressure time series. The second interpretation is more likely since it would be expected that the pressure peak would be largest when the drifter plunges into the pool.

By using the iterative query, 70% of the real steps in figure 4.6 were correctly identified. Using the single query 61% of the real steps were found. However, the ratio of real steps detected to the total amount of steps detected was slightly lower for the iterative query search than for the single query search, 69% and 73% respectively. This shows that the iterative query search is able to find more of the real steps, but that for every detected step there is a higher chance of it detecting false positives. In addition, the total number of steps detected using the iterative query search was 55, close to the actual number of steps in this channel segment, 54. 17 of these detected steps were classified as false positives, so these were weighing up for undetected real steps in the total number of detections. The single query search had a total step count of 45 in the same channel segment. The threshold could have been tuned to include more steps and get the correct total, but doing this led to the ratio between correctly identified steps and the total to drop to around 60%. The iterative query method produced better total step counts than the single query, when looking at the mean of multiple deployments (figure 4.6). This was not unexpected since the single query search only looked for 1 specific signal, while the iterative method included a wider range of signals, thereby capturing more steps.

Since the method is able to detect around 70% of the steps correctly in the cases where there was reference data, it is noteworthy that it is able to estimate the correct total number of steps to a better percentage than 70% from most cross sections. It is therefore likely that the false positive detections are weighing up for the undetected true steps.

The iterative method was slower by a factor of 11 compared to the single query method. Both methods were timed for how long they took to process 31 datasets from A25-A1 on a consumer laptop (Apple M1 CPU 2020, 16 GB ram). These datasets covered a 1080 m channel transect. The iterative query search used 32.2 s to process all the datasets, while the single query used 2.9 s. Although the iterative query search was slower it only took about a second to complete for each deployment.

The number of counted steps per deployment in a given channel segment varied; the largest spread between the highest and lowest step count was 50, using the single query, found in the deployments from cross section A18 (Figure 4.1). The true number of steps in this segment was 95. Though the spread in detected steps was large for individual deployments, averaging multiple deployments gave results closer to the true number of steps. This means that multiple repeated deployments were required to produce consistent results. This was not a big issue as drifters can be deployed rapidly and easily. The main limitation to this being how many can practically be carried to the deployment site, and also the utility rate of the drifters, i.e. how many are lost during deployment and how many are recovered with usable data.

To asses how many deployments were needed, the minimum sample size was calculated from equation 3.3 for the iterative and single query search. This was calculated for all successful deployments from A25-A1. There were 35 successfully deployments from A25-A1 between the 15.08, 16.08,17.08, 18.08 2020 on Austre Brøggerbreen. A velocity correction was applied to all days excluding the 18.08. The number of deployments needed for the single query method was 1.8, while it was 1.6 for the iterative method. Note that this was not the sample size needed to correctly estimate the true number of steps in the channel, but how many deployments were needed to produce a step count within 10% of the mean number of steps detected by all the deployments from A25 95% of the time. This shows that the iterative method produces a slightly more consistent step count than the single query method, but both methods needed at least two

deployments for a channel of ca 1000 m. Experience from fieldwork showed that drifters sometimes lost battery contact or had sensors that malfunctioned during deployment. Some drifters were also lost during retrieval. It is therefore required to have more than 2 because the drifter can fail in the field, or might be lost.

The number of required deployments was consistent with the findings of Alexander, Kruusmaa et al., 2020 who found that the required sample size using the same drifter platform was 2 using the 2 bar pressure sensors. They also included a utility rate of the sensors, which included how may sensors were lost during deployments and how many datasets were unusable due to sensor malfunction. Including this utility rate in the estimation of how many sensors would be needed they found that 3 drifter deployments were required for supraglacial channels (Alexander, Kruusmaa et al., 2020).

Comparing the detected steps to videos of the deployment (see figure 4.1) showed that a number of the counted steps were false positive detections, meaning that the detected steps did not correspond to a real step in the channel. There may therefore be processes in the channel that produce similar signals to steps. To find a possible explanation for this, the videos were analysed at the time of the false positives. There were in total 12 false positives in the filmed deployment from A14 on the 18.08.2020. Two false positives were found to correspond to very small steps that were not included in the initial analysis. Another corresponded to a small hydraulic jump, but due to the camera angle it was not possible to see if the hydraulic jump was associated with a step. Five false positives corresponded to long turbulent plunge pools following a step-pool. Three steps were detected around a real step within 1.6 s of each other. There was a real step within this time window, but only one was counted as a hit and the two remaining as false positives. The step directly followed a meander bend where the drifter collided with the channel wall. This step was long and the plunge pool coincided with the last detected step. This highlights a weakness in the method. Steps were noted down in the video as occurring in single points in time, while in reality the drifter uses some time to pass over a step. One false positive was the result of a data processing error where a small portion of data, that was recorded after the drifter was recovered from the channel, was not cut away, and one step was detected in this portion. One step was found in a place where the channel was not visible in the video because of the camera angle, there might have been a real step at this location but it is not possible to verify from the video.

The analysis of the false positive detections shows that most of these were in fact associated with step-like features. The problem was that only one detection could be matched to a single step. Using a flexible time window could potentially solve this problem. A minimum distance between detected steps could also partially solve this, but sometimes steps occurred in sequences in very rapid succession, so using a minimum distance might then lead to some of these steps not being identified.

In addition, is important to note that the drifters do not necessarily measure the actual conditions in a channel, they are in fact measuring their own motion through this channel. Fluctuations in the pressure readings occurred when the sensors moved up or down through the water column. These readings would not convey, e.g. the total pressure at the bottom of the channel. If two drifter deployments were made in a channel where the discharge is much higher during one deployment, the difference in discharge would not necessarily be visible in the total pressure logged by the drifters, since the drifters are mostly floating around the surface due to their slightly positive buoyancy. However, differing discharge is likely to cause a different flow motion, causing the drifter to dip up and down differently between the deployments, causing a distinct pressure signals and also different transit speeds.

Deployments from some cross sections produced too many steps, while from others, too few were detected. Both the single query and iterative query methods detected too few steps between cross sections A16 to the beginning of A13 (figures 4.4 and 4.8) Also, using the iterative

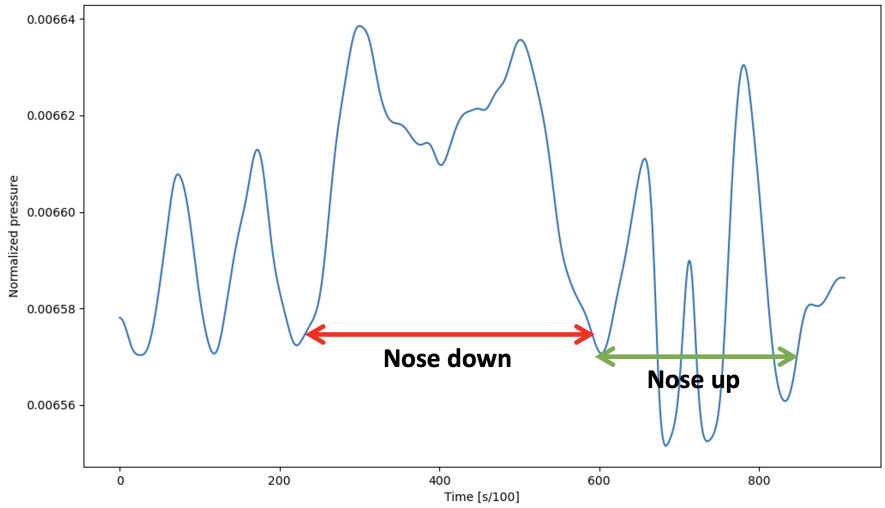

Figure 5.1: Example of pressure data when the sensor is oriented up or down, perpendicular to the water surface. The red arrow shows the area where the pressure sensor is pointing down, since it is deeper in the water column the pressure increases. The green arrow shows an area where pressure sensor is completely out of the water, resulting in a decrease in pressure. The segment is from a deployment between A8-A1 with drifter unit B80 on Austre-Brøggerbreen 18.08.2020.

query method, there were too many steps detected between A10 to the beginning of A7, compared to the real number of steps. There was no video taken of a drifter deployment from A16, but there was one taken from A15 to A1. By timing how long it took this drifter to move between A15 to A13 and A10 to A7 it was possible to derive a step frequency between the cross sections. The step frequency of A15-A13 was 0.58 steps per second, and A10-A7 was 0.28 steps per second. The step frequency was over double in A15-A13. Many of the steps in this transect were very close together, meaning that the steps flowed into each other with no space in between. This was likely caused a change in the appearance of the pressure signal, with no clear single step. Due to the chaotic movement of the drifter in the channel the pressure signal was constantly oscillating up and down as the pressure sensor moved deeper or shallower in the water column. There is always a chance that a random oscillation could be misinterpreted as a step. At lower velocities, or with a low step frequency, these random misinterpretations become a larger part of the total amount of counted steps.

The orientation of the drifter influenced the pressure readings. Comparing the pressure data to a video (figure 5.1), it became apparent that when the end cap with the pressure sensors was oriented down into the water, perpendicular to the water surface, the background water pressure became higher. When the nose tilted upwards, out of the water the background pressure became lower and had larger oscillations. The segment shown here was a slow flow channel segment, where the drifter changed its orientation constantly, while in faster flow the orientation of the drifter remained stable for longer stretches of the channel. These orientation changes could likely to result pressure signals that are misinterpreted as steps, and is a likely explanation for why more incorrect detections were made at slower flow velocities.

Method transferability

The previous discussion of the methods has been focused on one specific channel on Austre Brøggerbreen, with one drifter platform. For the methods to be practically usable they need to be transferable to different channels under different hydraulic conditions and possibly also different drifter platforms. The results showed that the B-series drifters deployed on Kongsvegen found too many steps on average (129% of the true number), but that it was possible to use the velocity

correction to get a count within 5% of the true number. However, only 8 B-series datasets were usable on Kongsvegen and these were all taken on the same day (13.07.2021). Surprisingly, the results from the M-series drifters, deployed on the same day (13.07.2021) gave better results than the B-series, with the mean step count being within 93% of the true number. Although the spread in the number of detected steps between deployments was much larger for the M-series drifters, with a difference of 94 detected steps between the highest and lowest step count, for comparison, the real number of steps in the channel was 95. For the B-series tubes deployed on the same day the difference was 27. The discrepancy between the highest and lowest values found in the M-series tubes was likely a function of the dataset length. The drifter deployment where the most steps were detected spent 200 s (58%) longer to complete the entire channel transect than the dataset where the least steps were found. Due to the large size of the M-series drifters, their flow was prone to being influenced by the channel bed and to a larger extent than the B-series. In some places in the channel, the water depth was so low that the M-series drifter scraped along the bottom of the channel, reducing the velocity. Also, supraglacial debris, like rocks, were frequent in the channel. The M-series drifters often collided with these rocks, bringing the drifter to a complete stop. These interactions with the channel could lead to deployments having different lengths. Since the B-series drifters were smaller, they had less contact with the bottom of the channel and were not as likely to impact debris. As was shown in the results from Austre Brøggerbreen, increased dataset length led to more steps being detected, possibly explaining the spread in results from the M-series.

Using the iterative query search on the M-series deployment filmed by drone on the 15.07.2021 (figure 4.15), revealed that 70% of the steps in the channel were correctly identified. This is comparable to what was found in the channel on Austre Brøggerbreen (4.6), where 70% of the steps were correctly identified. However the ratio of correctly identified steps to the total amount of detected steps, using the M-series, was lower on Kongsvegen: 58% on Kongsvegen against 69% on Austre Brøggerbreen. This could be due to the flow velocities being lower on Kongsvegen, allowing more time for misinterpretations of steps, or may be due to differences between the drifter platforms.

On the 15.07.2021 and the 18.07.2021, sets of M-series drifters were deployed twice, at different times during the day. In figure 4.13 it is visible that the number of detected steps per deployment occurred in two distinct clusters, six of them were higher than the real number of steps and three of them were lower. This difference could be explained by diurnal flow variations in the channel. Diurnal discharge variations are common on glaciers (Jansson et al., 2003). Although no measurements were made of diurnal discharge variations during the fieldwork on Kongsvegen, the pressure data collected on Austre Brøggerbreen in 2020 (figure 4.12) indicated that diurnal variations in water pressure did occur in the area. Two pressure peaks were visible in this time series, occurring between approximately 16:00-18:00. These pressure peaks likely mark the maximum daily discharge. In supraglacial channels, a higher discharge is primarily accommodated by a higher water velocity, relative to the width and depth of the channel (Gleason et al., 2016). The water depth also increased faster than the channel width (Gleason et al., 2016), which is likely why a pressure increase was seen from the static pressure logger.

Although the approach seems to be transferable from the supraglacial channel on Austre Brøggerbreen to the channel on Kongsvegen, the step features had different characteristics in the two channels that made a direct comparison difficult, in addition the two used drifter platforms had different characteristics. The channel on Kongsvegen had a lower slope angle than the Austre Brøggerbreen channel. Vatne and Irvine-Fynn, 2016 wrote that steps are characteristic of channels with a surface slope of more than 2°. The slope angle of the supraglacial channel on Kongsvegen was approximately 2.5° while the slope angle of the supraglacial channel on Austre Brøggerbreen was approximately 4°. The slope was calculated from the elevation difference of the deployment and recovery sites, divided by the horizontal straight line distance between them. The elevation difference was calculated using the Arctic digital elevation model (Porter et al., 2018). Kongsvegen was also crisscrossed by closed crevasses. Almost all step-pool like features formed along the closed crevasses, but these were not present in the channel on Austre Brøggerbreen, where other processes

are likely to dictate the position of step-pools. The features classified as steps on Kongsvegen were typically a deepening of the channel with a subsequent hydraulic jump. Overall they had a much smaller vertical drop than the steps on Austre Brøggerbeen, although there were also some steps with a comparable vertical drop on Kongsvegen.

5.2 Hydraulic geometries

The measurements of hydraulic geometry may be used to explain differences between the channel on Kongsvegen and on Austre Brøggerbreen, which in turn could be related to the step detection results. The measurements should be regarded as rough estimates of the channel conditions. The flow conditions in supraglacial channels can change rapidly over distances of only a few meters. Consequently, moving the cross section up- or downstream a fraction could have a large impact on the results. Measurements are biased towards more tranquil flow conditions since measurements are more difficult to take in turbulent water and steep reaches of channels.

Comparing the Reynolds and Froude number of the channel on Kongsvegen and on Austre Brøggerbreen showed that the channels had differing characteristics in terms of these numbers. The mean Reynolds number at the deployment point (C9 on Kongsvegen and A25 on Austre Brøggerbreen) showed the mean of all the cross sections down to the deployment point and gave an indication of the average turbulence that a drifter would experience while flowing through the entire channel. On Kongsvegen, the mean values from C9 were $12 \cdot 10^4$ on the 13.07.2021, $16 \cdot 10^4$ on the 15.07.2020 and $13 \cdot 10^4$ 18.07.2021. The mean Reynolds numbers from cross section A25 on Austre Brøggerbreen on the 18.08.2020 was higher $20 \cdot 10^4$ (12:00-13:00) and $21 \cdot 10^4$ (15:45-17:20). This shows that the conditions on Austre Brøggerbreen were likely more turbulent and faster flowing, a fact which could be confirmed visually by comparing videos of the two channels.

The Froude numbers were also higher on Austre Brøggerbreen than on Kongsvegen. On Kongsvegen, the mean Froude numbers from C9 were 1.3 on the 13.07.2021, 1.5 on the 15.07.2020 and 1.0 on the 18.07.2021. The mean Froude numbers from cross section A25 on Austre Brøggerbreen on the 18.08.2020 were both higher, 1.9 (12:00-13:00) and 2.0 (15:45-17:20). This indicates more supercritical flow on Austre Brøggerbreen. It is important to note that the Froude numbers on Austre Brøggerbreen are perhaps not representative for the entire measurement period during the 2020 fieldwork since they may be skewed towards higher discharge. The static pressure data (figure 4.12) showed that this was the day with the highest channel pressure, and consequently discharge. The Froude numbers found on Kongsvegen largely correspond to those found in other studies of supraglacial channels, which are between 0.45-3.11 (Gleason et al., 2016; Marston, 1983). On Kongsvegen, the maximum and minimum Froude numbers were 2.0 and 0.4 respectively. While Austre Brøggerbreen the maximum and minimum values were between 5.1 and 0.8 respectively.

The differing Froude numbers could be used to explain the different appearance of steps in the two channels. Kamintzis et al., 2019 found that with turbulent flow and high discharges, vertical incision of steps is strongest at the base of the step riser leading to steepening of steps in supraglacial channels. In contrast, when discharge is low and there is transitional flow (a mixture of laminar and turbulent flow) the erosion is fastest at the knickpoint of the step, causing a decrease in step height. This is supported by observations on Kongsvegen and Austre Brøggerbreen. On Kongsvegen the steps had a much smaller vertical descent than on Austre Brøggerbreen. The Froude number on Kongsvegen showed that there was transitional flow, while on Austre Brøggerbreen the flow was turbulent.

The more tranquil flow conditions on Kongsvegen, indicated by the lower Froude and Reynolds numbers, could explain why the B-series drifters detected too many steps on Kongsvegen. Slow flow caused the drifters to spend more time in the channel allowing small perturbations to be misinterpreted as steps. Also, there were areas of subcritical flow measured on Kongsvegen.

Subcritical flow allows waves created by local disturbances to travel upstream, which means that a local feature could create upstream patterns in the data, leading to more false positive detections. The method was also tuned to the flow conditions in the channel of Austre Brøggerbreen on the 18.08.2020, that was more turbulent and fast flowing, as indicated by the higher Reynolds and Froude numbers. However, this does not explain why the M-series drifters were able to produce relatively good results on Kongsvegen. This is likely a result of the less sensitive 30 bar pressure sensors on the M-series drifters, making them less susceptible to small perturbations and creating a more stable pressure signal, with pronounced pressure peaks only at larger perturbations of the flow. It could also be explained partly by the fact that the M-series drifters held a more stable orientation, relative to the water surface, doing less deep nosedives with the pressure sensors than the B-series.

Change point detection

Apart from the query search method, there are many time series analysis methods. A frequently used method is change point detection, which can be used to find abrupt changes in the underlying state of time series data (Aminikhanghahi and Cook, 2017). I theorised that steps would present such abrupt changes in the pressure data of the drifters. This is a completely unsupervised approach that allows the algorithm to find change points in the data. Applying this method to the pressure data of the drifters did not reveal a connection between the detected change points and the steps. An example of change point detection run on a filmed B-series drifter pressure time series can be seen in figure 5.2. This method proved to be unsuited to this investigation, likely because steps do not present a sustained change in the underlying state of the pressure time series. An example of a use case for change point detection is differentiating different human activities based on time series data collected by accelerometers (Truong et al., 2020). It can be used for example, to differentiate between walking, running and standing still. These different activities will result in sustained differences in, for example, the absolute acceleration, that can be found using change point detection. A step only creates a change in the pressure signal locally around the step, and in the case of Austre Brøggerbreen and Kongsvegen these steps typically had a duration of about 1 s. The pressure signal is also constantly oscillating, even when there is no step present. With a completely unsupervised approach there is no way to differentiate between oscillations caused by steps and those made by something else. However, using this method makes it possible to automatically find the deployment and recovery point of the drifter deployment. This could potentially be useful for automatically clipping the data to the deployment time, reducing the amount of manual work needed for processing. It is also possible that this method could be used to find areas where the flow conditions in the channel change, for example a transition from subcritical to supercritical flow. These different flow conditions would likely result in more sustained changes in the pressure signal. This potential warrants further attention.

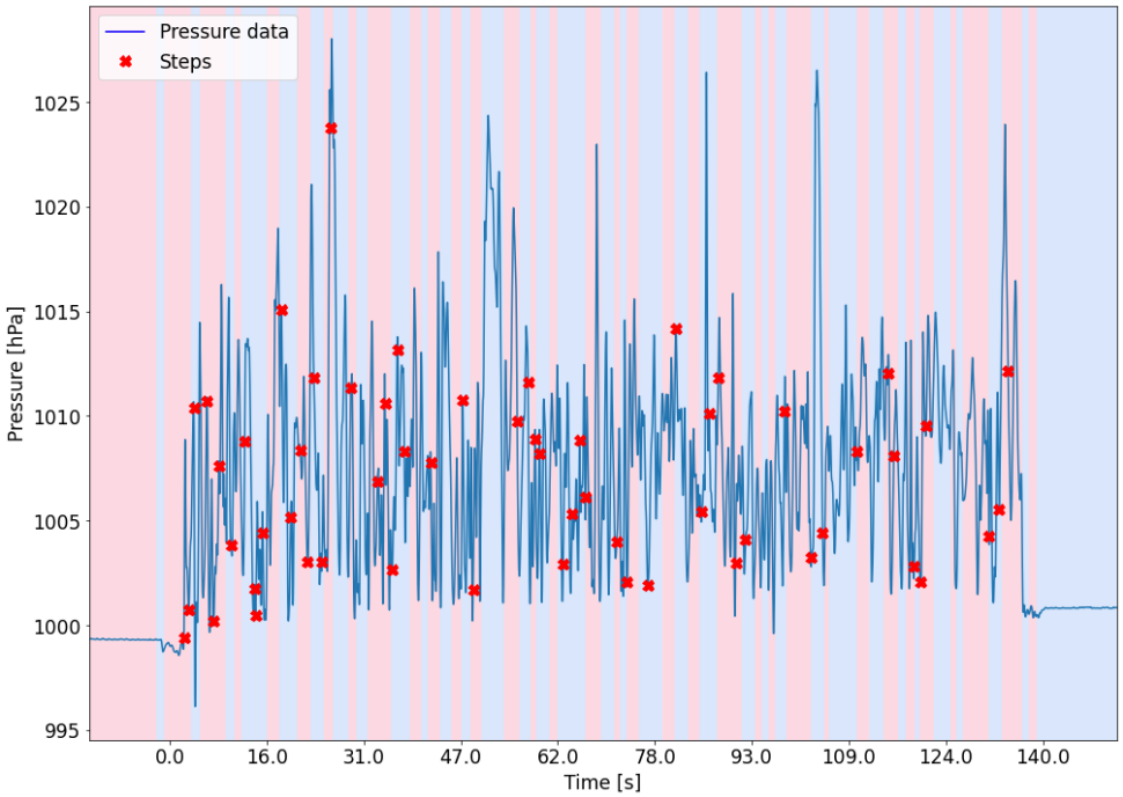

Figure 5.2: Detected change points on a deployment of drifter unit B56 18.08.2020 from cross section A14-A1 on Austre Brøggerbreen. The blue line shows the pressure recorded along the channel transect. Detected change points are shown by alternating blue and pink fields. Red crosses show steps found in a video of the deployment.

5.3 Potential applications

Detection of steps using drifters may have useful applications in investigations of glacial hydrology. The first and most obvious use for this method is to simply count steps, or other channel features that yield a characteristic signal in drifter data, for instance in long channel segments where manual counting may be impractical due to the scale or accessibility of the channel. Profiling the same channel over a whole melt season could give information about channel evolution as the step count changes over time through upstream migration of steps (Vatne and Irvine-Fynn, 2016). Piho and Kruusmaa, 2021 proved that englacial deployments of drifters is possible. The method could thus be used to analyse profiles of englacial channels, and studies have shown that steps form also in englacial channels (Vatne, 2001), where water reaching the glacier bed through moulins or crevasses can do so by cascading over several steps on the way down (e.g. Holmlund, 1988; Schroeder, 1998). Localising steps and tracking their migration over time in supra- and englacial channels can allow for a better understanding of the processes that link water from the surface to the the bed.

Vatne and Irvine-Fynn, 2016 surveyed an englacial channel for a 10 year period via speleological mapping and showed that over time, the average step height in the channel increased and the density of steps decreased, suggesting that larger steps migrated upstream at a faster rate, incorporating smaller steps. These results were the product of physically entering the englacial system, over multiple field campaigns. One could envision similar field campaigns using drifters instead of physically entering the system, which would significantly reduce the amount of work needed to gather the data and the risk associated with such operations. It would also allow profiling of multiple englacial channels in a shorter amount of time and to reach areas where the channels are too narrow to enter physically. Also, the speleological investigations were made during winter time, when there is little liquid water present in the channels. Drifters would allow direct observations of the channels with water flowing inside them, instead of having to indirectly deduce what is happening in the summer from winter observations.

Furthermore, Vatne and Irvine-Fynn, 2015 and Riverman, 2017 have suggested that the upstream migration of steps is one of the dominant processes of moulin formation in cold based glaciers, which acts through a process termed "cut and closure". The enhanced channel erosion around steps causes supraglacial channels to incise deep into the glacier surface. If the incision rates exceed the surface ablation, a roof can begin to form above the incised canyon, cutting off the supraglacial channel from the surface (Gulley et al., 2009). The vertical drop at a step can become increasingly pronounced, eventually forming a moulin. Moulins create a link between the glacier surface and the subsurface, sometimes all the way to the glacier bed, and often through cascading steps. In the subsurface, the presence of water may influence a number of dynamic properties of the glacier. Work by Covington et al., 2020 suggests that water-filled moulins on the Greenland ice sheet increase the pressure beneath the ice sheet, leading to accelerated ice sliding, potentially causing more rapid loss of ice into the ocean. Other observations on the Greenland ice sheet showed that steps were common across the supraglacial environment, although the cut and closure process is yet to be investigated (Riverman, 2017). If cut and closure moulin formation is a significant process occurring on large ice sheets, the inclusion of this process may have large implications for numerical models of ice movement and stability. To better understand how ice sheets will contribute to sea level rise, models will need better validation data on little studied areas of the glacial hydrologic system. Following the evolution of steps using drifter data in supraglacial channels could indicate where an englacial channel or moulin is likely to form, by tracking the migration of steps. This will allow for identification of regions where water could reach the glacier or ice sheet interior, and consequently what areas might be mobilised by surface meltwater, allowing better assessments of what changes might occur in the future.

One of the main issues of the drifter platform is that it requires recovery of the drifters in order to obtain data. This is especially a problem when deploying the drifters into the en- or subglacial system, where the flow path is unknown. Drifters could become stuck

somewhere underneath the ice or the exit of the channel may be unknown. Deployments in these systems would likely lead to a high loss rate of the units with no data obtained. The risk of losing all data can be mitigated using remote communication from the drifters. It is theoretically possible to send information from sensors beneath the ice via VHF radio (Prior-Jones et al., 2021) and from the supraglacial system through satellite communication, but these have a limited bandwidth that makes it impossible to send entire drifter datasets. As the query search computation is relatively simple and can produce results in near real time on a consumer laptop, it is possible to envision a similar method integrated onboard the drifters microcontroller. If certain key information could be calculated in real time onboard the drifter, for example the number of steps, the drifter could relay this information through remote communication. Instead of loosing the drifter and all the data onboard, it would be possible to at least gain some insights into what processes are happening beneath the glacier surface.

Another use of drifter data is to create flow path maps. Piho and Kruusmaa, 2021 used the IMU data of the 2020 B-series drifters on Austre Brøggerbreen to reconstruct a 2D flow path of the drifters using the deployment and recovery point as references. Longer flow paths were shown to give higher average errors. These reconstructions could be improved by adding known step locations, found using the proposed method, as additional references, thereby allowing the datasets to be split into smaller subsections. However, this would require known coordinates for the step location. Known coordinates could be obtained by mounting GNSS units on the drifters. When a step is detected in the channel it could be referenced to the corresponding coordinate recorded by the GNSS unit, although this would only be possible in supraglacial channels as GNSS signals would be blocked by ice, water and sediment in en- or subglacial channels. Another use for the reconstructions would be to use detected steps to align multiple drifter datasets. Since drifters can use a variable amount of time to pass through the same channel segment, alignment is a tricky process. If step locations could be estimated in a dataset, with a reasonable accuracy, these step locations could be used as reference points to segment the dataset into smaller subsequences. These subsequences could then be aligned and would allow statistics to be performed on the deployments to check that they are producing reliable results. This would improve upon the current method where datasets are segmented based on artificial criteria (Piho and Kruusmaa, 2021).

The query search method is very general and can in principle be applied to any time series with repeating motifs. This means that it could be used to search for other channel features, for example meanders. It could also be applied to other sensors than the pressure sensor, such as the acceleration sensor. It was not used in this investigation due to the insufficient accuracy of the accelerometer in the vertical direction. However, with a high quality acceleration dataset, detecting steps in acceleration data could be much more accurate than using the pressure data, particularly in pressurised channels. Since steps are areas of abrupt vertical slope change, one could search for large changes in vertical acceleration. The drifter platform is also versatile and a number of new sensors may be added in the future, which could also be analysed using the same method.

5.4 Errors, limitations and future improvements

There are a number of error sources in the methods presented in this thesis. Some of them are perhaps inherent to the chaotic flow of glacial channels, but some may be solved through technical or methodological improvements.

The methods I have used in this thesis attempted to classify all step features in one single class. Since the steps did in fact vary in magnitude, duration and shape, this may resemble fitting a square peg into a round hole. The accuracy and quality of information obtained from these methods certainly suffered from classifying all the steps in the same way. There were likely some step features that were consistently being missed if their signature in the pressure data was unique. Creating a catalogue of queries, gathered from different step

types, could allow steps to be placed into multiple classes. For each class a strict threshold could be applied, requiring a subsequence to have a high degree of similarity to the query, in order to be included. In addition to this, properties of different step types could be measured, for instance, hydraulic roughness, incision rates, etc. This would possibly not only provide additional accuracy in the counted steps, but also provide more information about each detected step.

A lot of false positive detected steps stemmed from the algorithms detecting multiple steps within one larger step feature. This was likely an effect of the fact that steps have different durations, as well as from drifters recirculating in pools. For instance, some steps had a long step-riser or plunge pool and some a short one. Both methods used in this thesis had a fixed window length of 0.74 s (single query) to 0.9 s (iterative query). This means multiple steps were detected within a step that had a duration of 2 or 3 seconds. This could be mitigated in the iterative query search by creating a reference dataset with variable window sizes. Occasionally, steps were also detected where a process other than a step, created a pressure signal similar to a step signal. Since the drifter moves chaotically in the water column there is always the chance of a false detection of a step. For datasets where the flow velocity in the channel was lower, the drifters had more time to detect signals that were not steps, than at faster flow velocities. A possible way to overcome this issue would be by using the acceleration data in addition to the pressure. If no significant vertical acceleration was registered at a point where the pressure data indicated a step, this step could be discounted.

It may also be useful to investigate the use of the 30 bar pressure sensors of the B-series drifters for step detection. When the B- and M-series drifters were deployed in the same channel on Kongsvegen (figure 4.13), the M-series gave better results, despite the method being developed for the 2 bar sensors on the B-series. This could be due to small perturbations in the flow not being registered by the 30 bar sensors, thereby reducing false positive detections.

The steps identified by video could be misaligned with the drifter data, causing the queries to search for signals that were not in fact steps. There was a systemic error introduced by the process of verifying if detected steps corresponded to a real step in the channel. This was a partly subjective process of seeing whether or not a detected step fell within one pressure peak of a real step. The steps identified by video could be misaligned to the dataset, further exaggerating this systemic error. Video reference measurements were only available for one day (18.08.2020) in the 2020 Austre Brøggerbreen dataset. Therefore, the step detection was highly tuned to this day. This caused problems when generalising to measurements on different days with a discharge different from this day. The results are likely biased towards this specific channel, the B-series drifter and the discharge conditions on this day.

Some small errors could have been introduced by cutting the data wrongly. This is a small error where some steps may have been detected before or after the drifter was deployed if the dataset was not correctly cut. Also, if there were steps directly after the deployment point these may not have been detected by the drifter since it needed a little time for the pressure sensors to fill with water. Deployment points should thus be placed so that they don't have a feature directly after the deployment.

Piho, Alexander et al., 2022 found that it was only possible to produce a planar topology of a supraglacial channel using the data from the IMU onboard the drifter because the vertical accelerations were found to have a large error. Theoretically it would be very easy to extract steps from vertical acceleration data as steps have been found to be one of the primary sources of elevation drops in supraglacial channels (Vatne and Irvine-Fynn, 2016).

Field methods

The most valuable source of validation for this feature detection is the filming of drifter deployments, even though during the fieldwork in 2021 not enough deployments were successfully filmed. This

was partly due to camera malfunctions and stumbling while filming. Analysing the videos is challenging, because the angle is not always good, the drifter is not always in frame and the camera is shaking as the cameraperson is running. Drone flights were found to be easier to analyse than handheld cameras. However, drones are limited by their battery life, which is also reduced by the cold conditions in the Arctic and on glaciers. This requires multiple spare batteries in the field, which were not available during the fieldwork on Kongsvegen. During the 2020 fieldwork, a lot of deployments were filmed, but during multiple important long channel transects the drifters failed. This left many videos without a matching data set. Long filmed channel sections are very valuable, because they can provide a lot more information for the same amount of work. When referencing the drifter data to the videos, the start and end of the deployment need to be aligned with the time in the video. This is tedious work that is prone to some error. However, referencing a long channel section is just as labour intensive as a short section. To ensure that long datasets are included, more films from long channel transects should be taken to increase the chances of capturing a successful deployment. Following long transects on foot is physically demanding, but increased use of drones would make this less of a problem.

Lastly, more continuous observations of the surveyed channels would also be useful. On Austre Brøggerbreen, a static pressure logger recorded continuous pressure data for three consecutive days, which made it easier to relate the channel conditions to the drifter data. Such continuous observations were not made on Kongsvegen.

CHAPTER 6

Conclusions

The goal of this thesis was to develop computational methods that could detect morphological features in glacial channels using drifter data. This thesis confirms that it is possible to detect steps in supraglacial channels using query searches of the pressure readings from drifters. For this, drifters were deployed in two supraglacial channels on two Arctic glaciers on Svalbard, one on Austre Brøggerbreen in 2020 and one on Kongsvegen in 2021. The methods were calibrated using reference data from the channel on Austre Brøggerbreen, and applied to the channel on Kongsvegen as a test case for the methods. Comparison of video reference measurements and detected steps showed that up to 70% of the real steps in the channel on Austre Brøggerbreen could be detected, utilising two different matrix profile query search methods, named "iterative query" and "single query". Using average step counts from multiple deployments it was possible to estimate the total number of steps in a channel segment. In the longest channel segment on Austre Brøggerbreen, which contained 155 steps, it was possible to estimate the total number number of steps with an error of 2% (iterative query), 6% (single query). This error was calculated from deployments on four different days.

The methods were calibrated to the channel conditions on one field day from Austre Brøggerbreen, where video reference data was available. When the same methods were applied to deployments on other days where the water flow velocity was lower than on the calibration day, too many steps were detected. It was possible to correct the total number of counted steps in a deployment using an empirical velocity correction. The velocity correction was created based on an observed empirical relationship between the transit time of drifters and the number of detected steps.

The methods were shown to be partly transferable between the two different channels and between different platforms. On Kongsvegen up to 70% of the real steps in the channel could be detected. However, more work is needed to reduce the amount of false detections and improve the accuracy of the detected steps. The methods proved to be sensitive to differing channel characteristics, especially flow velocity. A stronger base of reference measurements is therefore needed to make the methods directly applicable to a wider range of channel conditions.

Further research on the methods and drifter data in general may lead to new and interesting insights into the glacial hydrologic system. Linking drifter sensor signals to morphological features could allow to extract information from channels that are inaccessible to other measurement methods, places such as the en- and subglacial system. As these systems are known to influence the dynamics of glaciers, understanding how water reaches the subsurface and what processes are occurring there, could be vital for predictions of future changes to the worlds glaciers.

Appendices

APPENDIX A

Figures and Tables

Cross section	Water depth [m]	Water velocity [m/s]	Froude number	Reynolds number
A1	0.15	1.799	1.65	167795
A2	0.2	2.328	1.66	260548
A3	0.14	1.828	1.56	143226
A4	0.14.	1.503	1.28	117750
A5	0.2.	1.438	1.03	160940
A6	0.17.	1.977	1.53	188074
A7	0.11.	3.199	3.08	196916
A8	0.2.	2.46	1.76	275321
A9	0.17.	1.453	1.13	138226
A10	0.16.	2.141	1.71	191695
A11	0.2.	2.788	1.99	312031
A12	0.16.	1.552	1.24	138959
A13	0.13.	3.248	2.88	236297
A14	0.18.	2.003	1.51	201757
A15	0.15.	1.958	1.61	164381
A16	0.12.	2.345	2.16	157470
A17	0.1	3.773	3.81	211154
A18	0.15	2.869	2.37	240836
A19	0.17	1.418	1.10	134928
A20	0.15	1.656	1.37	139003
A21	0.1	5.075	5.12	283995
A22	0.17	3.29	2.55	312982
A23	0.15	1.674	1.38	140484
A24	0.18	2.206	1.66	222241
A25	0.13	2.626	2.33	191061

Table A.1: Hydraulic geometries from the different cross sections on Austre Brøggerbreen on 18.08.2020. The measurments are taken between 12:02 and 12:59.

Cross section	Water depth [m]	Water velocity [m/s]	Froude number	Reynolds number
A1	0.16	2.346	1.87	210001
A2	0.21	2.889	2.01	339512
A3	0.22	2.674	1.82	329199
A4	0.18	1.855	1.40	186849
A5	0.21	1.722	1.20	202340
A6	0.19	2.024	1.48	215159
A7	0.17	3.101	2.40	294986
A8	0.19	2.523	1.85	268225
A9	0.18	1.573	1.18	158393
A10	0.16	2.383	1.90	213363
A11	0.26	1.219	0.76	177358
A12	0.18	2.633	1.98	265215
A13	0.13	3.248	2.88	236284
A14	0.22	1.975	1.34	243144
A15	0.13	2.082	1.84	151447
A16	0.11	2.326	2.24	143178
A17	0.13	3.426	3.03	249233
A18	0.15	2.706	2.23	227170
A19	0.16	1.415	1.13	126652
A20	0.16	1.673	1.35	149748
A21	0.10	4.800	4.85	268606
A22	0.16	2.701	2.16	241835
A23	0.16	1.625	1.30	145454
A24	0.16	1.470	1.17	131617
A25	0.16	1.272	1.02	113872

Table A.2: Hydraulic geometries from the different cross sections on Austre Brøggerbreen on 18.08.2020. The measurments are taken between 15:45 and 17:20.

Cross section	Water depth [m]	Water velocity [m/s]	Froude number	Reynolds number
C1	0.45	1.59	1.60	88729
C2	0.70	1.90	1.62	148999
C3	0.85	1.46	1.24	114182
C4	1.10	2.06	1.83	149952
C5	0.90	0.90	0.46	202230
C6	1.30	2.09	1.78	163574
C7	1.10	1.71	1.65	105246
C8	0.80	1.17	1.08	78787
C9	0.95	0.59	0.55	39693

Table A.3: Hydraulic geometries from the different cross sections on Kongsvegen 13.07.2021.

Cross section	Water depth [m]	Water velocity [m/s]	Froude number	Reynolds number
C1	10	1.78	1.80	99555
C2	20	1.99	1.42	222705
C3	15	1.70	1.40	142770
C4	13	1.49	1.32	108283
C5	37	1.44	0.76	298419
C6	13	2.11	1.87	153700
C7	15	2.37	1.95	198909
C8	15	1.32	1.09	110991
C9	12	1.97	1.82	132518

Table A.4: Hydraulic geometries from the different cross sections on Kongsvegen 15.07.2021.

Cross section	Water depth [m]	Water velocity [m/s]	Froude number	Reynolds number
C1	13	0.61	0.54	44387
C2	14	1.91	1.63	149953
C3	17	0.88	0.68	83857
C4	13	0.72	0.63	52535
C5	40	1.12	0.56	249797
C6	15	2.08	1.72	174598
C7	20	1.56	1.12	174999
C8	10	1.64	1.66	91814
C9	35	0.68	0.37	133578

Table A.5: Hydraulic geometries from the different cross sections on Kongsvegen 18.07.2021.

APPENDIX B

Computer Code

All computer code used to generate the results and analysis in this thesis can be found at my github repository: https://github.com/gecocowie/Master_thesis

Bibliography

Adakudlu, M., Andresen, J., Bakke, J., Beldring, S., Benestad, R., Bilt, W. v. d., Bogen, J., Borstad, C. P., Breili, K., Breivik, Ø. et al. (2019). 'Climate in Svalbard 2100'. In:

Akbarinia, R. and Cloez, B. (2019). 'Efficient Matrix Profile Computation Using Different Distance Functions. arXiv 2019'. In: *arXiv preprint arXiv:1901.05708*.

Alexander, A., Kruusmaa, M., Tuhtan, J. A., Hodson, A. J., Schuler, T. V. and Kaab, A. (2020). 'Pressure and inertia sensing drifters for glacial hydrology flow path measurements'. In: *The Cryosphere* vol. 14, no. 3, pp. 1009–1023.

Alexander, A., Obu, J., Schuler, T. V., Kääb, A. and Christiansen, H. H. (2020). 'Subglacial permafrost dynamics and erosion inside subglacial channels driven by surface events in Svalbard'. In: *The Cryosphere* vol. 14, no. 11, pp. 4217–4231.

Aminikhanghahi, S. and Cook, D. J. (2017). 'A survey of methods for time series change point detection'. In: *Knowledge and information systems* vol. 51, no. 2, pp. 339–367.

Anthoff, D., Nicholls, R. J. and Tol, R. S. (2010). 'The economic impact of substantial sea-level rise'. In: *Mitigation and Adaptation Strategies for Global Change* vol. 15, no. 4, pp. 321–335.

Armstrong, R. L., Rittger, K., Brodzik, M. J., Racoviteanu, A., Barrett, A. P., Khalsa, S.-J. S., Raup, B., Hill, A. F., Khan, A. L., Wilson, A. M. et al. (2019). 'Runoff from glacier ice and seasonal snow in High Asia: separating melt water sources in river flow'. In: *Regional Environmental Change* vol. 19, no. 5, pp. 1249–1261.

Arnold, N., Banwell, A. and Willis, I. (2014). 'High-resolution modelling of the seasonal evolution of surface water storage on the Greenland Ice Sheet'. In: *The Cryosphere* vol. 8, no. 4, pp. 1149–1160.

Bagnall, A., Lines, J., Bostrom, A., Large, J. and Keogh, E. (2016). 'The great time series classification bake off: a review and experimental evaluation of recent algorithmic advances'. In: *Data Mining and Knowledge Discovery* vol. 31, no. 3, pp. 606–660.

Bagshaw, E., Lishman, B., Wadham, J. L., Bowden, J. A., Burrow, S. G., Clare, L. R. and Chandler, D. (2014). 'Novel wireless sensors for in situ measurement of sub-ice hydrologic systems'. In: *Annals of glaciology* vol. 55, no. 65, pp. 41–50.

Bagshaw, E. A., Burrow, S., Wadham, J. L., Bowden, J., Lishman, B., Salter, M., Barnes, R. and Nienow, P. (2012). 'E-tracers: Development of a low cost wireless technique for exploring sub-surface hydrological systems'. In: *Hydrological Processes* vol. 26, no. 20, pp. 3157–3160.

Bhardwaj, A., Sam, L., Martin-Torres, F. J., Kumar, R. et al. (2016). 'UAVs as remote sensing platform in glaciology: Present applications and future prospects'. In: *Remote sensing of environment* vol. 175, pp. 196–204.

Brown, G. H. (2002). 'Glacier meltwater hydrochemistry'. In: *Applied Geochemistry* vol. 17, no. 7, pp. 855–883.

Burgess, E. W., Forster, R. R., Larsen, C. F. and Braun, M. (2012). 'Surge dynamics on Bering Glacier, Alaska, in 2008-2011'. In: *The Cryosphere* vol. 6, no. 6, pp. 1251–1262.

Chanson, H. (1994). 'Hydraulics of skimming flows over stepped channels and spillways'. In: *Journal of Hydraulic Research* vol. 32, no. 3, pp. 445–460.

Chartrand, S. M. and Whiting, P. J. (2000). 'Alluvial architecture in headwater streams with special emphasis on step–pool topography'. In: *Earth Surface Processes and Landforms* vol. 25, no. 6, pp. 583–600.

Covington, M., Gulley, J., Trunz, C., Mejia, J. and Gadd, W. (2020). 'Moulin volumes regulate subglacial water pressure on the Greenland ice sheet'. In: *Geophysical Research Letters* vol. 47, no. 20, e2020GL088901.

Curran, J. H. and Wohl, E. E. (2003). 'Large woody debris and flow resistance in step-pool channels, Cascade Range, Washington'. In: *Geomorphology* vol. 51, no. 1-3, pp. 141–157.

Dau, H. A. and Keogh, E. (2017). 'Matrix profile v: A generic technique to incorporate domain knowledge into motif discovery'. In: *Proceedings of the 23rd ACM SIGKDD international conference on knowledge discovery and data mining*, pp. 125–134.

Davis, W. (1932). 'Piedmont benchlands and Primärrümpfe'. In: *Bulletin of the Geological Society of America* vol. 43, no. 2, pp. 399–440.

Eyles, N. (2006). 'The role of meltwater in glacial processes'. In: *Sedimentary Geology* vol. 190, no. 1-4, pp. 257–268.

Ferguson, R. (1973). 'Sinuosity of supraglacial streams'. In: *Geological Society of America Bulletin* vol. 84, no. 1, pp. 251–256.

Generate pseudo-random numbers (2022). *https : //docs.python.org/3/library/random.html*.

Gleason, C. J., Smith, L. C., Chu, V. W., Legleiter, C. J., Pitcher, L. H., Overstreet, B. T., Rennermalm, A. K., Forster, R. R. and Yang, K. (2016). 'Characterizing supraglacial meltwater channel hydraulics on the Greenland Ice Sheet fromin situobservations'. In: *Earth Surface Processes and Landforms* vol. 41, no. 14, pp. 2111–2122.

Gulley, J., Benn, D., Müller, D. and Luckman, A. (2009). 'A cut-and-closure origin for englacial conduits in uncrevassed regions of polythermal glaciers'. In: *Journal of Glaciology* vol. 55, no. 189, pp. 66–80.

Holmlund, P. (1988). 'Internal geometry and evolution of moulins, Storglaciären, Sweden'. In: *Journal of Glaciology* vol. 34, no. 117, pp. 242–248.

Hou, H., Deng, Z. D., Martinez, J. J., Fu, T., Duncan, J. P., Johnson, G. E., Lu, J., Skalski, J. R., Townsend, R. L. and Tan, L. (2018). 'A hydropower biological evaluation toolset (HBET) for characterizing hydraulic conditions and impacts of hydro-structures on fish'. In: *Energies* vol. 11, no. 4, p. 990.

Hugonnet, R., McNabb, R., Berthier, E., Menounos, B., Nuth, C., Girod, L., Farinotti, D., Huss, M., Dussaillant, I., Brun, F. et al. (2021). 'Accelerated global glacier mass loss in the early twenty-first century'. In: *Nature* vol. 592, no. 7856, pp. 726–731.

Iken, A., Röthlisberger, H., Flotron, A. and Haeberli, W. (1983). 'The uplift of Unteraargletscher at the beginning of the melt season—a consequence of water storage at the bed?' In: *Journal of glaciology* vol. 29, no. 101, pp. 28–47.

IPCC, S. (2019). *IPCC Special Report on the Ocean and Cryosphere in a Changing Climate [H.-O. Pörtner, DC Roberts, V. Masson-Delmotte, P. Zhai, M. Tignor, E. Poloczanska, K. Mintenbeck, A. Alegría, M. Nicolai, A. Okem, J. Petzold, B. Rama, NM Weyer*.

Jansson, P., Hock, R. and Schneider, T. (2003). 'The concept of glacier storage: a review'. In: *Journal of Hydrology* vol. 282, no. 1-4, pp. 116–129.

Jennings, S. J., Hambrey, M. J., Glasser, N. F., James, T. D. and Hubbard, B. (2016). 'Structural glaciology of Austre Brøggerbreen, northwest Svalbard'. In: *Journal of Maps* vol. 12, no. 5, pp. 790–796.

Kamintzis, J., Irvine-Fynn, T., Holt, T., Jones, J., Tooth, S., Griffiths, H. and Hubbard, B. (2019). 'Knickpoint evolution in a supraglacial stream'. In: *Geografiska Annaler: Series A, Physical Geography* vol. 101, no. 2, pp. 118–135.

Karlstrom, L., Gajjar, P. and Manga, M. (2013). 'Meander formation in supraglacial streams'. In: *Journal of Geophysical Research: Earth Surface* vol. 118, no. 3, pp. 1897–1907.

Karner, F., Obleitner, F., Krismer, T., Kohler, J. and Greuell, W. (2013). 'A decade of energy and mass balance investigations on the glacier Kongsvegen, Svalbard'. In: *Journal of Geophysical Research: Atmospheres* vol. 118, no. 10, pp. 3986–4000.

Kohler, J. et al. (2018). 'On the verge of a surge; Kongsvegen, northwestern Svalbard.'

König, M., Wadham, J., Winther, J.-G., Kohler, J. and Nuttall, A.-M. (2002). 'Detection of superimposed ice on the glaciers Kongsvegen and midre Lovénbreen, Svalbard, using SAR satellite imagery'. In: *Annals of Glaciology* vol. 34, pp. 335–342.

Li, H., Beldring, S., Xu, C.-Y., Huss, M., Melvold, K. and Jain, S. K. (2015). 'Integrating a glacier retreat model into a hydrological model–Case studies of three glacierised catchments in Norway and Himalayan region'. In: *Journal of Hydrology* vol. 527, pp. 656–667.

Marston, R. A. (1983). 'Supraglacial stream dynamics on the Juneau Icefield'. In: *Annals of the Association of American Geographers* vol. 73, no. 4, pp. 597–608.

McKean, J., Nagel, D., Tonina, D., Bailey, P., Wright, C. W., Bohn, C. and Nayegandhi, A. (2009). 'Remote sensing of channels and riparian zones with a narrow-beam aquatic-terrestrial LIDAR'. In: *Remote Sensing* vol. 1, no. 4, pp. 1065–1096.

Murzyn, F. and Chanson, H. (2009). 'Free-surface fluctuations in hydraulic jumps: Experimental observations'. In: *Experimental Thermal and Fluid Science* vol. 33, no. 7, pp. 1055–1064.

Nuth, C., Kohler, J., König, M., Von Deschwanden, A., Hagen, J., Kääb, A., Moholdt, G. and Pettersson, R. (2013). 'Decadal changes from a multi-temporal glacier inventory of Svalbard'. In: *The Cryosphere* vol. 7, no. 5, pp. 1603–1621.

Phillips, T., Rajaram, H. and Steffen, K. (2010). 'Cryo-hydrologic warming: A potential mechanism for rapid thermal response of ice sheets'. In: *Geophysical Research Letters* vol. 37, no. 20.

Piho, L., Alexander, A. and Kruusmaa, M. (2022). 'Topology and pressure distribution reconstruction of an englacial channel'. In: *The Cryosphere Discussions*, pp. 1–19.

Piho, L. and Kruusmaa, M. (2021). 'Subsurface Flow Path Modeling From Inertial Measurement Unit Sensor Data Using Infinite Hidden Markov Models'. In: *IEEE Sensors Journal* vol. 22, no. 1, pp. 621–630.

Pitcher, L. H. and Smith, L. C. (2019). 'Supraglacial Streams and Rivers'. In: *Annual Review of Earth and Planetary Sciences* vol. 47, no. 1, pp. 421–452.

Ponce, V. M. (1979). 'On the classification of open channel flow regimes'. In: *Fourth National Hydrotechnical Conference*. Vancouver, B.C., Canada.

Porter, C. et al. (2018). *ArcticDEM. https : //doi.org/*10.7910/*DVN/OHHUKH*, Harvard Dataverse. Version V1.

Prior-Jones, M. R., Bagshaw, E. A., Lees, J., Clare, L., Burrow, S., Werder, M. A., Karlsson, N. B., Dahl-Jensen, D., Chudley, T. R., Christoffersen, P. et al. (2021). 'Cryoegg: development and field trials of a wireless subglacial probe for deep, fast-moving ice'. In: *Journal of Glaciology* vol. 67, no. 264, pp. 627–640.

Riverman, K. L. (2017). 'Flow dynamics of the NE Greenland Ice Stream with hydrological insights from englacial exploration of Larsbreen, Svalbard'. PhD thesis. The Pennsylvania State University.

Ryan, J. C., Hubbard, A., Stibal, M., Irvine-Fynn, T. D., Cook, J., Smith, L. C., Cameron, K. and Box, J. (2018). 'Dark zone of the Greenland Ice Sheet controlled by distributed biologically-active impurities'. In: *Nature communications* vol. 9, no. 1, pp. 1–10.

Schroeder, J. (1998). 'Hans glacier moulins observed from 1988 to 1992, Svalbard'. In:

Schuler, T. V., Kohler, J., Elagina, N., Hagen, J. O. M., Hodson, A. J., Jania, J. A., Kääb, A. M., Luks, B., Małecki, J., Moholdt, G. et al. (2020). 'Reconciling Svalbard glacier mass balance'. In: *Frontiers in Earth Science* vol. 8, p. 156.

TE connectivity sensors (2017). *https : //www.te.com/global − en/product − CAT − BLPS*0059.*html*.

Tesaker, A. (2021). 'Investigation of glacial water flow using lagrangian drifters.' In: *Master's thesis, Universitetet i Oslo*.

Thang, H. M., Viet, V. Q., Thuc, N. D. and Choi, D. (2012). 'Gait identification using accelerometer on mobile phone'. In: *2012 International Conference on Control, Automation and Information Sciences (ICCAIS)*. IEEE, pp. 344–348.

The matrix profile (2022). *https : //stumpy.readthedocs.io/en/latest/*$Tutorial_{T}he_{M}atrix_{P}rofile.html$.

Truong, C., Oudre, L. and Vayatis, N. (2020). 'Selective review of offline change point detection methods'. In: *Signal Processing* vol. 167, p. 107299.

Tuhtan, J., A., A., Kruusmaa, M. and Fuentes-Pérez, J. (2020). 'Multiscale change detection in a supraglacial stream using surface drifters'. In: *River Flow*.

Van Benschoten, A. H., Ouyang, A., Bischoff, F. and Marrs, T. W. (2020). 'MPA: a novel cross-language API for time series analysis'. In: *Journal of Open Source Software* vol. 5, no. 49, p. 2179.

Vatne, G. and Irvine-Fynn, T. (2015). 'Morphological dynamics of an englacial channel.' In: *Hydrology & Earth System Sciences Discussions* vol. 12, no. 8.

Vatne, G. (2001). 'Geometry of englacial water conduits, Austre Brøggerbreen, Svalbard'. In: *Norsk Geografisk Tidsskrift* vol. 55, no. 2, pp. 85–93.

Vatne, G. and Irvine-Fynn, T. (2016). 'Morphological dynamics of an englacial channel'. In: *Hydrology and Earth System Sciences* vol. 20, no. 7, pp. 2947–2964.

Yang, X., Zhao, Y., Street, G., Huang, Y., To, S. F. and Purswell, J. (2021). 'Classification of broiler behaviours using triaxial accelerometer and machine learning'. In: *Animal* vol. 15, no. 7, p. 100269.

Yeh, C.-C. M., Zhu, Y., Ulanova, L., Begum, N., Ding, Y., Dau, H. A., Zimmerman, Z., Silva, D. F., Mueen, A. and Keogh, E. (2017). 'Time series joins, motifs, discords and shapelets: a unifying view that exploits the matrix profile'. In: *Data Mining and Knowledge Discovery* vol. 32, no. 1, pp. 83–123.

Zhu, Y., Zimmerman, Z., Senobari, N. S., Yeh, C.-C. M., Funning, G., Mueen, A., Brisk, P. and Keogh, E. (2016). 'Matrix profile ii: Exploiting a novel algorithm and gpus to break the one hundred million barrier for time series motifs and joins'. In: *2016 IEEE 16th international conference on data mining (ICDM)*. IEEE, pp. 739–748.